AN EVALUATION OF SHADOW SHIELDING FOR LUNAR SYSTEM WASTE HEAT REJECTION

A Thesis

by

CHEYN LAYTON WORN

Submitted to the Office of Graduate Studies of
Texas A&M University
in partial fulfillment of the requirements for the degree of

MASTER OF SCIENCE

May 2012

Major Subject: Nuclear Engineering

AN EVALUATION OF SHADOW SHIELDING FOR LUNAR SYSTEM WASTE HEAT REJECTION

A Thesis

by

CHEYN LAYTON WORN

Submitted to the Office of Graduate Studies of
Texas A&M University
in partial fulfillment of the requirements for the degree of

MASTER OF SCIENCE

Approved by:

Chair of Committee,	Pavel V. Tsvetkov
Committee Members,	Shannon Bragg-Sitton
	Yassin A. Hassan
	Tim J. Jacobs
Head of Department,	Yassin A. Hassan

May 2012

Major Subject: Nuclear Engineering

ABSTRACT

An Evaluation of Shadow Shielding for Lunar System Waste Heat Rejection. (May 2012)
Cheyn Layton Worn, B.S., Texas A&M University
Chair of Advisory Committee: Dr. Pavel V. Tsvetkov

Shadow shielding is a novel and practical concept for waste heat rejection from lunar surface spacecraft systems. A shadow shield is a light shield that shades the radiator from parasitic thermal radiation emanating from the sun or lunar surface. Radiator size and mass can reduce if the radiator is not required to account for parasitic heat loads in addition to system energy rejection requirements. The lunar thermal environment can be very harsh towards radiative heat rejection. Parasitic heat loads force the radiator to expand in size and mass to compensate. On the Moon, there are three types: surface infrared, solar insolation, and albedo. This thesis tests shadow shielding geometry and its effect on the radiator and nuclear reactor in a reactor-powered Carnot heat engine. Due to the nature of cooling by radiative heat transfer, the maximum shaft work a Carnot system can produce and the minimal required radiator area occurs when the Carnot efficiency is 25%.

First, a case for shadow shielding is made using an isothermal, control radiator model in Thermal Desktop. Six radiator temperatures and three latitudes are considered in the tests. Test variables in this section include radiator shapes and shade geometry. The simulations found that shadow shielding is best suited for a low-temperature radiator at the lunar equator. Optimized parabolic shade geometry includes a focus right above or at the top of the radiator and full to three-quarters shade height. The most useful rectangular radiator shape for shadow shielding is that which has a low height and long width.

All simulations were conducted using a shade with a 10 kg/m^2 area mass. A sensitivity study was conducted for different shade area masses using high and low values found in the literature. The shade is the most useful when the shade's area mass is less than or

equal to that of the radiator. If the shade mass is below this threshold, the shade would be applicable to all radiator temperatures tested.

Optimized shade and radiator geometry results were then factored into a second model where the radiator is comprised of heat pipes which is similar to radiators from actual system designs. Further simulations were conducted implementing the SAFE-400[1] fast fission nuclear reactor design. The study found that shadow shielding allowed the system to use a low-temperature radiator where other configurations were not viable because shadow shielding drastically improves radiative heat transfer from the radiator, but at the consequence of raising radiator mass.

ACKNOWLEDGMENTS

I must thank many people for their guidance and support. First, I thank my mother, father, and sister for always believing in me and their love. Next, I would like to thank Dr. Fred Best and Dr. Cable Kurwitz for their guidance and aid. I would also like to thank Dr. Pavel Tsvetkov and my committee (Dr. Yassin Hassan, Dr. Shannon Bragg-Sitton, and Dr. Tim Jacobs) for their patience and help.

NOMENCLATURE

Upper-Case Letters

A	Area
C	Configuration
D	Diameter
E	Energy
F	View Factor
G	Solar Flux
L	Length
Q	Energy Load
$\dot{Q}$	Heat Load
R	Radius
T	Temperature
V	Volume
$\dot{W}$	Shaft Work Rate

Lower-Case Letters

a	Area Ratio
c_p	Specific Heat
e	Specific Energy
h	Specific Enthalpy
$\hat{h}$	Unitless Height
$\vec{i}$	Unit Vector
k	Thermal Conductivity
l	Line
m	Mass
$\dot{m}$	Mass Flow Rate

n	Number of Items
p	Focal Length
q	Specific Energy Load
$\dot{q}$	Specific Heating Rate
$\dot{q}'$	Linear Heating Rate
$\dot{q}''$	Heat Flux
r	Radial Axis
s	Specific Entropy
t	Thickness or Width
x, y, z	Cartesian Axes

Subscripts

B	Base
C	Carnot
F	Fin
H	Hot
IR	Infrared
R	Rejection
S	Sink
T	Tip

ad	Adhesive
al	Albedo
b	Bottom
co	Radiator Core
f	Fissile Nuclear Fuel
fi	Filler
fs	Radiator Face Sheet

hp	Heat Pipes
ls	Lunar Surface
o	Origin
ra	Radiator
re	Lunar Regolith
rx	Reactor
rxsh	Reactor Shielding
sh	Shade (Shadow Shielding)
so	Solar
t	Top
x$\rightarrow$y	From x to y
x$-$y	Between x and y

Greek

Γ	Surface
Δ	Difference
Σ	Macroscopic Neutron Fission Cross-Section
Ω	Solid Angle

α	Solar Absorptivity
β	Angle
ε	Emissivity
η	Efficiency
λ	Wavelength
θ	Temperature Ratio
ϑ	Latitude
σ	Stefan-Boltzmann Constant
ς	Specularity

ρ	Reflectivity
ρ	Density
ρ'	Linear Density
ρ''	Areal Density
τ	Time
ϕ	Neutron Flux
ζ	Dimensionless Ratio of Radiative Heat Transfer to Conduction

GLOSSARY

MLI	multi-layer insulation
IR	infrared thermal radiation
SAFE	Safe Affordable Fission Engine
UV	ultraviolet thermal radiation
Albedo	ultraviolet thermal radiation reflected by a surface
Regolith	lunar surface sand

TABLE OF CONTENTS

Page

Page

LIST OF FIGURES

FIGURE Page

FIGURE Page

FIGURE Page

FIGURE Page

LIST OF TABLES

1. INTRODUCTION

As the world pushes forward into the twenty-first century the goals of space exploration and research have shifted with the changing millennium. The National Aeronautics and Space Administration (NASA) has considered landing and establishing a continual human presence on the Moon to pioneer future established human presence on Mars. NASA has been developing a new lunar landing module for sustainable, extended operational use.

Space systems often employ solar power or fuel cells to generate electricity. A nuclear reactor system has been proposed as a heat source for a lunar surface system because nuclear power is reliable, energy dense, and does not depend on the sun's presence to operate. However, a heat source is one part of a thermodynamic system which must also include a method for waste energy rejection. Radiators are used for space systems for the following reasons.

Radiators emit thermal radiation to space from exposed faces; operation does not require a power source beyond the establishment of a temperature gradient between the radiative surface and sink. Radiators are typically the only long duration choice for waste heat rejection in lunar landing module designs because no viable alternative options exist. For one, there is minimum atmosphere and no water on the lunar surface, ruling out system cooling through convection. Lunar surface sand (regolith) has very poor thermal conductivity; a cooling system would need to be very large to sustain system waste energy rejection. By elimination, a radiator is the best option.

Problems arise in radiator design due to the thermal lunar environment. Other objects thermally interact with the radiator and these include the sun and the lunar surface; a parasitic radiative heat load develops on the radiator if the face plates come within view of the sun or moon. Parasitic thermal radiations can reduce a radiator's effectiveness because the radiator will need to emit both the parasitic heat load and the original waste energy; this typically means the radiator must either be larger or operate at a higher temperature.

This thesis follows the style of Journal of Thermophysics and Heat Transfer.

Many solutions exist to reduce parasitic heat loads originating from the sun or lunar surface. Shadow shielding is a novel, feasible, and useful concept for waste heat rejection from landed lunar spacecraft. Fig. 1.1 is a graphic displaying a radiator with shadow shielding. It is an isometric drawing looking towards the lunar surface, which is the graphic background. The dark, square object in the center is the radiator, vertical in orientation, and the shades are parabolic ear-like projections extending from the radiator sides.

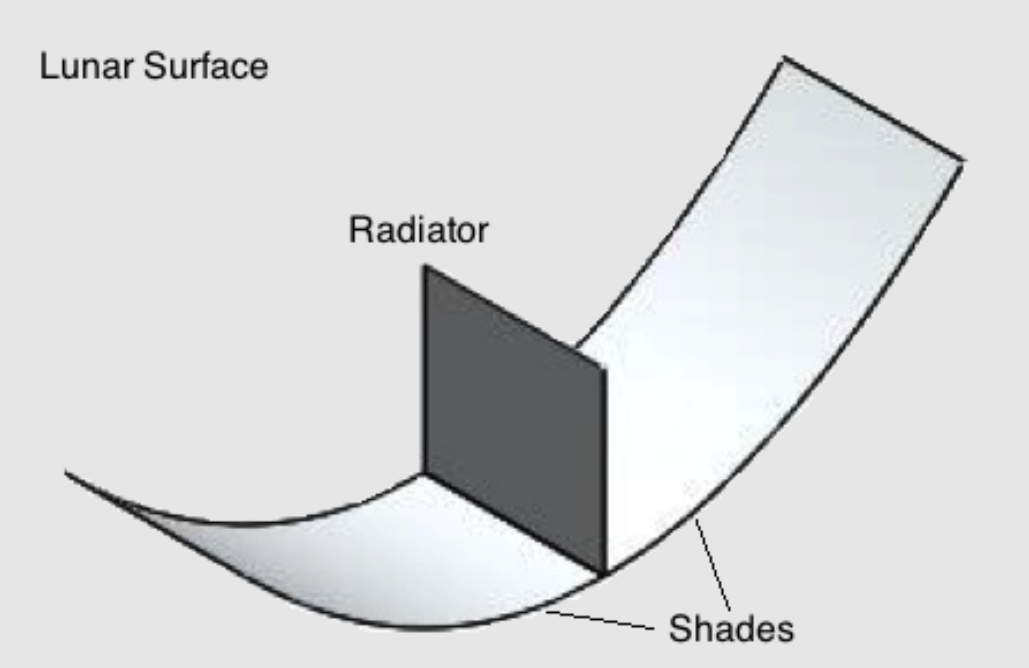

Fig. 1.1: Isometric concept drawing of a shaded radiator.

As shown, a shadow shield is a light shield that shades the radiator from parasitic thermal radiation originating from the sun or lunar surface. The radiator can shrink in size and mass if the radiator is not required to account for solar and lunar parasitic loads.

Radiator design arises as a challenge for lunar reactor systems because lunar gravity is seldom considered. The problem is shown in Fig. 1.2 which is an artist's conception of the lunar surface nuclear reactor proposed in Houts and Mason.[2]

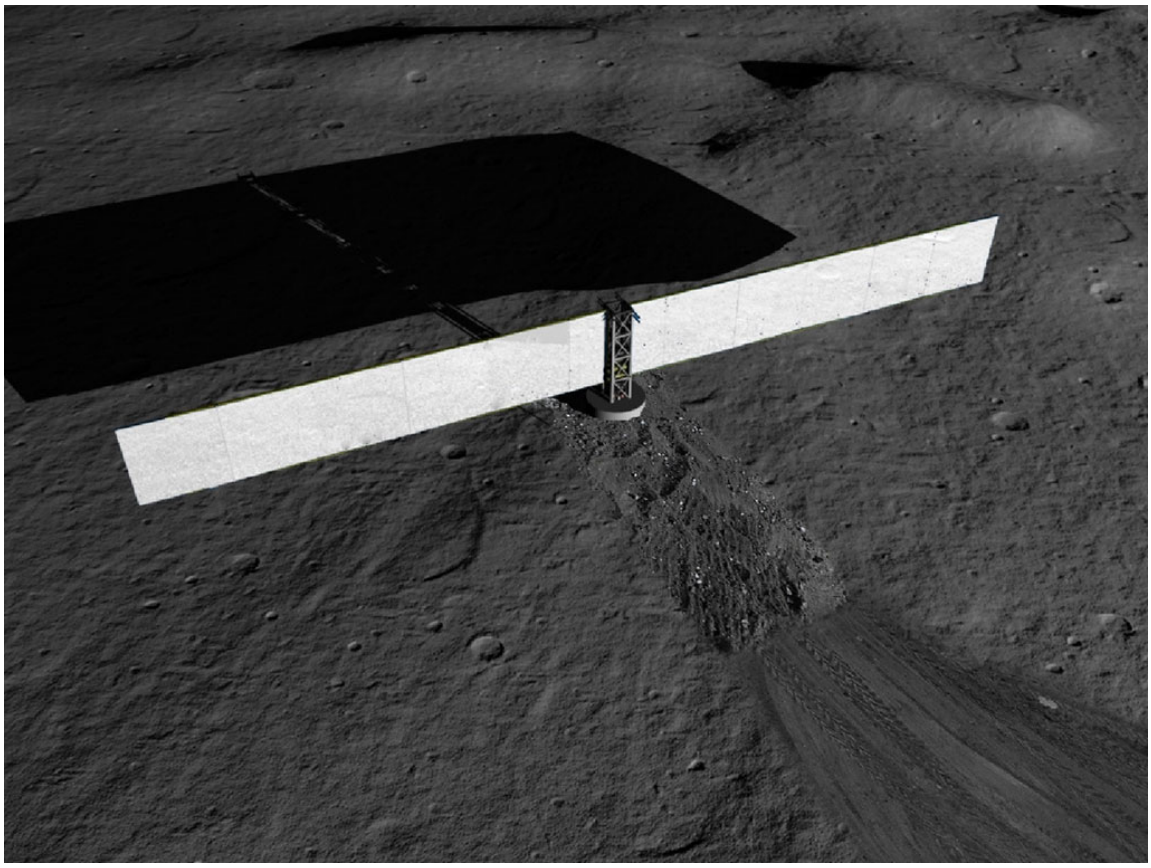

Fig. 1.2: Artist's conception of the lunar surface nuclear reactor proposed in Houts and Mason.[2] System reactor buried beneath the lunar surface.

The enormous white rectangles are radiators which reject waste energy from the thermodynamic system. The radiators in the design are better suited to operate in orbit around the Earth because the design lacks support structure and the design study does not mention its need. The radiator design needs support, and this arises because of lunar gravity; gravity in Earth orbit is minimum and radiator designers can ignore weight. However, the moon has one sixth Earth gravity. A large radiator conditioned for micro-gravity cannot be the best option in lunar gravity because its weight would require support structures for operation, driving up the specific mass with respect to area. This factor has a tremendous

impact on system mass optimization.[2,3] The radiator can shrink in area and mass with shadow shielding, reducing transportation and construction costs.

1.1 Lunar Radiator and Reactor System Studies

Nuclear-powered space systems have been studied and designed since the late 1960s; Dieckamp[4] published a starting guide for system designers in 1967. Analysis began with an in-depth discussion on reactor physics and design and then implemented thermodynamic system as a whole using the ideal Carnot cycle with starting emphasis on the radiator system. One paramount conclusion was that although nuclear systems may tend towards high Carnot efficiency, a high Carnot efficiency would not necessarily lead to the lightest or smallest radiator.

Multiple lunar reactor systems have been proposed in the past. Houts and Mason[2] and Elliott et al.[3] both proposed a lunar nuclear reactor system design in the past decade. A keystone of each design is the massive radiators protruding from the system top. This obvious feature was a factor which drove this thesis, the desire to lower radiator mass and size through alternative radiator design.

Radiator design arises out of a need to balance radiator performance and mass. Since space system mass transport is very expensive, the key is to find the design which gives the best performance for the lightest mass. Fin efficiency is a measure of how well the radiator performs its task, but is not as big a concern as mass. Concentrating on the tradeoffs associated with radiator mass, performance, and efficiency, in 1984 Chang[5] presented a mass model for a realistic radiator design. The radiator should be composed of four items: face sheets, filler, adhesive, and a mechanism for moving energy from the system to the radiator (typically heat pipes, which will be used in analysisminimum). The face sheets and adhesive hold the radiator together. The face sheets emit the waste energy to the surroundings. Adhesive is supposed to be spread evenly and thinly across the inward-facing side of the face sheets. Filler is very light material and provides the radiator with structure. Heat pipes are the primary mechanism for transporting energy from the system to the radiator. They

are devices that combine thermal conductivity and phase transition to efficiently transfer energy from one end to the other.

Chang's work is an application of work performed by Truong and Mancuso[6] in 1980. Using a simple fin, Truong and Mancuso developed a correlation expression for fin effectiveness and performance using the Runge-Kutta numerical method to solve a heat transfer equation for this fin. The pair also analyzed how various factors such as radius, sink temperature, and materials would affect results. Chang applied their model to radiator design by altering the fin geometry to be rectangular in overall shape. Chang then developed a computer model to find the optimal heat pipe spacing within a radiator. Chang did not specify the operating environment but, similar to Truong and Mancuso, did implement sink temperature terms for each side of the fin. Sink temperature is tied to radiator performance; a thermodynamic sink is a system with a heat capacity large enough such that its temperature remains effectively constant (at what is known as the sink temperature) when in thermal equilibrium.[7]

Radiator performance is dictated by many competing factors such as the operational environment, radiating surface properties, and radiative heat transfer itself. Radiative heat transfer is proportional to the temperature of the radiating surface raised to the fourth power. It is relatively weaker than the other two forms of heat transfer (conduction and convection). Radiative heat transfer is also correlated to the surface properties of the radiating surface, namely emissivity and absorptivity; absorptivity is a ratio of the absorbed part of incoming thermal radiation to the total incoming thermal radiation and emissivity is a ratio of the energy emitted by a surface to the energy that would be emitted by a black surface at the same temperature. A black body is an ideal physical body that absorbs all incident electromagnetic radiation, regardless of frequency or angle of incidence, and emits as much or more energy at every frequency than any other body at the same temperature.[8]

Another aspect of radiator performance is the operational environment, namely the Moon. The lunar thermal environment can be very harsh towards a radiative heat rejection system due to parasitic heat loads. Parasitic heat loads force the radiator to expand in

size and mass to compensate. On the Moon, there are three types: surface infrared, solar insolation, and albedo, all introduced and discussed by Gilmore.[9] Surface infrared thermal radiation is emitted by the lunar surface during all times of the lunar day but is most extreme where surface temperatures are highest (i.e. the lunar equator at noon). A lunar surface temperature map is useful for visualizing the extremes. In 2008 Christie et al.[10] developed a transient thermal model of the lunar surface using analytical techniques with numbers from previous studies and observations. Analysis predicted temperatures and regolith properties which are very close to actual measured properties. The thermal model will be used to set lunar temperatures and regolith properties in analysis.

Solar insolation directly comes from the sun, which circles overhead at lower latitudes (causing a day and night cycle) but circles around the horizon at the lunar hot pole. Albedo is solar thermal radiation reflected by the lunar surface; it is the least intense of the three types. Shadow shielding is meant to block a vertical radiator's view of the lunar surface, minimizing surface infrared and albedo loads; it also occasionally blocks out the radiator's view of the sun at the hot pole. This is just a basic view of the lunar thermal environment. Location and radiator orientation also play a role in radiator performance. Dallas et al.[11] studied the effects of orientation, lunation, and location on the performance of bare, vertical lunar radiators in 1971. Their analysis provided a method of rapidly approximating the effective sink temperature and size of a lunar system radiator.

Shadow shielding emerged as a concept to shade the radiator from the lunar surface in the early 1990s. In 1990 Costello and Swanson[12] proposed a parabolic, specular reflector to shade the radiator from the hot lunar surface and reflect the sun's rays. They found, using an analytical model, that radiative heat transfer from a vertical radiator surface is greatly enhanced using this method; they also assumed the shade completely blocked the radiator's view of the lunar surface. This assumption is not realistic unless the radiator and shade are extremely long or use end caps, neither of which the study assumes.

Barron et al.[13] conducted a design study on shadow shielding for a low temperature lunar equatorial system radiator in 1991. They researched the lunar environment at this lat-

itude and studied the thermodynamic and mass effects of a shade on a vertical, 270 Kelvin radiator array-based heat rejection system. Early in analysis they proved the low temperature radiator could not operate on the lunar surface without a shadow shield; the shade serves to block out the high amounts of infrared thermal radiation emitted by the lunar surface at noon. The team considered several shade geometries that included parabolic, wing-shaped, and step-shape shades. In order to compare all designs, the team formed a decision matrix that included shade mass, radiator performance (using sink temperature), and ease of deployment. They concluded that a parabolic-shaped shade with the focus slightly above the top of the radiator was fairly heavy and difficult to deploy; in fact their parabolic shade had an area mass of 20 kg/m^2 which also accounted for structure for holding up the shade as well. Despite the mass, the parabolic shade provided the greatest improvement in radiative heat transfer from the radiator surface. Much like Costello and Swanson,[12] Barron et al.[13] assumed that the shade completely blocked the radiator's view of the lunar surface by making the radiator very wide.

In 1995 Keller[14] and Ewert et al.[15] presented studies on parabolic shade properties; results in both papers were quantified using the sink temperature and the Thermal Synthesizer System (TSS). Keller found that the shade surface facing the radiator should be highly specular in both the infrared and ultraviolet spectra to obtain better radiator performance. He also found that the shade bottom should be essentially black. Ewert et al. confirmed Keller's results using the TSS and a scaled-down version of the system in a laboratory vacuum chamber. Keller and Ewert et al. also used a very light shade area mass of 0.56 kg/m^2; they did not account for shade structure like Barron et al. Similar to Costello and Swanson[12] and Barron et al.[13] both analyses assumed the radiator to be very long so the shade would completely block out the radiator's view of the lunar surface, simplifying view factor calculation for thermal analysis.

1.2 Temperature and Efficiency

All thermodynamic cycles must reject waste energy. The heat rejection system is the only interface between a thermodynamic system and the environment if the heating source is internal (like reactor designs) and properly thermally insulated. Radiator optimization arises out of a desire to minimize mass and view factor to various thermal sinks.

The basic requirement of a space power system to maintain the thermodynamic cycle cold temperature by the radiative rejection of thermal energy introduces unique considerations and constraints. A generic system schematic, using a reactor for heating and a radiator for cooling, is shown in Fig. 1.3

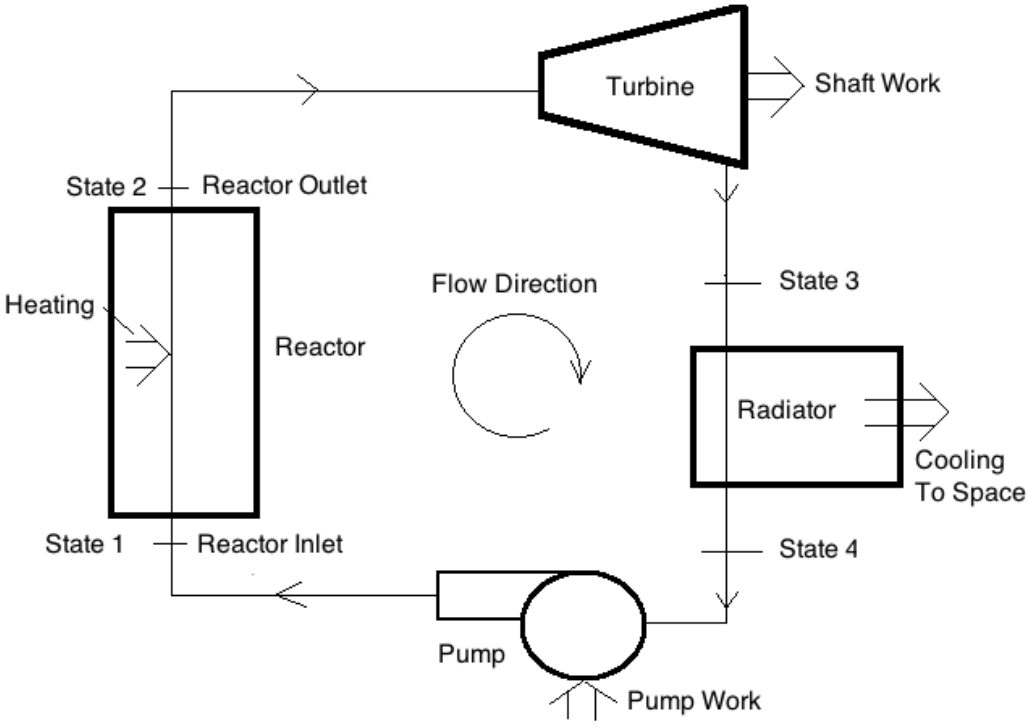

Fig. 1.3: Generic heat engine with reactor heating source and radiator cooling.

The system working fluid heats in the reactor (expanding from state 1 to 2), expands in the turbine to produce shaft work (moving from state 2 to 3), cools in the radiator

(compressing from state 3 to 4), and is compressed and returned to the reactor by the pump (moving from state 4 back to 1).

This thesis will use the Carnot heat engine[7] for analysis as it is simple and ideal, providing an upper limit on thermodynamic cycle efficiency. The Carnot cycle is ideal in that all processes involved are considered reversible. Friction, energy loss to surroundings, and unrestrained expansion are three examples of irreversible processes important to system design. Truly reversible processes cannot be achieved in reality because many of these irreversibilities cannot be prevented. Neglecting them simplifies analysis.

For the Carnot cycle, as applied to the reactor system, working fluid heating/expansion in the reactor and cooling/compression in the radiator are isothermal processes; expansion in the turbine and compression in the pump or compressor are isentropic processes. All processes in the Carnot cycle are reversible, as Carnot analysis ignores processes such as friction, unwanted heat transfer, and unrestrained expansion. Table 1.1 summarizes and relates the Carnot cycle to the previous Fig. 1.3.

Table 1.1: Carnot cycle processes with reactor heating source and radiator cooling.

Process	Component	Energy or Work Transfer Rate	Process Description
1→2	Reactor	$\dot{Q}_H$	Reversible, Isothermal Heating and Expansion
2→3	Turbine	$\dot{W}_{shaft}$	Reversible, Isentropic Expansion
3→4	Radiator	$\dot{Q}_R$	Reversible, Isothermal Cooling and Compression
4→1	Pump/Compressor	$\dot{W}_{pump}$	Reversible, Isentropic Compression

High Carnot efficiency requires minimum cycle cold temperature which increases the radiator area requirement because of the T^4 dependence of the radiator area.[4] Since radiator size will have a significant influence on system design criteria, concept selection, and weight, it is important to evaluate and understand the trade off between system efficiency and radiator area. In general if η_C is defined as the system Carnot efficiency, and the system heat input $\dot{Q}$, is related to the system shaft work $\dot{W}_{shaft}$ such that

$$\dot{Q} = \frac{\dot{W}_{shaft}}{\eta_C}, \tag{1.1}$$

then the rate at which energy is rejected by the radiator, $\dot{Q}_R$, is the difference between the heat input and shaft work such that

$$\dot{Q}_R = \dot{Q} - \dot{W}_{shaft} = \dot{W}_{shaft}\left(\frac{1}{\eta_C} - 1\right). \tag{1.2}$$

If T_H is defined as the reactor outlet temperature and T_R as the system heat rejection temperature, then

$$\eta_C = 1 - \frac{T_R}{T_H}, \tag{1.3}$$

and if T_S is defined as the sink temperature, using a simplified radiative heat transfer equation,

$$\dot{Q}_R = A_{ra}\varepsilon_{ra}\sigma\left(T_R^4 - T_S^4\right), \tag{1.4}$$

where A_{ra} represents the radiator area, ε_{ra} the radiator surface emissivity, and σ the Stefan-Bolzmann constant.

If one were to define a parameter θ_S as the ratio of the sink temperature to the system heat rejection temperature as

$$\theta_S = \frac{T_S}{T_R},\ \theta_S \in [0 \ldots 1], \tag{1.5}$$

then

$$\dot{Q}_R = A_{ra}\varepsilon_{ra}\sigma T_R^4\left(1-\theta_S^4\right) \tag{1.6}$$

and furthermore, substituting Eq. (1.3)

$$\dot{Q}_R = A_{ra}\varepsilon_{ra}\sigma T_H^4\left(1-\eta_C\right)^4\left(1-\theta_S^4\right). \tag{1.7}$$

Substitution of Eq. (1.2) into Eq. (1.7) and simplification allows one to find Eq. (1.8),

$$\frac{\dot{W}_{shaft}}{A_{ra}} = \varepsilon_{ra}\sigma T_H^4\cdot\eta_C\left(1-\eta_C\right)^3\left(1-\theta_S^4\right). \tag{1.8}$$

The maximum work (or minimum radiator area) occurs where

$$\begin{array}{rcl} \frac{\partial}{\partial\theta_S}\left(\frac{\dot{W}_{shaft}}{A_{ra}}\right) & = & 0 \\ \frac{\partial}{\partial\eta_C}\left(\frac{\dot{W}_{shaft}}{A_{ra}}\right) & = & 0, \end{array} \tag{1.9}$$

and the results are

$$\begin{array}{rcl} \eta_C|_{\text{min. } A_{ra}} & = & 25\% \\ \theta_S|_{\text{min. } A_{ra}} & = & 0. \end{array} \tag{1.10}$$

The calculus behind the calculation of Eq. (1.10) from Eqs. (1.8) and (1.9) may be found in Appendix A; it is important to note that no additional numbers or properties are necessary to obtain these values. The sink temperature ratio and Carnot efficiency that provide the minimum radiator area and greatest amount of shaft work are not dependent on materials, physical constants, or temperature values.

Figs. 1.4 and 1.5 are plots of Eq. (1.8); Fig. 1.4 is a plot of unitless shaft work over a range of Carnot efficiencies with constant sink temperature ratios, constant radiator area, and a constant isothermal system heating temperature. The equation plotted is simply Eq. (1.8) with the radiator emissivity, Stefan-Boltzmann constant, and system heating temperature divided out. The curves in Fig. 1.5 are inverses of the curves in Fig. 1.4 and represent the required radiator area for a constant shaft work and system heating temper-

ature over a range of sink temperature ratios. The four separate sink temperature ratios plotted in each figure are 0, 0.3, 0.6, and 0.9.

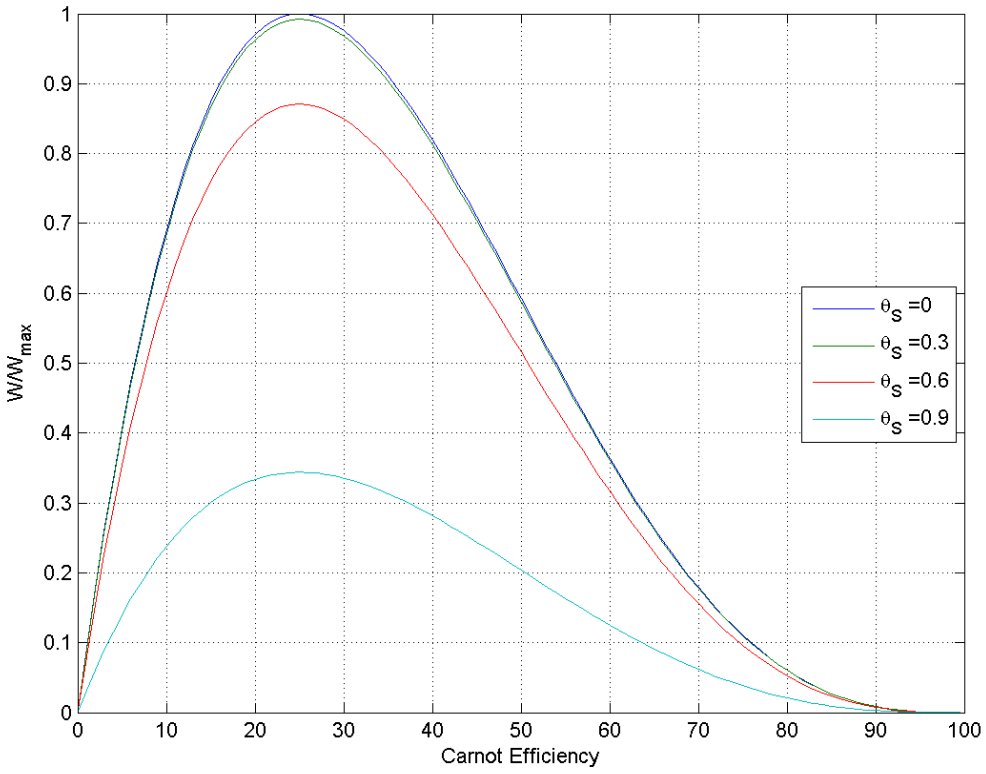

Fig. 1.4: Plot of shaft work versus Carnot efficiency for four sink temperature ratios.

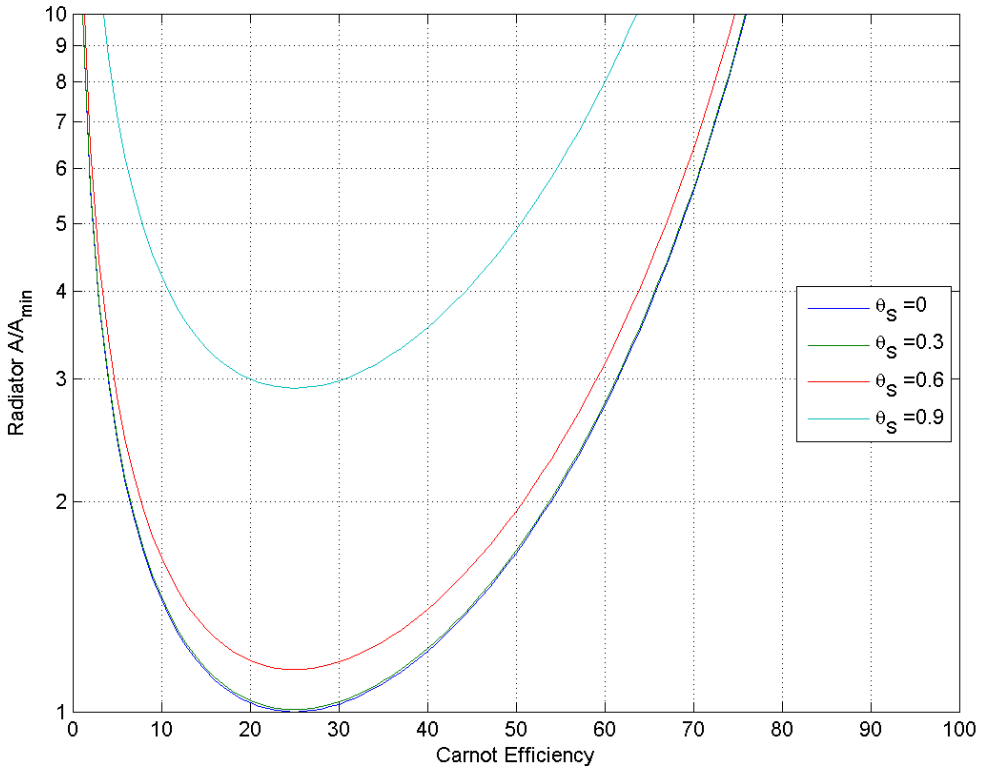

Fig. 1.5: Plot required radiator surface area versus Carnot efficiency for four sink temperature ratios.

As predicted in Eq. (1.10), maximum shaft work produced and minimum radiator area occur at 25% Carnot efficiency for all sink temperature ratios. It is important to note that rising sink temperature ratios either reduce shaft work production or require an increase in radiator size but the optimal Carnot efficiency does not change. Nuclear systems are very energy dense and tend towards the optimum Carnot conditions, but the Carnot efficiency that corresponds with the minimum radiator area and maximum shaft work produced is not necessarily high. In fact, higher Carnot efficiencies require an increase in radiator area and produce a decrease in shaft work; a minimum radiator temperature does not correlate with a minimum radiator area or mass.

It is also not necessarily true that the minimum radiator mass occurs at the minimum radiator area. The smallest radiator area calls for a radiator with coolant lines packed together with no space or material in between them; while this provides a very high radiator efficiency, the radiator has become extremely heavy in the process. It is important to balance radiator mass and area due to transport costs and required radiator structure.

Structure must also be considered when designing a landed system that will be subject to gravity. Fig. 1.6 is an artist's depiction of a lunar nuclear reactor-heated system designed by Elliott et al.[3] The radiator (the teal panel) in the depiction is very large, almost 30 meters wide and 5.5 meters tall raised 3.6 meters from the lunar surface. Struts protrude from the bottom to uphold the radiator wings. A radiator with a lower mass reduces support structure needs and transport costs. A radiator with a minimum area could allow for easier set-up and transportation in that it would be better capable of being stored in a compact configuration such that it can be packed in a launch vehicle. The two parameters area and mass must be balanced although mass takes precedence due to cost.

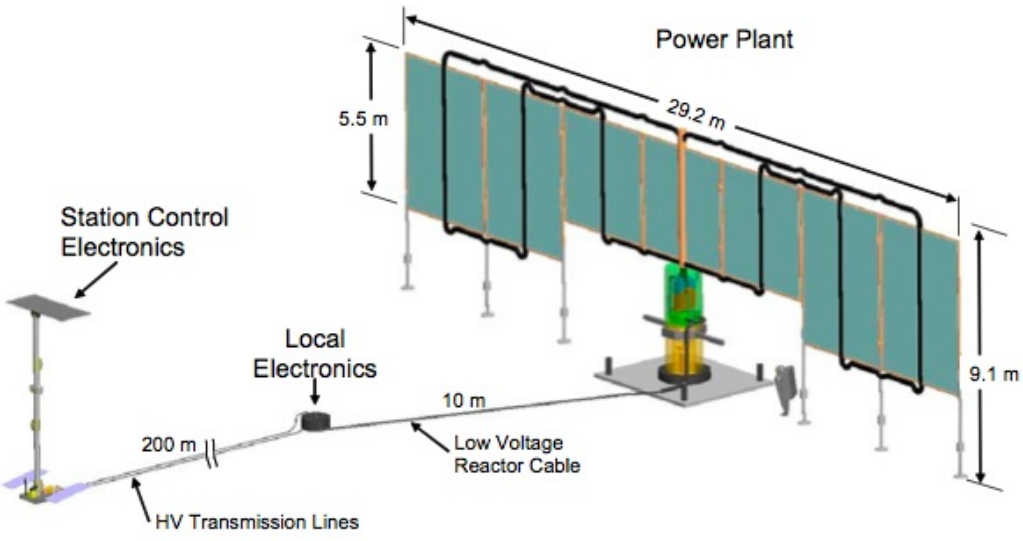

Fig. 1.6: Artist's conception of a lunar surface nuclear reactor system proposed by Elliott et al.[3]

Sink temperature reduction is one way to reduce radiator size, but the concept of a sink temperature requires further expansion. If no net energy radiated from the radiator surface then

$$\dot{Q}_R = A_{ra}\varepsilon_{ra}\sigma\left(T_R^4 - T_S^4\right) = 0$$

and the radiator surface temperature would equal to sink temperature ($\theta_S = 1$). Sink temperature is an effective temperature that includes the effects of parasitic thermal loads. To gain perspective one must now consider the radiator's relationship with the lunar environment.

1.3 The Lunar Thermal Environment and Radiator Configuration

Radiator orientation with respect to the lunar environment is an extremely important consideration because the orientation directly impacts parasitic thermal loading. Radiator

designs must account for parasitic thermal loads associated with the desired operational lunar latitude day and night cycles. Studies conducted so far have primarily considered the thermal extremes of the lunar poles and equator. In any lunar latitude, one must consider parasitic heat loads emanating from the lunar surface and parasitic loads originating from the sun. Lunar system radiator designs are usually oriented either vertically or horizontally; both types deal with parasitic heat loads in different ways. First, however, the lunar thermal environment must be explained, starting with the surface infrared thermal radiation.

1.3.1 Surface Infrared Radiation

The lunar north and south poles both experience 180 day periods of alternating darkness and light; the lunar poles maintain surface temperatures around 295 Kelvin in direct sunlight and 70 Kelvin during the night.[9] The lunar equator experiences the greatest temperatures and temperature shifts compared to other latitudes. A lunar day and night cycle at the equator lasts about one earth month and surface temperatures can reach up to 390 Kelvin. Lunar night at the equator lasts the same length of time but the surface temperature drops to near 100 Kelvin. A radiator on the lunar equator should work best during the night time due to minimum surface infrared thermal radiation (IR) and the absence of solar or albedo thermal radiation. Lunar noon is the opposite; all parasitic radiations are at their maximum during this time. Sunset and sunrise on the moon are also extreme periods during the lunar day. Lunar surface temperatures dramatically drop or rise over 100 Kelvin at dusk or dawn respectively.[9] Fig. 1.7 displays the lunar surface temperature versus latitude for a lunar day.

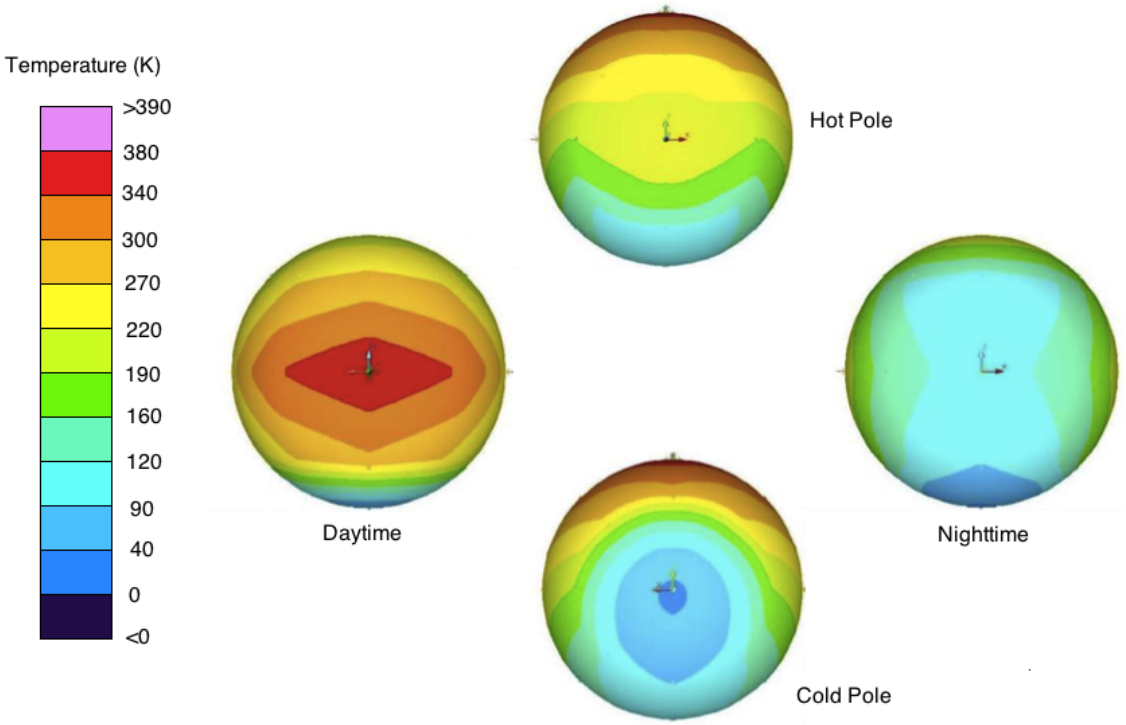

Fig. 1.7: Lunar surface temperatures.

As predicted by Wienn's displacement law the lunar surface primarily emits thermal radiation in the infrared spectrum.[8] The parasitic load on a single radiator face is represented by Eq. (1.11)

$$\dot{Q}_{fs,IR} = A_{fs}\sigma F_{ls\to fs}\varepsilon_{ls}T_{ls}^4(t,\vartheta), \tag{1.11}$$

where A_{fs} represents the area of one radiator face, $F_{ls\to fs}$ the view factor from the lunar surface to the radiator face, ε_{ls} the lunar surface emissivity, and T_m the lunar surface temperature. Infrared radiation radiates any area in view of the lunar surface at any time of the lunar day, regardless of the sun's presence.

1.3.2 Solar Insolence

Solar insolence is the thermal radiation from the sun that radiates a surface. Fig. 1.8 is a simple graphic that depicts the suns trajectory over a shaded radiator at the lunar equator. During the lunar day the sun is overhead. Fig. 1.9 is another simple graphic that depicts the sun's trajectory over the lunar hot pole rather than the equator. At this latitude the sun is constantly encircling the pole from horizon.

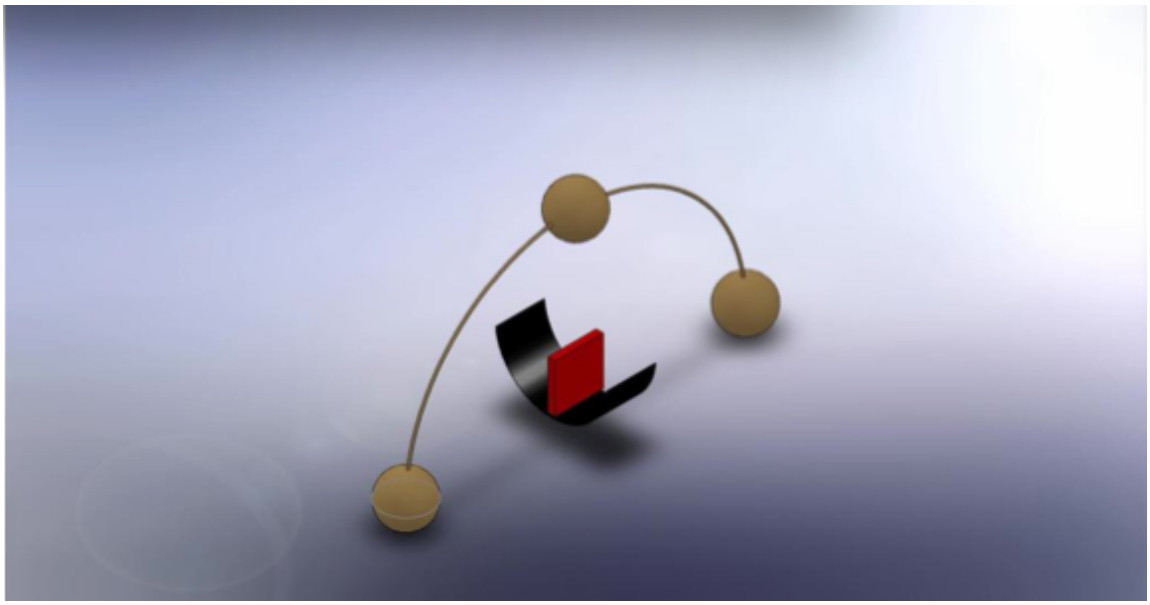

Fig. 1.8: Sun's trajectory over equator.

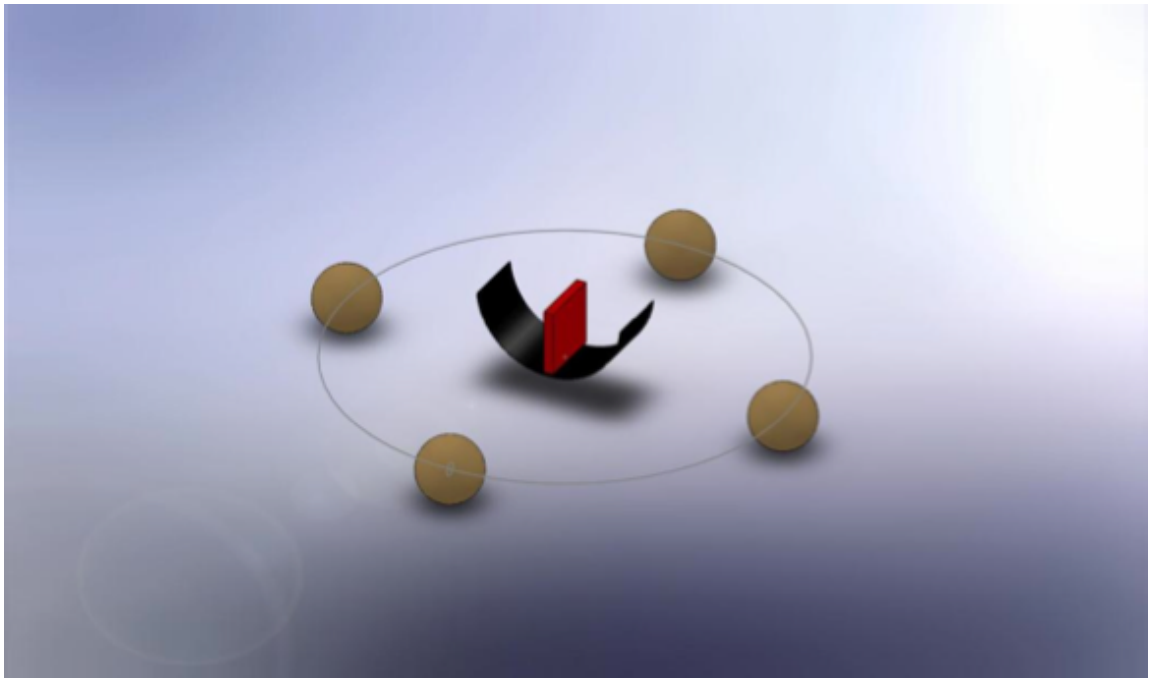

Fig. 1.9: Sun's trajectory over hot pole.

Mathematically, the solar insolence upon the radiator is represented by Eq. (1.12)

$$\dot{Q}_{fs,so} = A_{fs}\alpha_{fs}G_{so}\cos\left(\beta_{fs-so}\right), \tag{1.12}$$

where α_{fs} represents the radiator face surface absorptivity, G_{so} the solar heat flux at 1 AU (1370 W/m^2), and β_{fs-so} the angle between a unit vector normal to the radiator surface and a line connecting the radiator's latitude to the sun. Fig. 1.10 displays a simple graphic visualizing how the beta angle could be calculated for a vertical, two-sided radiator facing north and south. The moon's orbital plane is inclined 1.53° relative to the sun, and this is important in calculating that beta angle.

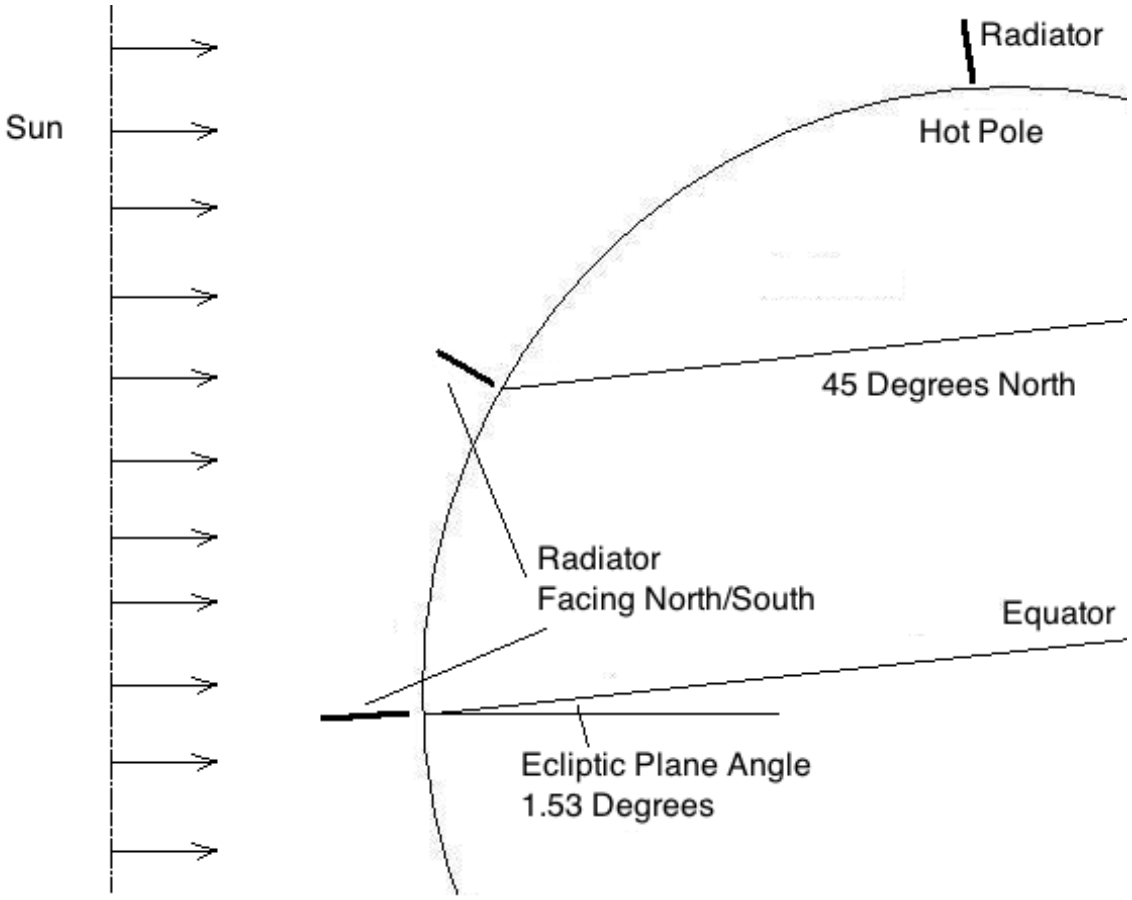

Fig. 1.10: Radiator latitudinal orientation.

1.3.3 Albedo

Albedo is thermal radiation reflected of a body; for this thesis, albedo refers only to the solar radiation that is reflected by lunar surface regolith. Albedo from the Earth is negligible on the lunar surface. The parasitic heat load may be mathematically represented by Eq. (1.13),

$$\dot{Q}_{fs,al} = A_{fs}\alpha_{fs}\rho_{ls}G_{so}F_{ls\rightarrow fs}, \tag{1.13}$$

where the only new term, ρ_{ls}, represents the lunar surface regolith reflectivity; this is the difference between regolith absorptivity and one. The view factor for this type of parasitic radiation is the same as the view factor for lunar surface-IR calculations. Discussing albedo helps characterize the lunar thermal environment but in actual design lunar albedo thermal load tend be very small compared to IR and solar loads.

Solar and albedo loads are only present when the sun is present in the lunar sky. A lunar day is comprised of 29 earth days; at the equator 14 days are in darkness with the other half in light. Polar latitudes experience 180 day stretches of sunlight or darkness.

1.3.4 Sink Temperature

If no net energy radiated from the radiator surface and the entire radiator surface is one uniform temperature then the heat rejected from the radiator is zero, as in Eq. (1.14),

$$\dot{Q}_R = A_{fs} \sum_{n=1}^{2} \varepsilon_{fs,n} \sigma \left(T_R^4 - T_S^4 \right) = 0 \tag{1.14}$$

and the radiator surface temperature would equal to a quantity known as sink temperature represented by T_S. Now consider the radiator's relationship with the lunar environment. Equation (1.14) and a summation of the parasitic radiations (Equation (1.11), (1.12), and (1.13)) may be equated, resulting in Eq. (1.15),

$$A_{fs} \left(\sum_{n=1}^{2} \varepsilon_{fs,n} \right) \sigma \left(T_R^4 - T_S^4 \right) = A_{fs} \left(\sum_{n=1}^{2} \varepsilon_{fs,n} \right) \sigma T_R^4 - A_{fs} q''_{ps}(C)$$

$$T_S = \sqrt[4]{\frac{q''_{ps}(C)}{\sigma \sum_{n=1}^{2} \varepsilon_{fs,n}}} \tag{1.15}$$

where the subscripts 1 and 2 represent two separate radiator sides. It is assumed that the radiator is isothermal as a whole. $q''_{ps}(C)$ represents the parasitic heat load per unit face sheet area. Following through substitution and rearrangement, one can find the expression

for the sink temperature for a radiator, vertical (Eq. (1.16)) or horizontal (Eq. (1.17)), such that the effective sink temperature, T_S, is calculated as

$$T_S(V) = \sqrt[4]{\frac{\alpha_1 \cos(\beta_{1-so})}{\sum_{n=1}^{2} \varepsilon_{fs,n}} \frac{G_s}{\sigma} + \frac{\sum_{n=1}^{2} F_{ls\to n}}{\sum_{n=1}^{2} \varepsilon_{fs,n}} \varepsilon_{ls} T_m^4 + \frac{\sum_{n=1}^{2} \alpha_{fs,n} F_{ls\to fs,n}}{\sum_{n=1}^{2} \varepsilon_{fs,n}} \rho_{ls} \frac{G_s}{\sigma}} \tag{1.16}$$

for the vertical configuration and as

$$T_S(H) = \sqrt[4]{\frac{\alpha_t \cos(\beta_{t-so})}{\sum_{n=1}^{2} \varepsilon_{fs,n}} \frac{G_s}{\sigma} + \frac{F_{ls\to b}}{\sum_{n=1}^{2} \varepsilon_{fs,n}} \left(\varepsilon_{ls} T_m^4 + \alpha_b \rho_{ls} \frac{G_s}{\sigma} \right)} \tag{1.17}$$

for the horizontal radiator configuration. Side 1 of the vertical radiator has been designated as the side which deals with solar insolence in this equation; this may change based on radiator alignment with the lunar lines of latitude, a concept that will be expanded upon in the next section. Both sides are equally radiated by the lunar surface. In Eq. (1.17) (for the horizontal radiator), subscripts t and b represent the radiator top and bottom respectively. The top deals with solar insolence while the bottom is irradiated by the lunar surface.

Table 1.2 displays the lunar surface properties[1] to be used in sink temperature calculations.

Table 1.2: Lunar environment properties.

Property		Value	Units
Regolith Temperatures	Equator Noon	384	Kelvin
	Equator Night	120	
	Hot Pole	220	
	Cold Pole	70	
Regolith	Absorptivity, α_{ls}	0.93	Unit-Less
	Emissivity, ε_{ls}	0.93	
	Reflectance, ρ_{ls}	0.07	
Inclination of the Lunar Equator Relative to the Sun		1.53	Degrees
Solar Thermal Flux		1370	W/m^2

1.3.5 Radiator Orientation

Radiator orientation is paramount to radiator operation; it can render a design completely useless if improperly considered. The two most common radiator configurations studied are horizontal and vertical with respect to the lunar surface. Both configurations have their benefits and drawbacks. Fig. 1.11 displays these configurations and the types of parasitic heat loads they will encounter at noon on the lunar equator. Table 1.3 provides the magnitude of the parasitic heat loads for several radiator configurations, with the configurations shown in the figures in bold text.[16] Every configuration has the same emissivity and solar absorptivity (0.9 and 0.23 respectively) for comparison and uses the lunar surface thermal model developed in Perez-Davis et al.[1]

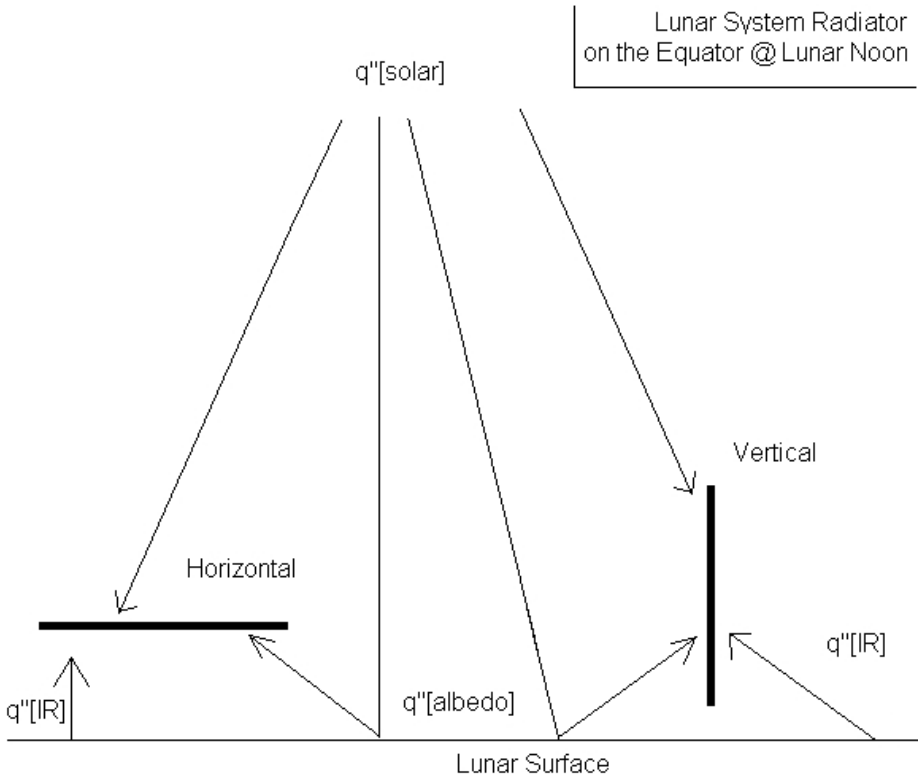

Fig. 1.11: Horizontal and vertical radiator orientations with specified worst-case parasitic heat loads at noon on the lunar equator. Adapted from Clark and Ewert.[16]

Table 1.3: Worst-case parasitic heat loads and sink temperatures for several radiator configurations.

Orientation	Lunar Latitude	Rotation Angle	Time of Lunar Day	Albedo	IR	Solar	Sink Temperature
				W/m^2			Kelvin
Horizontal	Equator	N/A	Noon	9.72	1220.97	325.10	351.38
	45°N		Noon	9.72	863.35	236.02	322.87
	Hot Pole		N/A	9.72	36.04	8.68	151.98
Vertical	Equator	0°	Late Morning	9.72	1220.43	313.95	350.72
		90°	Noon	9.72	1220.97	8.68	331.96
	45°N	0°	Late Morning	9.72	862.61	314.37	328.38
		90°	Noon	9.72	863.35	223.74	321.97
	Hot Pole	N/A	N/A	9.72	36.04	325.10	245.52

Horizontal radiator designs take direct solar loads throughout the day at any sub-polar latitude; the radiator would have to expand in size to accommodate these massive solar thermal loads. Horizontal radiators are mainly considered for polar missions because the configuration eliminates nearly all solar insolation. One drawback to the horizontal design is that it rejects waste energy using only the top side of the panel. The bottom side is insulated to prevent lunar surface irradiation. For this reason, horizontal radiators are seen as inefficient. Vertical radiators are perceived as more efficient due to their ability to utilize both sides of the panel, but this can be easily nullified if the radiator is improperly aligned with the lunar lines of latitude.

Vertical radiator alignment with lunar latitude line is a property which requires explanation. Fig. 1.12 serves to define the rotation angle, $\beta_{fs-\vartheta}$.

The radiator surface vector is simply a unit vector perpendicular to (pointing outwards from) one of the radiator's faces. With this in mind, the radiator rotation angle $\beta_{fs-\vartheta}$ can now be defined.

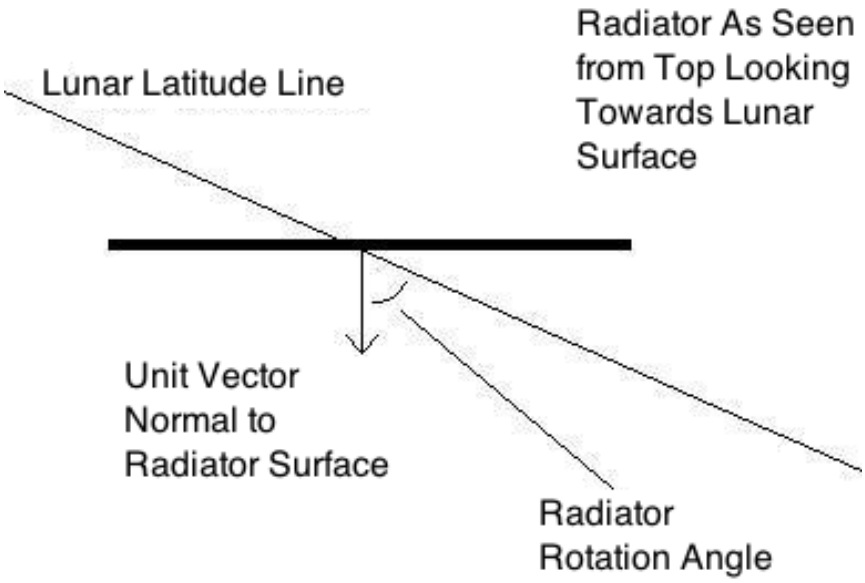

Fig. 1.12: Definition of radiator rotation angle $\beta_{fs-\vartheta}$.

The radiator rotation angle $\beta_{fs-\vartheta}$ is simply the angle between the radiator surface vector and the lines of latitude along the lunar surface. Now that this parameter has been defined, discussion of the vertical radiator and its relationship with the lunar thermal environment (as shown in Table 1.3) may continue.

At the lunar equator, if the vertical radiator is properly aligned (a 90° rotation angle with radiating surface facing north and south) the design can reduce solar insolation by as much as ninety six percent over the horizontal configuration. One side is constantly irradiated by the sun over the lunar day, but this value is very small and nearly zero when compared to the infrared load. If the radiator is rotated 90° such that it faces east and west (a 0° rotation angle with radiating surface facing east and west), this benefit is completely nullified. This configuration completely escapes solar insolation at noon when lunar surface temperatures are maximum, but late morning and early afternoon pose a problem.

However, infrared radiation emanated from the moon is the primary concern for the vertical radiator because its two large sides combined absorb the same amount of infrared radiation as the bottom side of the horizontal radiator. Many design studies and papers have

proposed solutions to mitigate this major problem; two solutions are shadow shielding and raising the radiator surface temperature.

As stated before radiative heat transfer is proportional to the difference in radiator and sink temperature to the fourth power. Unfortunately, the sun and the lunar surface both thermally load the radiator, as has been demonstrated, which hampers radiator performance. Fig. 1.13 displays a plot of waste heat rejected versus the ratio of the sink to radiator surface temperatures.

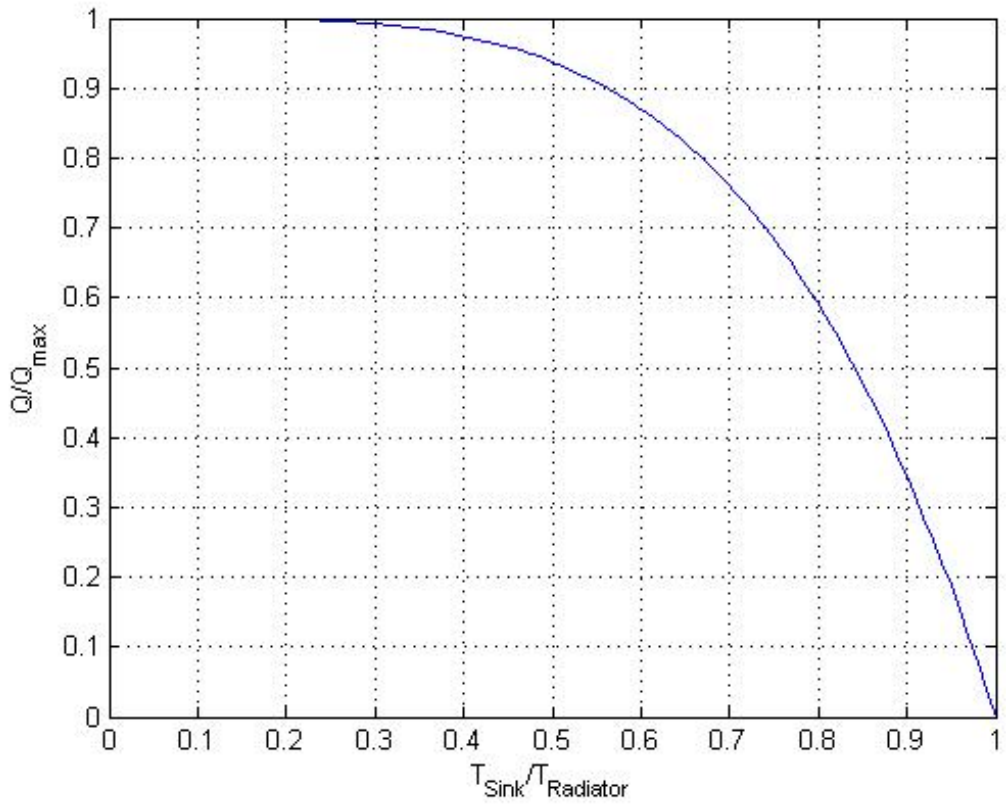

Fig. 1.13: Heat rejected from a radiator as a function of the ratio of sink temperature to the system heat rejection temperature.

In Fig. 1.13 a radiator rejects the greatest amount of energy when the ratio of sink temperature to radiator surface temperature is zero. This fraction can translate to a zero Kelvin sink temperature or a radiator surface temperature which dwarfs the sink temperature. Unfortunately a zero sink temperature is difficult to obtain on the moon (unless the radiator has a high surface temperature) due to parasitic radiations from the sun and the lunar surface. High radiator temperatures may not be an option for small-scale power systems, and the exotic materials required may not be readily available, easy to manufacture, or allow the smallest radiator mass. Shadow shielding is an effective method for reducing the radiator sink temperature; although it may increase configuration mass, shadow shielding would be much easier to implement than an exotic material and high radiator temperature.

1.4 Objectives

The overall goal of the proposed research is to evaluate the benefits shadow shielding offers for radiators in lunar nuclear reactor designs. This thesis will first present theory on radiative heat transfer, a heat pipe radiator mass model, the thermal lunar environment, advanced shadow shield geometry, the associated energy transfer, and the nuclear reactor as a heating source in a thermodynamic system that uses a radiator for rejecting waste energy. Then, this thesis will validate shadow shielding with shaded radiator models in Thermal Desktop.

The first round of simulations (using a solid, isothermal radiator) will find optimal radiator and shade geometry for each combination of six radiator temperatures at three lunar latitudes. Simulation variables include radiator shapes and shade attributes such as height and openness. The optimized shade geometry, a radiator heat pipe mass model, and the Safe Affordable Fission Engine nuclear reactor (designed to produce 400 kW of thermal power; acronym SAFE-400) will then be combined to compare to several radiator models from current lunar reactor designs.

2. MODELING APPROACH

Shadow shielding is a beneficial and useful technology for a low-temperature lunar system radiator. In order to build the case for shadow shielding, this thesis must first delve into shadow shielding theory.

2.1 Shadow Shielding Theory

The point of shadow shielding is to reduce parasitic heat loads on the radiator surface that originate from the lunar surface. Vertical radiators do not need shielding from solar insolation if the radiator is orientated correctly. Infrared and albedo radiations emanating from the lunar surface, however, are far more problematic. Shadow shielding for vertical radiators nominally blocks the view of the lunar surface, as seen in Fig. 2.1.[14]

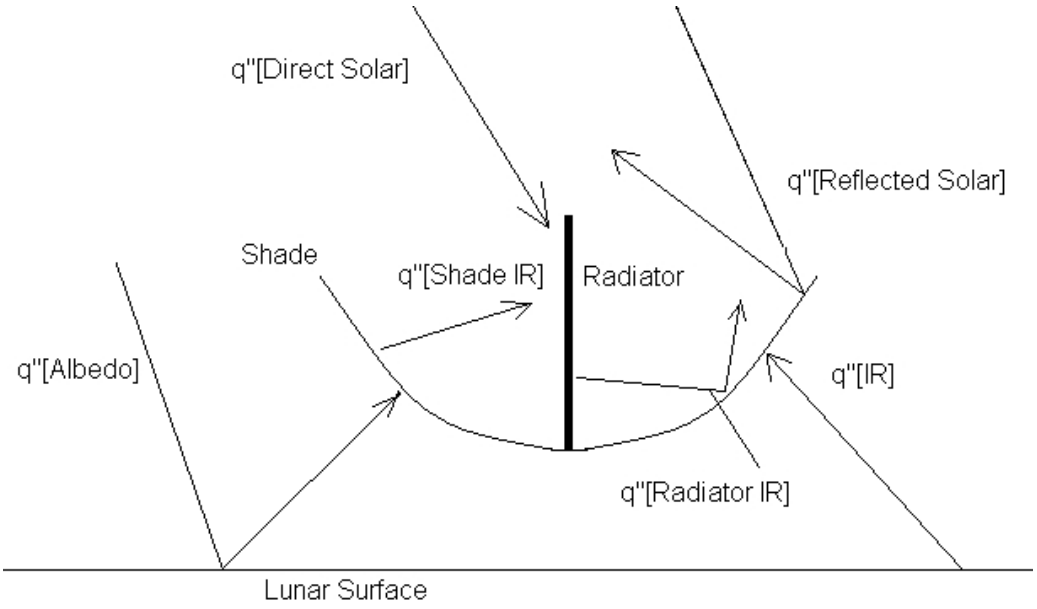

Fig. 2.1: Parasitic radiation loads experienced by a vertical radiator with shadow shielding.[14]

The figure is a side view of the radiator and shade. As shown, the radiator is a thin, dark item, and the shields are the parabolic, thin lines off the sides. It is important to note how this figure is different from the vertical radiator in Fig. 1.11. The radiator is not irradiated by the lunar surface; the bottom sides of the shades now absorb or reflect these loads. Albedo and IR formerly incident upon the radiator face are replaced by the infrared emission from the shade. Solar insolation incident upon the radiator has not changed, but now solar insolation also reflects off of the shade and collects at the shade focus.

The shade optical properties provide the opportunity to replace the regolith with something much less emissive, thereby mitigating the infrared parasitic heat load. This is a good demonstrative assumption but not entirely true. The shade blocks out most of the radiator's view of the lunar surface but not all. Fig. 2.2 is a graphic showing the lunar thermal landscape from a the face of a shielded vertical radiator.

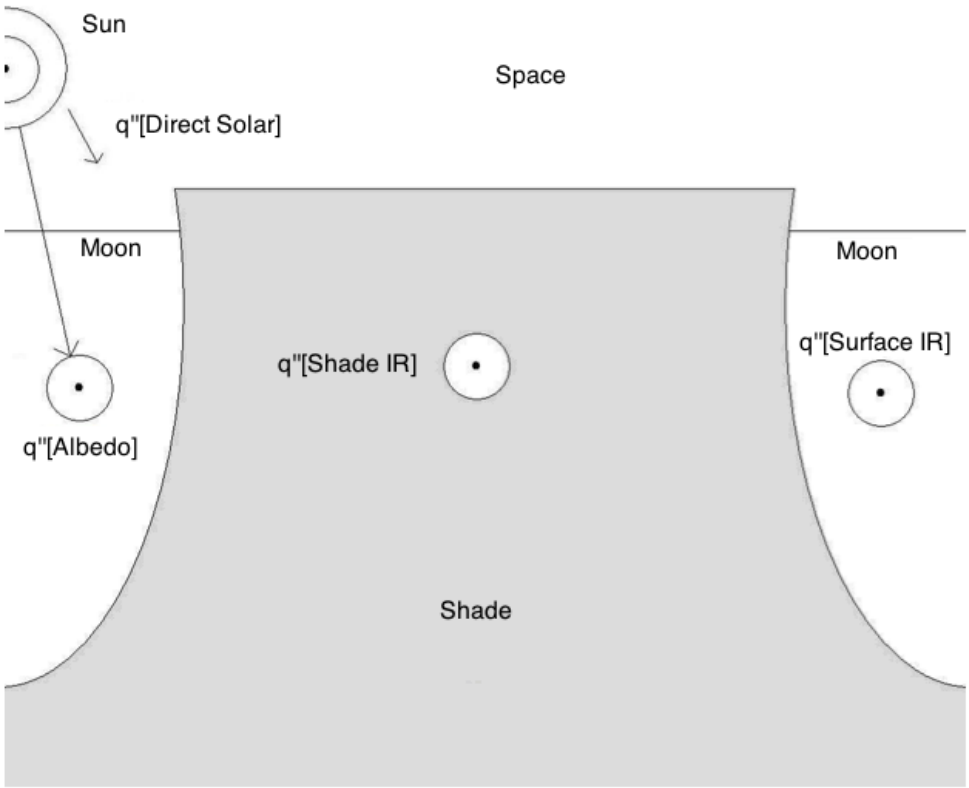

Fig. 2.2: View from shielded radiator surface including parasitic radiations.

The sides beyond the edge of the shade allow the lunar surface to still irradiate the radiator's face. One geometrical sidestep lies in the radiator area aspect ratio. Decreasing this ratio, which means increasing the radiator width and decreasing the radiator height, blocks out more of the radiator's view of the lunar surface.

Shade optical and geometric properties are the keys to shade usefulness. These parameters bear further discussion, beginning with shade geometric properties and continuing on to surface optical properties.

2.1.1 Geometric Properties

Shade geometry is paramount to shade operation. Barron et al.[13] found the optimal shade geometry to be parabolic in cross-sectional area with a focus slightly above the radiator top. For all designs, they kept the shade height the same as the radiator height. Their goal was to evaluate a myriad of different shadow shade geometries, and they found that the parabolic shade provided the greatest improvement in radiative heat rejection, but they did not optimize the geometry of their design. In this thesis, there are three areas of shade geometry that will be covered: shade focal length, shade height, and radiator area aspect ratio.

These three geometric parameters will be discussed further in the next few subsections. Each subsection offers at least a plot of shade mass and reduction in the radiator's view of the lunar surface versus the shade geometric property described as quantitative predictions of the models that will be completed in analysis. A view factor is the ratio of energy emitted by a surface directly toward and intercepted by another surface to the total energy emitted by the former surface. View factors between two surfaces are calculated by a double contour integral around the surface boundaries, as in Eq. (2.1),

$$F_{1\to 2} = \frac{1}{2\pi A_1} \oint_{\Gamma_1} \oint_{\Gamma_2} \ln\left(L_{1-2}\right) d\vec{l}_2 \cdot d\vec{l}_1, \tag{2.1}$$

where $F_{1\to2}$ represents the view factor from surface 1 to surface 2, A_1 the area of surface 1, Γ each surface's boundary, L the line connecting the surfaces, and $\vec{l}$ the position vector for points along the contour of its respective surface.[8]

A fundamental assumption of the view factor reduction calculations is that a shade half as high as the radiator blocks out the maximum amount of the radiator's view of the lunar surface; a taller shade does not further alter the radiator's view of the lunar surface, but instead begins to interfere with the radiator's view of space. This assumption mathematically derives from quantifying the view factor of an unshaded radiator; from Modest,[8] space and the lunar surface each occupy half of a flat, vertical surface's view. However, this assumption is crude and very simple.

Additionally, the control radiator and shade configuration is comprised of a one meter wide by one meter tall radiator; the control-sized shade is the same height as the radiator and maintains a focus ten centimeters above the radiator top. For all charts, all radiator faces are one meter square in area. The charts serve as predictions of mass and heat transfer curves in the results section.

2.1.1.1 Shade Height

Shade height is an important shade geometric parameter. This parameter directly controls shade mass and how much of the lunar surface a radiator face sees. Fig. 2.3 is a plot of the reduction in the radiator's view of the lunar surface and shade mass as a function of shade height. Shade mass has been assumed to be 10 kg/m^2.

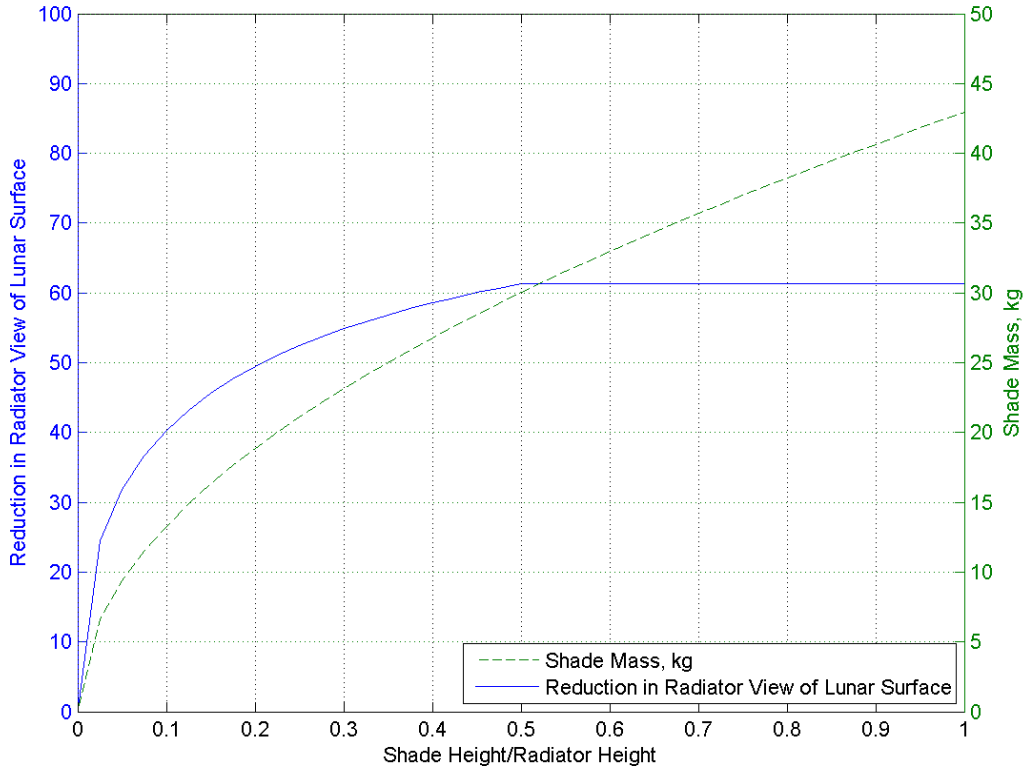

Fig. 2.3: Plot of shade mass and reduction in the radiator's view of the lunar surface versus shade height with shade focus 10 cm above radiator top and radiator area aspect 1.

The radiator in question is square in shape (one meter per side) and the shade has a focus ten centimeters above the radiator top. The shade height was varied from no shade to full shade in 1% radiator height steps for these calculations. The fundamental assumption, that the half radiator height shade blocks out the most of the radiator's view of the lunar surface, explains the flattening of the view factor reduction curve in the right half of the plot. Shade mass, naturally, rises with increasing shade height. The shade mass and the left half of the view factor reduction curves both resemble square root functions which is tied back to the nature of the parabolic shade geometry.

2.1.1.2 Radiator Area Aspect Ratio

Radiator area aspect ratio also plays a role in shade effectiveness, the underlying assumption being that the shade is as wide as the radiator. The radiator area aspect ratio a_{ra} is defined as the ratio of the radiator height to the radiator width. Fig. 2.4 is a plot of the reduction in the radiator's view of the lunar surface and shade mass as functions of this aspect ratio.

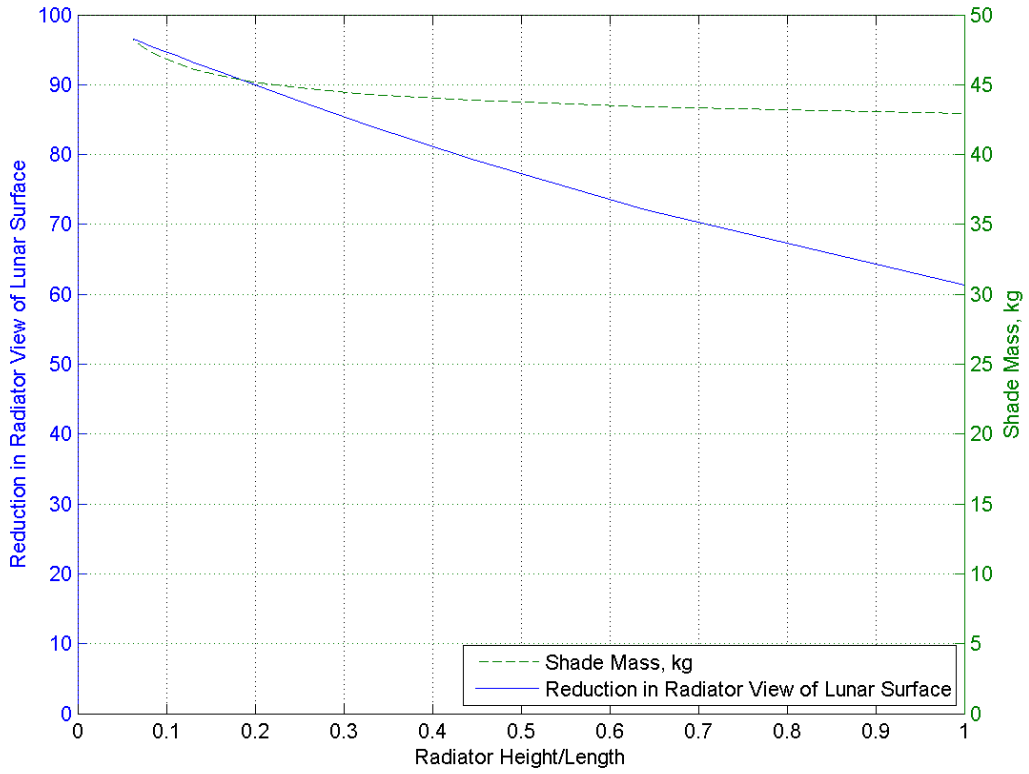

Fig. 2.4: Plot of shade mass and reduction in the radiator's view of the lunar surface versus radiator area aspect ratio with full shade and focus 10 cm above radiator top.

The radiator in question is rectangular in shape but maintains a one meter squared per side surface area; the shade has a focus ten centimeters above the radiator top and is the same height as the radiator. From left to right on the curve, radiator and shade height increase and the width decreases. The radiator's view of the lunar surface also increases with rising radiator area aspect ratio but shade mass decreases. This suggests that a short but wide radiator may be preferable as far as heat transfer is concerned, that the wider and shorter the radiator, the greater the shield's effect.

Dividing the radiator-lunar surface view factor reduction by the shade mass provides a curve which displays an obvious maximum, as in Fig. 2.5.

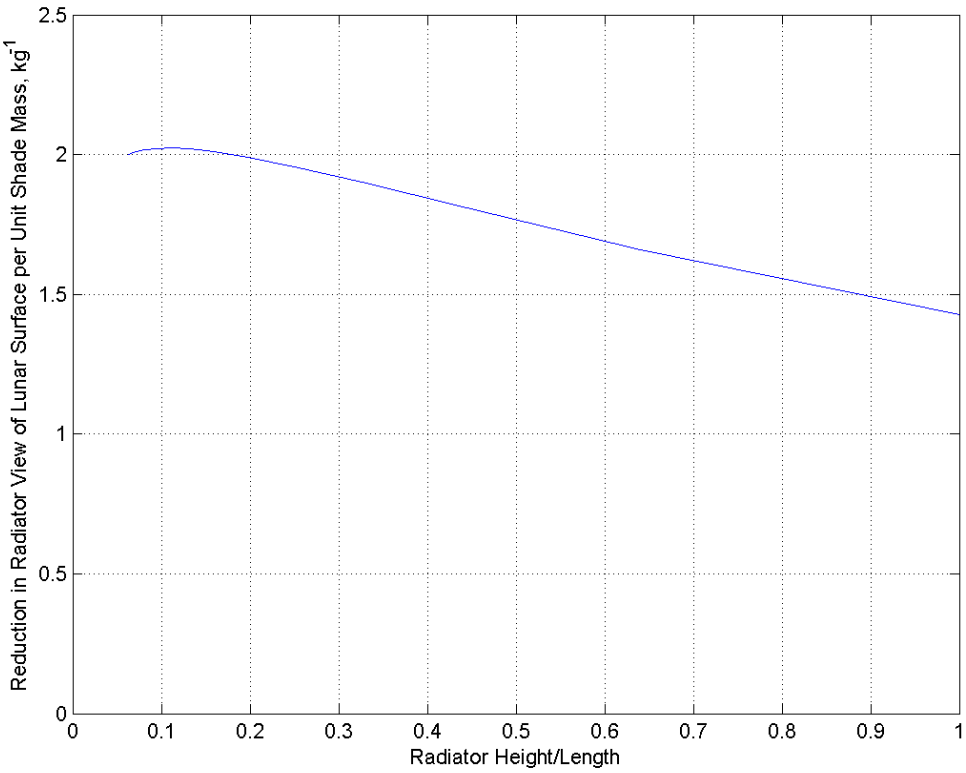

Fig. 2.5: Plot of specific reduction in the radiator's view of the lunar surface versus radiator area aspect ratio with full shade and focus 10 cm above radiator top.

The greatest radiator-lunar surface view factor reduction for the least shade mass occurs at a radiator area ratio of 0.0625, meaning the radiator should be sixteen times longer than it is tall.

2.1.1.3 Shade Focal Length

Shade focal length is one important geometric quantity for shade optimization. It is a parameter intertwined with both shade mass and optical properties. In theory, if the shade is highly specular, thermal radiation incident upon the shield's radiator-facing surface will reflect and collect at the focus; therefore the focus should be above the radiator. However, there are repercussions to raising this parameter. A longer focal length means the shade will extend out further to maintain a specific height. This also corresponds with a rise in shade mass. Radiator thermal performance must be balanced with shade mass in this respect.

2.1.2 Optical Properties

Shade optical properties are also key to shade operation. The shade is meant to block the radiator's view of the lunar surface, which has optical properties very close to a black body. The regolith absorbs and emits nearly all thermal radiation incident upon it due to very high absorptivity and emissivity. The shade represents a chance to replace regolith with a less emissive surface. To that end, the shade side facing the radiator should have very low emissivity, as detailed in several design studies. However, the shade does absorb energy from the radiator and the lunar environment. To cut down further on shade infrared emissions, the shade side facing the lunar surface should provide the shade the opportunity to cool itself.

To make use of the parabolic shape the shade surface facing the radiator should specularly reflect as much incident as possible. Surface specularity refers the manner in which thermal radiation reflects off a surface. Fig. 2.6 displays this concept. The diffusely reflect-

ing surface reflects incident thermal radiation back in all directions. The highly specular surface reflects incident thermal radiation back at the same angle in which it struck the surface.[8]

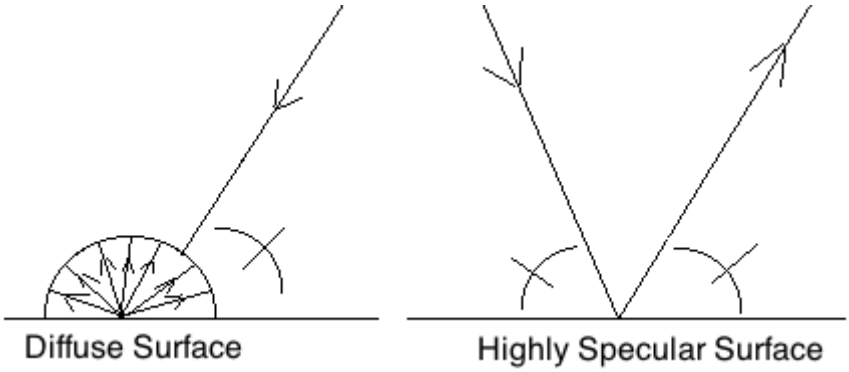

Fig. 2.6: Diffuse and specular reflecting surfaces.

2.2 Radiator Mass Model

Real radiators are not just metal slabs; modern radiators are comprised of four components: heat pipes, face sheets, adhesive, and filler, as illustrated in Fig. 2.7.

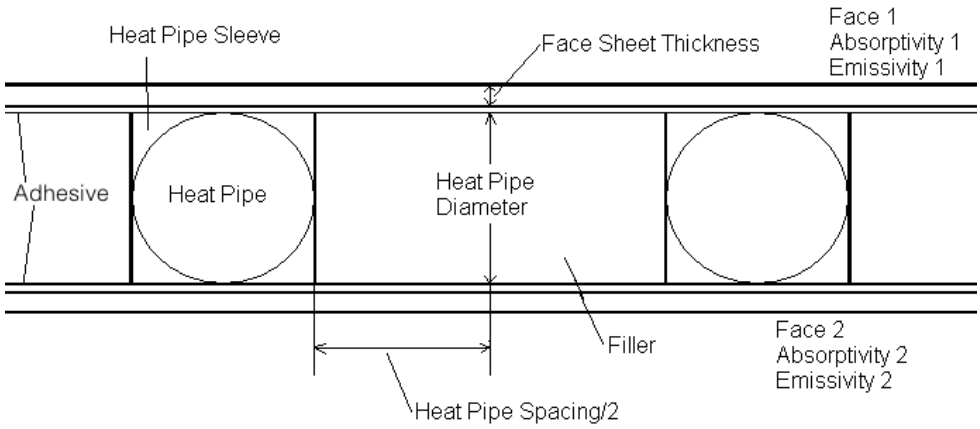

Fig. 2.7: Radiator cross-section.

The face sheets and adhesive hold the radiator together. The face sheet has an associated thickness, which effects thermal conductivity as well as mass. The two must be balanced. Adhesive is supposed to be spread evenly and thinly across the inward-facing side of the face sheets. Filler is supposed to be very light (lighter than the heat pipes) and provides the radiator with structure.

Heat pipes are the primary mechanism for transporting energy from the system to the radiator. They are devices that combine thermal conductivity and phase transition to efficiently transfer energy from one end to the other. In order to produce a true isothermal surface temperature, a radiator would need heat pipes closely spaced with a thick face sheet thus resulting in minimum temperature gradients between heat pipes. This produces an efficient but heavy radiator. The minimum radiator mass typically does not occur near efficiency values of 100%. A balance between radiator thermal performance and fin efficiency is achieved by spacing the heat pipes or coolant lines and varying the thickness of the face sheet. The loss of efficiency due to a face sheet temperature gradient is offset by a reduction in mass of the entire radiator due either to less piping, decreased face sheet thickness, or a combination of the two. An important aspect is that different materials will have different optimization points e.g. an aluminum face sheet radiator will have different spacing and thickness than a stainless-steel face sheet radiator and comparing similar geometries may be misleading.

To ensure a radiator of minimum mass, a model must incorporate coolant tubes and study the spacing of those pipes along with the face sheet thickness. The smallest radiator could be achieved if one were to use close pipe spacing for maximum fin efficiency. However, such a radiator would be very heavy due to the high number of pipes. Mass, as stated before, is a critical driver for space system development; therefore a lighter but less efficient radiator is preferred.

For any radiator, the optimum balance of heat-pipe spacing and fin thickness should found to minimize the total radiator mass. The generic heat equation for a fin radiating to an effective thermal sink is Eq. (2.2),

$$\frac{d^2T}{dx^2} - \frac{(t_B - t_T)}{Lt_T + (t_B - t_T)(L-x)}\frac{dT}{dx} - \frac{\sigma\left(\sum_{n=1}^{2}\frac{\varepsilon_n}{\cos\beta_n}\right)L}{2k\left[Lt_T + (t_B - t_T)(L-x)\right]}\left(T^4 - T_S^4\right) = 0 \qquad (2.2)$$

with appropriate boundary conditions Eq. (2.3)

$$T|_{x=0} = T_R \qquad (2.3a)$$

$$\left.\frac{dT}{dx}\right|_{x=L} = 0 \qquad (2.3b)$$

Equations (2.2) and (2.3) represent a generalized Fig. 2.7. Parameters ε_1 and ε_2 are the emissivities of radiator sides 1 and 2, L the heat pipe spacing divided by two, t_B the thickness at the heat pipe, and t_T the thickness at the middle between the heat pipes. The parameter k represents the radiator material thermal conductivity; this property, as well as the emissivities, are functions of the base heat pipe temperature, but this will be ignored for analysis. The beta angles (β_1 and β_2) represent the angles between the face sheet and a plane resting on either side of the heat pipes, as shown in Fig. 2.8.

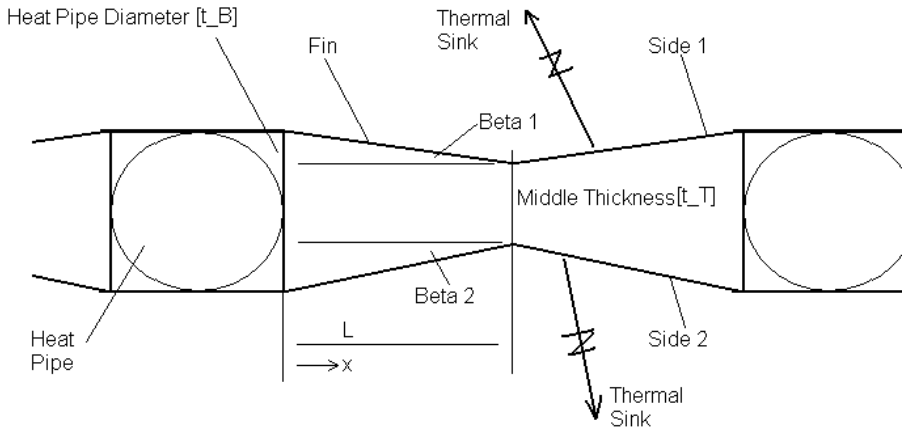

Fig. 2.8: Radiator cross-section with beta angles indicated.

A numerical expression was derived to calculate the radiator fin efficiency, η_F. This parameter accounts for the thermal effects of the sink temperature, radiative heat transfer from both sides, and the heat transfer characteristics of the radiator as a fin.[5] Equation (2.4) assumes a fin of uniform thickness, with

$$\eta_F = \left(1-\theta_S^4\right)\cdot \begin{cases} 1-1.25\zeta+1.60\zeta^2 & \text{if } 0.01 \le \zeta \le 0.2 \\ 0.532-0.405\log\zeta & \text{if } 0.2 \le \zeta \le 2.0 \end{cases} \tag{2.4}$$

and parameter ζ is defined as Eq. (2.5)

$$\zeta = \frac{\sigma L^2}{k t_B} T_R^3 \sum_{n=1}^{2} \varepsilon_n. \tag{2.5}$$

Parameter θ_S was defined previously. L the heat-pipe spacing divided by two, T_R the heat pipe base temperature, T_S the effective sink temperature, and t the radiator face sheet thickness.

Once the fin effectiveness has been calculated, the heat rejected from the radiator can be expressed as Eq. (2.6)

$$\dot{Q}_{ra} = A_{fs} \sum_{n=1}^{2} \varepsilon_n \eta_F \sigma T_R^4 \tag{2.6}$$

where the sink temperature term and radiator fin heat transfer characteristics have been absorbed by the fin efficiency. For a given required heat rejection rate, one may easily find the required face sheet area. Naturally, many heat pipe spacings and face sheet thickness must be tested to find the right sizes that correspond with the lowest radiator mass, which is an optimization process.

The mass of the radiator as a whole is Eq. (2.7)

$$m_{ra} = 2m_{fs} + m_{fi} + m_{hp} + m_{ad} \tag{2.7}$$

where subscript fs represents the face sheet, fi filler between the heat pipes and face sheets, hp heat pipes, and ad the adhesive binding face sheets to the heat pipes and filler.

Adhesive mass is the product of the face sheet area and the adhesive density. Before calculating the filler and heat pipe masses one must figure out how the radiator, as a rectangle, is orientated and how many heat pipes the design requires.

The number of heat pipes, n_{hp}, is expressed in Eq. (2.8)

$$n_{hp} = \text{floor}\left(\frac{L_o}{L_{hp}}\right) - 1 \tag{2.8}$$

where L_o is the length of radiator side from which the heat pipes emanate. The other radiator side is labeled as L_{hp}. If the radiator side aspect ratio is one then L_{hp} and L_o are equivalent.

Once L_{hp} and L_o have been found, heat pipe and filler masses are easy to calculate. Heat pipe mass is the product of the heat pipe linear density, the number of heat pipes, and the heat pipe running length, L_{hp}. The linear density also includes the heat pipe sleeve. Filler mass is the product of the filler density, the filler thickness (assumed to be the heat pipe diameter), and the cross-sectional filler area along radiator side o. The area is the difference between the cross-sectional radiator area along side o and the area occupied by the heat pipes as in Eq. (2.9)

$$m_{fi} = \rho_{fi} L_{hp}\left(L_o D_{hp} - n_{hp} D_{hp}^2\right) \tag{2.9}$$

Note that the heat pipe area is treated like a square due to the extrusion.

The mass densities for each radiator component and operation material are displayed in Table 2.1. To obtain the density for when the components are not made of aluminum, one must multiply said density by a fraction of the new material density to that of aluminum.

Table 2.1: Mass densities of radiator components.

Component	Density				Units
	Aluminum	Titanium	Stainless Steel	Molybdenum	
Heat Pipe	0.3715	0.6192	1.1007	1.4145	kg/m
Honeycomb Filler	33.69	56.15	99.82	128.27	kg/m^2
Adhesive	0.1463	0.2438	0.4335	0.5570	
Face Sheet	2700	4500	8000	10280	kg/m^3

The first part of testing determines the optimal radiator face sheet thickness and heat pipe spacing given the operational environment, reactor operation temperature, and heat pipe temperature. Fig. 2.9 plots the specific mass versus specific area for a radiator with a 400 K nominal operating temperature. The chart is a plot of specific mass and area for several face sheet thicknesses and heat pipe spacings and two sink temperature ratios. The zero sink temperature ratio represents a radiator that is in deep space and the 0.83 sink temperature ratio represents a bare, vertical radiator at noon on the lunar equator rotated such that it faces north and south. The important point to note for each set of curves is the minimum specific mass; at this point the radiator area mass (found by dividing the specific mass by the specific area) will be at minimum, providing the heat pipe spacing and face sheet thickness that correspond with the lowest radiator mass. Several trends are obvious. For one, the smallest face sheet thickness provides the lowest radiator mass. This is the product of a simplification of face sheet and filler thermal conductivities. A higher sink temperature fraction requires more radiator mass. The closest heat pipe spacing makes for a very high radiator specific mass but also the lowest specific area; as this parameter grows, the specific mass falls but begins to grow again after a clear minimum region.

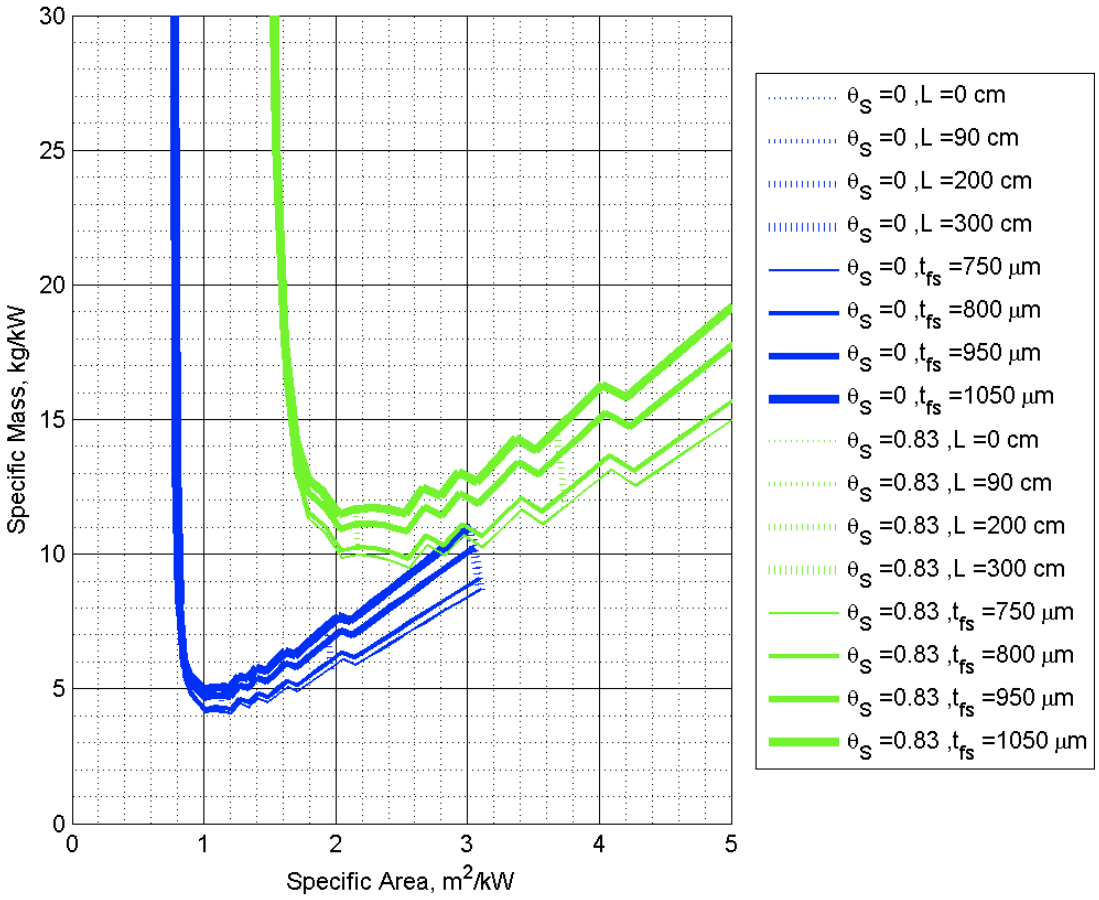

Fig. 2.9: Specific mass versus specific area for a 400 K radiator.

What can be taken from this graphic is the effect of the sink temperature on radiator mass; lowering the sink temperature allows the radiator to shrink in size and mass, as claimed previously. The point of shadow shielding is to reduce this effective sink temperature, but the shade is certainly a mass driver.

2.3 The Reactor

Thermal power output from a nuclear reactor $\dot{Q}_H$, as described in Eq. (2.10)

$$\dot{Q}_H = V_f E_f \Sigma_f \phi, \tag{2.10}$$

is proportional to the reactor fuel volume V_f, the energy released per fission E_f, the macroscopic fuel fission cross-section Σ_f, and the neutron scalar flux ϕ. E_f is dependent on the type of fuel and Σ_f is dependent both on fuel type and reactor design.[17]

From a coolant standpoint, this relationship can also be modeled as Eq. (2.11)

$$\dot{Q}_H = \dot{m} c_p (T_H - T_C), \tag{2.11}$$

where $\dot{m}$ is the coolant mass flow rate, c_p the coolant heat capacity (assumed to be constant with temperature), and T the coolant temperature. The subscripts for the temperatures indicate either the temperatures at the reactor outlet (subscript H) at the reactor inlet (subscript C). The equation is only valid if the coolant does not change phases during the heating process and remains close to isobaric; otherwise specific enthalpy (h) must be used, such as Eq. (2.12),

$$\dot{Q}_H = \dot{m} (h_H - h_C). \tag{2.12}$$

Therefore,

$$\dot{Q}_H = V_f E_f \Sigma_f \phi = \dot{m} (h_H - h_C). \tag{2.13}$$

This expression must be altered if one desires to model the reactor thermodynamic system based on the Carnot cycle. Equation (2.11) can be reformatted to Eq. (2.14)

$$\dot{Q}_H = \dot{m} \langle T_H \rangle (s_H - s_C), \tag{2.14}$$

where $\langle T_H \rangle$ represents the average core heating temperature and s the working fluid entropy. A caveat here is that nuclear reactors maintain constant heating rates rather than

temperatures; therefore an average heating temperature must be used. The average heating temperature is defined as Eq. (2.15)

$$\langle T_H \rangle = \frac{1}{(s_H - s_C)} \int_{q_H} T ds, \tag{2.15}$$

where s represents the working fluid entropy and q_H the specific heating rate. Δs represents the change in the coolant fluid entropy between the reactor inlet and outlet and is identical to the change in entropy in Eq. (2.14). The use of lower-case refers to specific quantities with respect to mass. If one sets temperature to be the derivative of energy with respect to entropy, Eq. (2.15) simplifies to Eq. (2.16)

$$\langle T_H \rangle = \frac{1}{\Delta s} \int_{q_H} \frac{de}{ds} ds = \frac{q_H}{\Delta s}. \tag{2.16}$$

Reactor mass is linearly related to reactor volume, given reactor density. Fuel mass can be represented as Eq. (2.17)

$$m_f = \rho_f \frac{\dot{Q}_H}{E_f \Sigma_f \phi}. \tag{2.17}$$

Combining Eq. (2.11) and Eq. (2.17) one gets Eq. (2.18)

$$m_f(T_H) = \frac{\rho_f \dot{m}(s_H - s_C)}{\dot{q}} \langle T_H \rangle \tag{2.18}$$

and one can see that the fuel mass is a linear function of the average heating temperature. This implies that the masses of other parts of the core (coolant, cladding, and structure) should also be functions of the average heating temperature.

2.3.1 The SAFE-400 Design

This thesis chose the SAFE-400[1] space fast spectrum fission reactor design for system analysis. The reactor has been designed to constantly deliver 400 kW, thermal. The core is hexagonal in shape with a flat-to-flat size of 26 cm and a radial beryllium reflector 48

cm in diameter. The core is 58 cm in height, 50 cm of which is fueled; the heat pipes extend an additional 50 cm above the core to couple with the heat exchanger. For reactor control, there are six identical drums 12 cm in diameter on the sides of the core; each circular drum is made of beryllium (a neutron reflector) with a 120° boron carbide neutron absorber on one side. This side can be rotated to control the reactor because the B_4C is a neutron poison, and prevents criticality when facing towards the core. Axial cross-sections of the core are presented in Fig. 2.10; Fig. 2.10a is a close-up of the core configuration and Fig. 2.10b is a picture of the entire core with the B_4C control drums rotated facing out from the core (a control drum rotation of 180°).

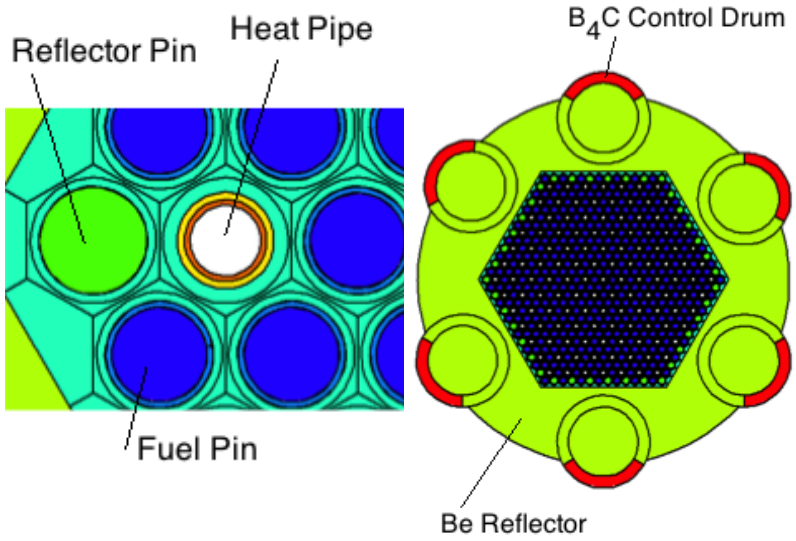

(a) Core configuration close-up (b) Control drums at 180°.

Fig. 2.10: Axial cross-section of the SAFE-400 core.[1,18]

The core is comprised of 127 identical modules arranged in a hexagonal shape. Each module is centered on one heat pipe surrounded by three fuel pins held together by a molybdenum tricusp, shown in Fig. 2.11. Fuel pins are comprised of the fuel (8.36 mm

outer diameter) at the center, rhenium cladding (0.51 mm thickness), and a helium-filled gap in between the other components. For analysis, the fuel and clad gap will be ignored because of its tiny size, thickness 0.025 mm, relative to fuel and cladding. The heat pipe at the center of a module is clad in molybdenum as well, and uses pure, two-phase sodium as the working fluid. The fuel material itself is uranium nitride, 97% enriched in fissile isotope uranium-235.

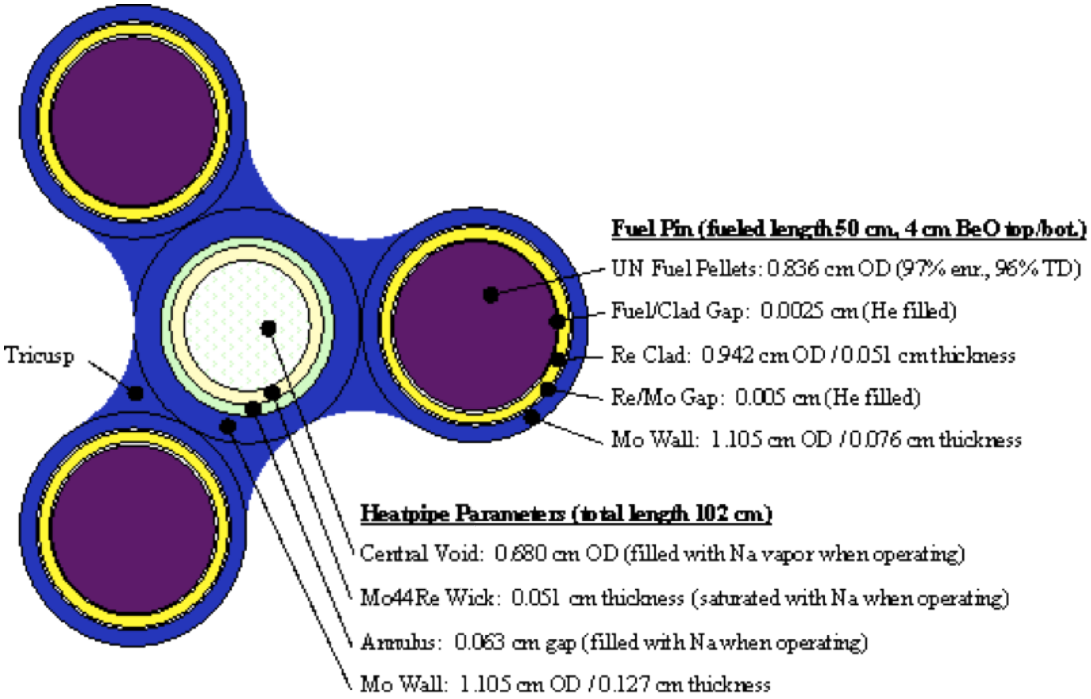

Fig. 2.11: SAFE-400 module.[1, 18]

For analysis, the molybdenum and rhenium materials (comprising heat pipes, fuel cladding, and fuel walls) from the original design will be replaced with materials that correspond with the reactor outlet temperature. This is a simplifying assumption; further, detailed analysis would be required for a realistic design.

2.4 System Thermodynamics and Mass

Low rejection temperatures allow for better thermodynamic efficiency but radiators emit greater amounts of energy with higher surface temperature. These conflicting constraints formulate radiator configurations that will reject enough waste heat without impairing work output. Fig. 2.12 displays the contrast by plotting unit-less system work and rejection energies versus the ratio of system heat rejection temperature to heating temperature. The maximum on the electrical power curve occurs when the radiator rejection temperature T_C is 75% of the cycle heating temperature T_H, producing a 25% cycle efficiency, while the rejected power has a maximum where T_C is equal to T_H. The underlying equations behind Fig. 2.12 assume the radiator emits its heat to a thermal sink with zero temperature, but, as seen before, this is not an option for a radiator in operation on the moon.

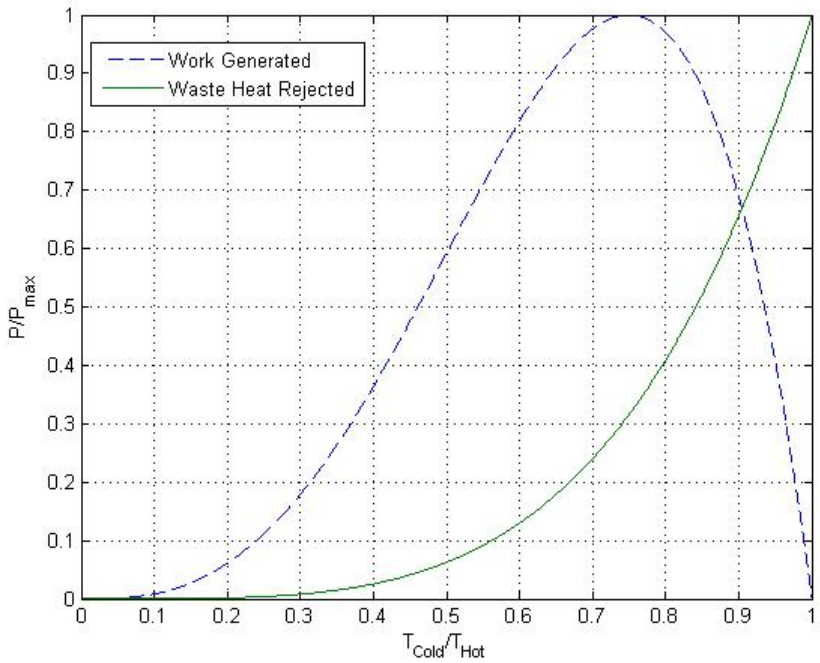

Fig. 2.12: Rejected power and shaft work generated versus the ratio of cold to hot temperature. Ideal Carnot cycle using radiative heat transfer for heat rejection.[4]

The two curves represent the shaft work produced by the cycle and energy rejected from a radiator with a zero Kelvin sink temperature. Naturally, a higher sink temperature would reduce radiative heat transfer from the radiator and require an increase in radiator mass and size. The shade is meant to lower the effective sink temperature at the expense of mass.

The previous sections have derived reactor and radiator masses and system efficiencies as functions of the reactor outlet temperature, radiator temperature, and the sink temperature of the lunar environment. System mass is composed of the reactor, radiator (heat rejection), power conversion system, pump, shielding, and the coolant masses, as in Eq. (2.19),

$$m_{Sys} \approx m_{ra} + m_{rx} + m_{pc} + m_p + m_{rxsh} + m_{co} \ , \tag{2.19}$$

where m_{ra} is the radiator mass, m_{rx} the reactor mass, m_{pc} the power conversion system mass, m_p the pump, m_{rxsh} reactor shielding mass, and m_{co} the coolant mass.

In order to evaluate the sensitivity between system mass and changes in the lunar thermal environment, one must make a few assumptions and examine the individual properties and figures of merit that comprise radiator and reactor masses to find an appropriate balance between mass and performance. To this end, this paper will consider only the effect reactor outlet and radiator temperatures have on the size and mass of the radiator and the reactor core fuel and cladding.

3. METHODS

Validating shadow shielding requires quantifying its effects on radiator performance. One must model a radiator and shadow shielding in a program which can perform the complex heat transfer calculations required. This thesis chose to use the CAD program Thermal Desktop to do so, with Matlab to aid in analysis. This thesis began analysis by adopting control radiator and shade geometry and then applied optima gathered from those tests towards a more realistic, heat-pipe based design. Thermal Desktop must be understood before progression into plotting and analysis. This chapter will then discuss plotting programs and calculations performed. Then the radiator models will be discussed.

3.1 Thermal Desktop

Thermal Desktop is an AutoCAD add-on that performs numerical heat transfer calculations, including energy transfer rates, thermal capacitance, and temperatures, to generate thermal models of electronics and vehicles. Thermal Desktop has thermal analysis-specific types of capabilities such as applying contact conductance, insulation, heat loads, and heaters.[19]

The Thermal Desktop environment develops a capacitance and conductance network for input to computational codes SINDA, FLUINT, and RadCAD. SINDA completes finite-difference, lumped parameter calculations for heat transfer design analysis and FLUINT completes fluid flow analysis.[19]

SINDA and FLUINT provide conduction and convection calculations, but this thesis primarily concerns radiative heat transfer on the lunar surface. RadCAD expands the capabilities of Thermal Desktop to include radiative models of spacecraft orbit. The module uses a deterministic Monte Carlo ray tracing technique to calculate view factors, radiation conductors, and heating rates for surface for input into SINDA/FLUINT.[19]

A full Thermal Desktop model must include at least one node to act as a boundary temperature or heat load. One can then set up an orbit through the Orbit Manager. Many

kinds of orbits can be simulated, but the specific type this problem calls for is the geographic latitude, longitude, and altitude type orbit. This type of orbit was chosen because it can simulate static landing craft and surface conditions. Other types of orbit are better suited to simulating orbiting spacecraft like satellites.

Setting up the orbit requires specifying the body the model will orbit and the path the model will take. Vehicle positions for a series of time values are entered using planet-centered values for latitude, longitude, and altitude. The altitude is measured from the surface of a perfect sphere using the planet's radius; a three meter altitude will be used for all orbits in all models. As discussed before, most radiators designed for lunar nuclear-powered systems sit directly above the reactor; additionally, keeping radiator from touch the surface eliminates potential contact problems.

The list of times tells Thermal Desktop when to calculate heat transfer. For this thesis, the radiator in every Thermal Desktop run will start at noon and endure an entire day and night cycle, ending at noon on the following lunar day at time 29.5 Earth-days. Test points occur every 2.5 days, or every 30°.

Latitude is positive to the East and negative to the West. The z-axis has been designated as pointing outward from the lunar surface. Nominally the x-axis points to the east and the y-axis to the north, as in Fig. 3.1. The large red arrow points in the direction which the model in Thermal Desktop moves around the body. The separate x-y-z coordinates indicate the specific points where Thermal Desktop performs heat transfer calculations.

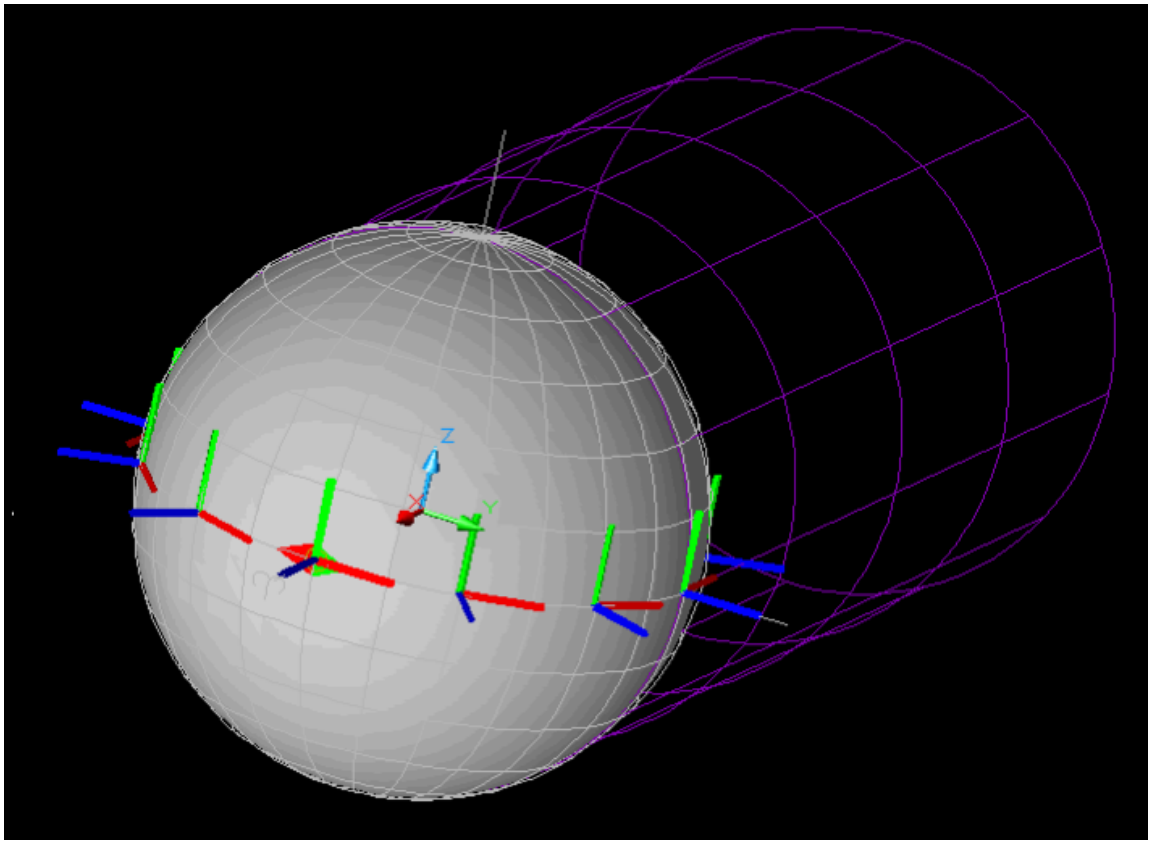

Fig. 3.1: Equatorial orbit modeled in Thermal Desktop.

The radiator is supposed to remain static for each and every test so longitude and latitude need to remain at the same value; otherwise Thermal Desktop models the orbiting object as though it is moving. The z-axis may also be rotated; this ability was made use of for the rotation angle $\beta_{fs-\vartheta}$ tests. Test types will be discussed after the next section; the next section discusses how supplementary Matlab programs handle, compile,and plot data from Thermal Desktop

3.2 Plotting and Calculations

Plotting and analysis programs may be found in Appendix D. Thermal Desktop outputs a text file containing a node summary on RadCAD and SINDA/FLUINT calculations performed, providing node capacitance, temperature, and energy transfer. For plots the graphing program selects and saves the appropriate heat transfer data which is the heat conducted from either core node (for the control tests) or the heat pipe nodes (optimum tests).

The program finds the minimum waste heat rejected from the radiator over the lunar day to make the graphs of heat rejected per unit system mass versus varied parameters. This is an effort to be conservative.

3.3 Models

Several models were developed and tested inThermal Desktop. First, a control model, consisting of a solid radiator was developed and tested. Once the optimum shade parameters were determined, they were fed into another Thermal Desktop desktop model that accounts for heat pipes.

3.3.1 Initial Control

The initial control model consisted of a thin metal plate that orbits the moon constructed in Thermal Desktop. A total of six temperatures (from 200 Kelvin to 600 Kelvin in 100 Kelvin increments) and three latitudes (Equator, 45°N, and hot pole) are tested to find optimal shade geometry for each latitude and each temperature. Optimum, in this case, means a high ratio of rejected heat to system mass.

The initial control models have the following properties in Table 3.1 (radiator) and Table 3.2 (shade); these properties were suggested from the literature review.

Table 3.1: Control radiator properties.

Property		Value	Units
Absorptivity/Emissivity		0.23/0.9	Unitless
Radiator Area		1	m^2
Radiator Thickness		0.01	cm
Radiator Material	$T_{ra} \leq 400K$	Aluminum	N/A
	$T_{ra} > 400K$	Titanium	
Radiator Density, ρ	$T_{ra} \leq 400K$	2700	kg/m^3
	$T_{ra} > 400K$	4500	

Radiator materials and suggested operating temperature came from Angelo and Buden.[20] Shade mass was chosen as a compromise between Barron et al.[13] (high shade area density at 20 kg/m^2; accounts for any and all structure) and Costello and Swanson[12] (low shade area density at 0.56 kg/m^2; accounts for only the shade). The area shade density chosen is a simplification but should include at least some structure and deployment components. All previous shade design studies[12–15] were unanimous in choosing kapton as the shade material, and this thesis will use it as well. Kapton is a light but strong plastic film that acts well as thermal insulation; it is able to withstand temperatures of up to 670 K.[9]

Table 3.2: Shade properties.

Property		Value	Units
Absorptivity/Emissivity	Shade Top	0.01/0.01	Unitless
	Shade Bottom	0.9/0.9	
Shade Shape		Parabolic	N/A
Material		Kapton	N/A
Area Density, ρ''_{sh}		10	kg/m^2

There are three sets of tests, one for each variable analyzed. The first two tests concern shade focal length and shade height. The third test considers the radiator area configuration, whether the radiator is rectangular or square in shape. The first two tests use a square, vertical radiator, but all tests keep a 1 m^2 area per active side.

The distance from the radiator top to the shade focal height, p', was varied from 0 cm to 20 cm above the radiator top in 5 cm increments for a total of five runs per radiator temperature for each latitude. As postulated in the Theory chapter, if the shade is specularly reflective, all thermal radiation incident upon the parabolic shade surface will reflect towards and collect at the focus. This round of tests seeks to test this hypothesis.

The shade height was varied from no shade to full shade in at least 25% increments for a grand total of five separate runs for each radiator temperature and each tested operating latitude. The ratio of the shade height to the radiator height, h_{sh}, is an important dimensionless parameter used in this context. The so-called full shade has the same height as the radiator and thus has an h_{sh} ratio of 1. A 25% increase in shade height means the shade height rises by a quarter of the radiator height.

The third test required modifying both radiator and shade geometry; keeping the radiator area constant, radiator height was reduced and radiator and shade lengths were increased. a_{ra} is defined as the ratio of radiator height to radiator length. Four separate ratios were tested with 0.25/4 (0.0625), 0.5/2 (0.25), 0.8/1.25 (0.64), and 1/1 (1).

3.3.2 Radiator with Heat Pipes

The next round of testing adds heat pipes to the previous design. Initially, three heat pipes are sandwiched between two face sheets with material filling the rest of the cross-section. An adhesive glue holds face sheets to the filler material and the heat pipes. The concept is displayed in Fig. 3.2.

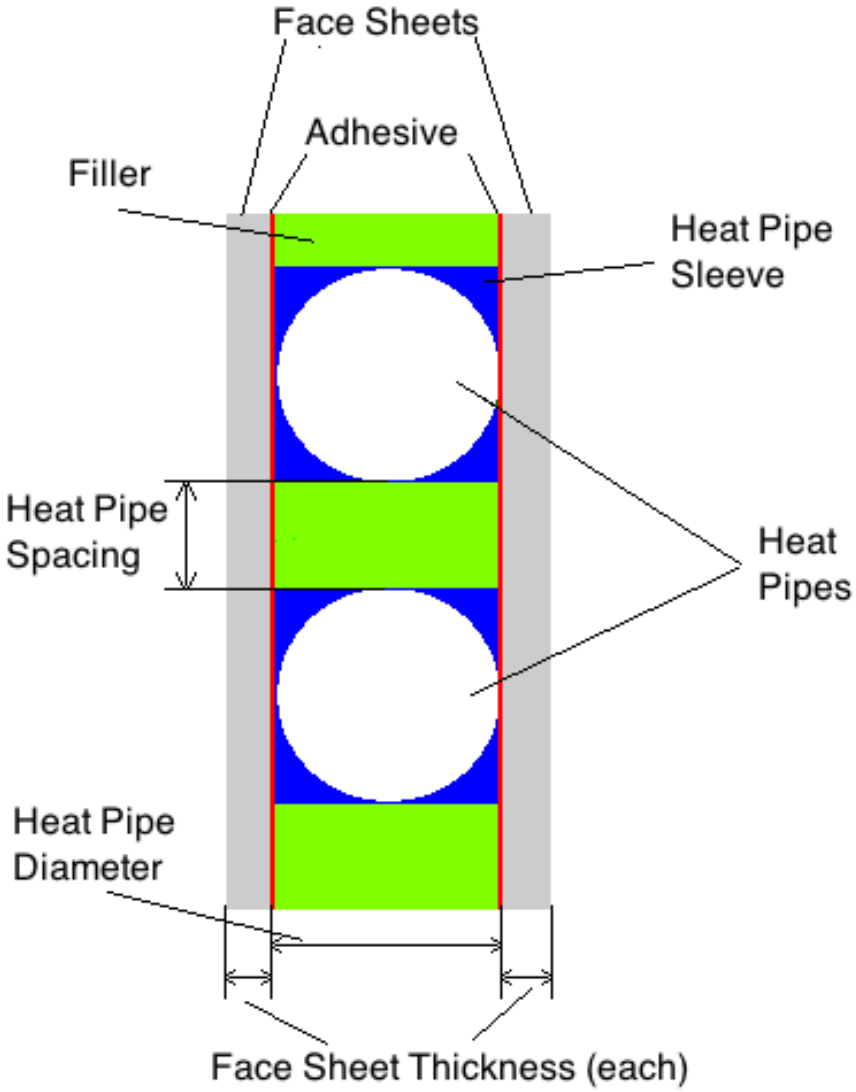

Fig. 3.2: Heat pipe radiator cross-section.

Table 3.3 lists the actual radiator properties that will be used during testing, including materials and densities for heat pipes, core materials, and face sheets.

Table 3.3: Heat pipe radiator properties

Property	Value		Units
	$T_{ra} \leq 400$K	$T_{ra} > 400$K	
Material	Aluminum	Titanium	N/A
Filler Material	Metal Honeycomb		
Density Ratio	1	1.67	Unitless
Filler Material Density, ρ_{co}	33.69	56.26	kg/m^3
Heat Pipe Linear Density, ρ'_{hp}	0.375	0.626	kg/m
Adhesive Area Density, ρ''_{co}	0.146	0.244	kg/m^2
Heat Pipe Diameter, Filler Thickness	0.3		cm

One assumption is that honeycomb material may be made out of any material required for testing; this is made in order to provide a standard of comparison. In reality, only aluminum honeycomb can be manufactured at present. Given the new mass and Thermal Desktop models, the results and numbers will be fed into a heat pipe radiator and system mass model.

4. RESULTS AND DISCUSSION

This chapter presents the results of testing outlined in the previous chapter on methods. This chapter will begin with the control radiator tests to find the optimal shade and radiator geometry. Plots of rejected thermal energy per unit mass versus the change in shade or radiator geometry will be presented. Then the results will be charted and tabulated. The second section will combine the heat pipe radiator and shade mass models and compare the areal masses calculated to radiators in current designs.

4.1 Control Radiator Tests and Shadow Shield Optimization

The control radiator design (a slab of metal) will be used to establish optimal radiator and shade geometry; in this case, optimal geometry corresponds to the highest ratio of the rate at which energy is emitted by the radiator to the mass of said radiator and its shade.

First, the initial control shade and radiator model will be presented and analyzed. Three radiator configurations, horizontal, vertical, and shielded vertical are compared. All radiators are square in shape (an aspect ratio of one) and one meter per side. The shade remains the same height as the radiator and has a focus ten centimeters above the radiator top.

The next three sections concern modifying a control-sized radiator and shade to find the optimum shade or radiator parameter for each type of test. The tests, in order, will modify the radiator area configuration a_{ra}, the ratio of shade height to radiator height $\hat{h}_{sh}$, and the shade focal length minus the radiator height p'.

4.1.1 Initial Control

The plots in this section establish the initial model. Each plot corresponds to a lunar latitude test: equator, 45°N, and hot pole. For each plot the x-axis is radiator surface temperature and the y-axis is the rate at which energy is emitted from the radiator divided by the configuration mass. Each plot has three lines for each of the following configurations:

horizontal, vertical, and shaded vertical. All radiators are square in shape, 1 m^2 per side. For the shaded configuration, the shade has a focus 10 cm above the radiator top and is the same height as the radiator.

The first plot presented, Fig. 4.1, is that of the radiator at the Equator, the second (Fig. 4.2) at 45°N, and the third (Fig. 4.3) at the lunar hot pole.

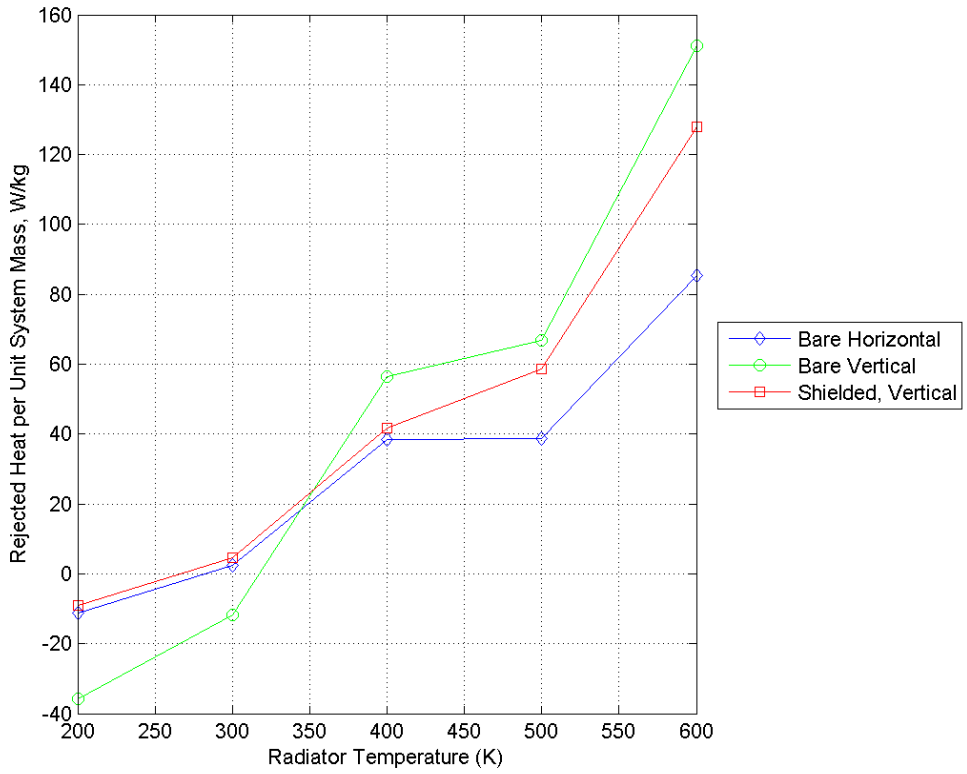

Fig. 4.1: Rejected heat per unit mass versus radiator surface temperature, vertical equatorial radiators aligned with lunar latitude line ($\beta_{fs-\vartheta}$ =90°); shade focus 10 cm above radiator top.

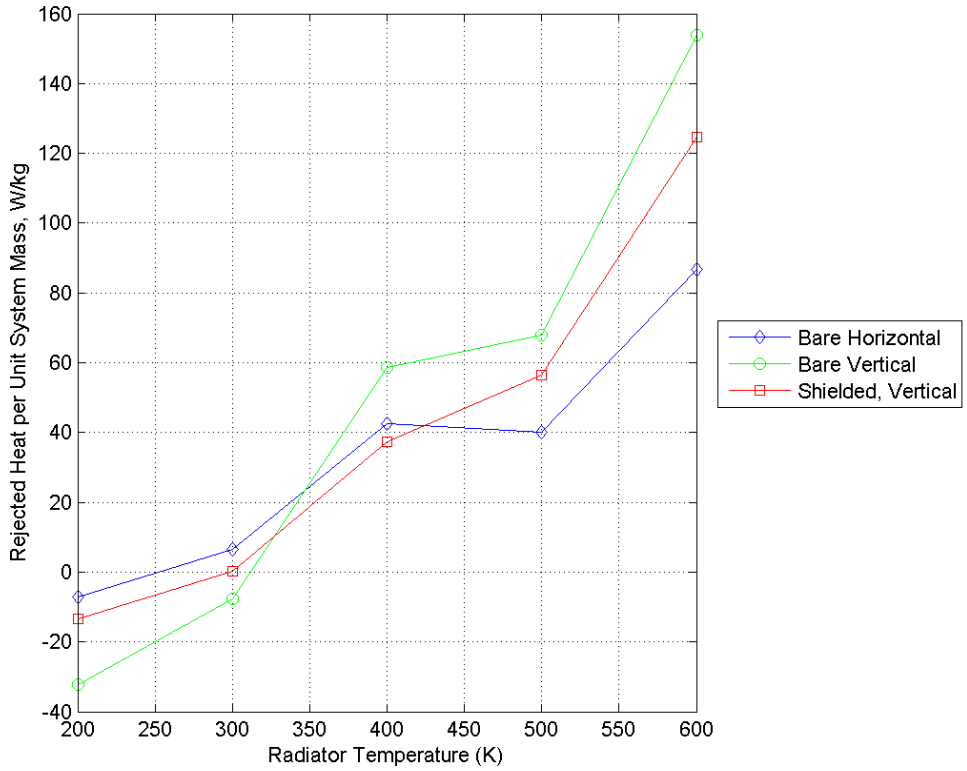

Fig. 4.2: Rejected heat per unit mass versus radiator surface temperature, vertical equatorial aligned with lunar latitude line ($\beta_{fs-\vartheta}$ =90°); shade focus 10 cm above radiator top.

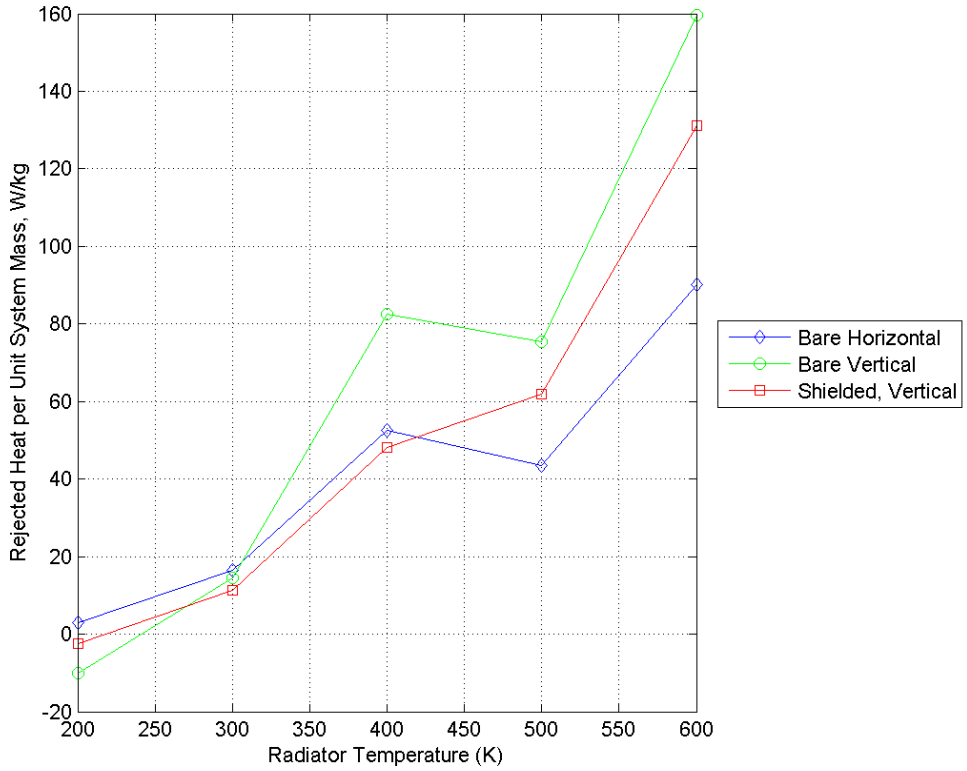

Fig. 4.3: Rejected heat per unit mass versus radiator surface temperature, vertical radiator-sat hot pole; shade focus 10 cm above radiator top.

An initial glance shows the shade may in fact raise mass and hamper heat transfer, but keep in mind that these are all square radiators; the shade may not be very effective at its job given this type of configuration. This demonstrates the need for the next round of tests to optimize the radiator and shade geometries.

4.1.2 Radiator Area Configuration

Focus will now shift to the radiator area configuration. Radiator area configuration tests results for the equator region are shown in Fig. 4.4 . Results from the same tests conducted

at 45° and the hot pole may be found in Appendix C. For all tests, the shade held a focus 10 cm above the radiator and remained the same height as the radiator.

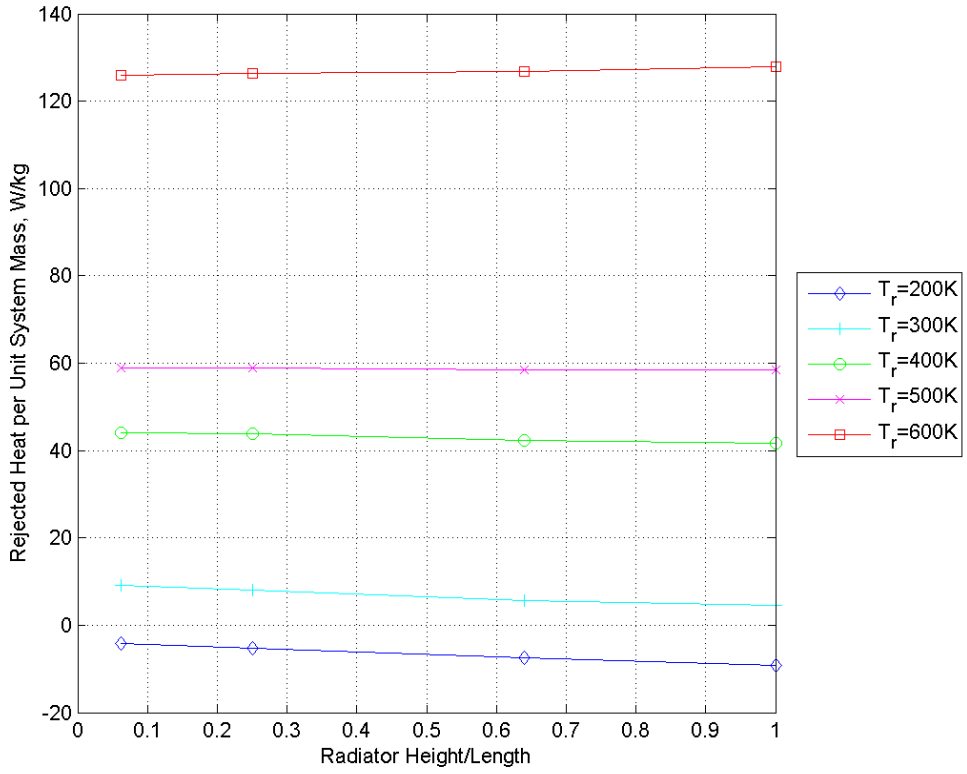

Fig. 4.4: Rejected heat per unit mass versus ratio of radiator height to length at equator; radiator aligned with lunar latitude line; full shade with focus 10 cm above radiator top

The lower temperature curves do resemble the view-factor reduction and shade mass curves developed in the theory section on shadow shielding geometry, but the higher temperature curves do not. The less of the lunar surface that the lower temperature radiator sees, the better. The opposite is true for the higher temperature radiators.

4.1.3 Shade Height

Shade height is the second parameter to be tested. The results of testing for the equatorial model are presented in Fig. 4.5.Test results for the hot pole and 45°N may be found in Appendix C. In all tests, the shade focus was kept 10 cm above the radiator and the radiator was kept square.

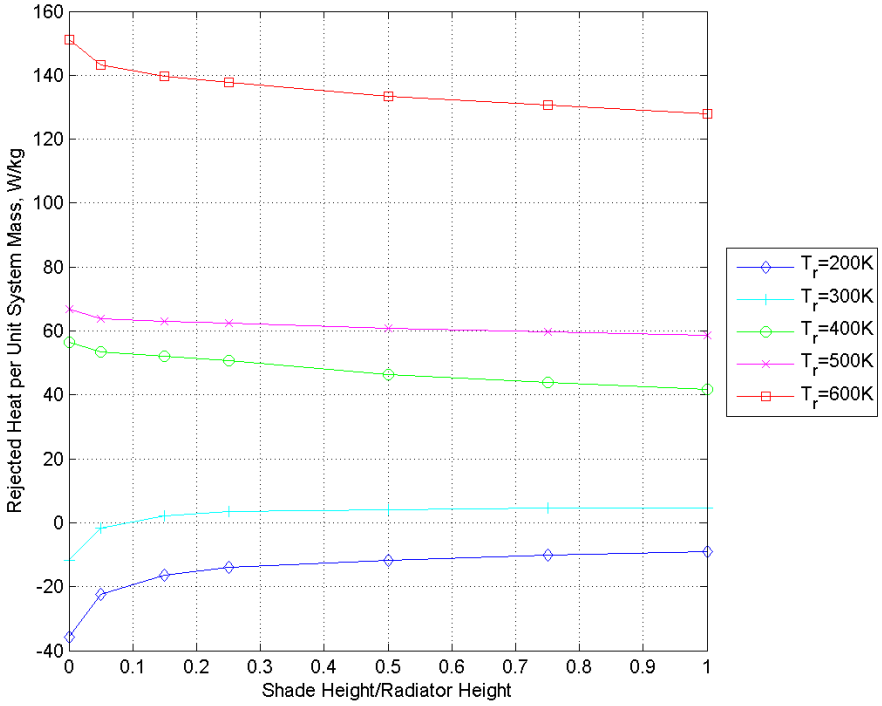

Fig. 4.5: Rejected heat per unit mass versus shade height, equatorial radiator aligned with lunar latitude line; shade focus 10 cm above radiator top

The radiators with temperatures 400 K and above seem to suggest the shade actually is not worth the additional mass, as the bare, vertical radiator performs better than those shaded. Heat transfer from two lower temperatures improves dramatically with greater shade height up until about a shade to radiator height ratio of 0.3, but begins to level off

thereafter due to the rising shade mass (although radiative heat transfer does improve, just not as drastically as earlier).

4.1.4 Shade Focal Length

This section focuses on the results from the altering the shade focal length. For all tests, the radiator is kept at an area ratio of one and the shade remains the same height as the radiator. Fig. 4.6 is a plot of the rate at which the radiator emits energy divided by the radiator's and the shade's combined mass for a radiator on the equator that is aligned with lunar latitude lines (i.e. a 90° beta angle). Plots for the hot pole and 45°N may be found in Appendix C.

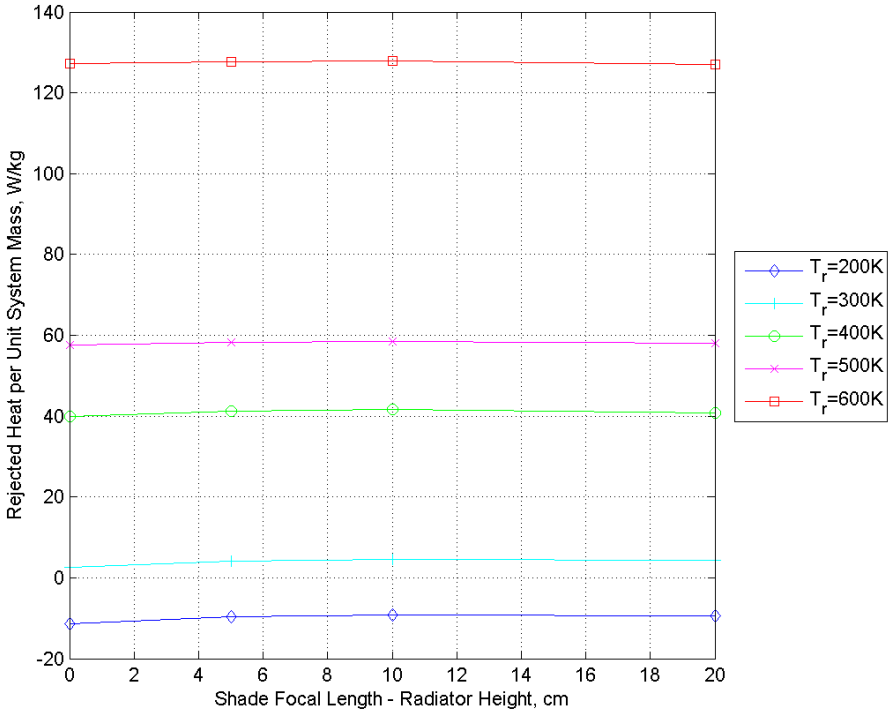

Fig. 4.6: Rejected heat per unit mass versus distance between shade focus and radiator top, equatorial radiator aligned with lunar latitude line; full shade.

Changing the shade focal length does not seem to have much of an effect on the results. A maximum, though difficult to discern, may be found when the shade focal length is 10 cm above the radiator's top for this latitude and for all temperatures. Naturally, shade mass grows as the focus rises, and this effect is showing in the chart.

4.1.5 Results

Tests found several optimal geometry conditions. Figs. 4.7, 4.8, and 4.9 chart the optimal shade and radiator parameters p', $\hat{h}_{sh}$, and a_{ra} versus radiator temperature at the lunar equator, 45°N, and the hot pole, respectively. The charts summarize results from the previous three tests. Table 4.1 summarizes the results displayed in the charts.

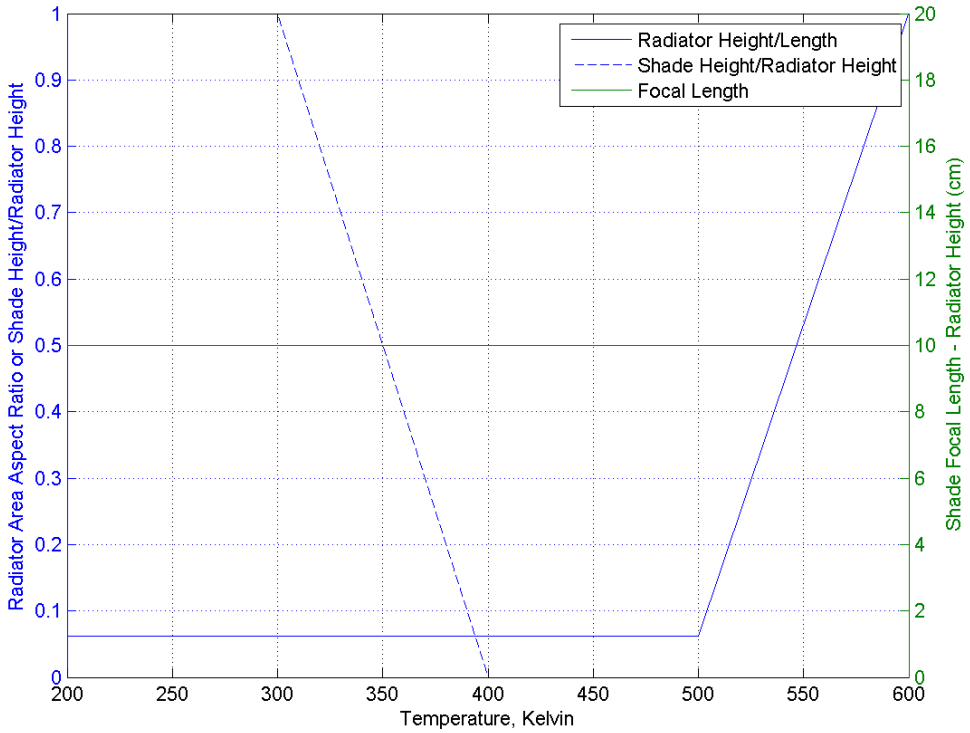

Fig. 4.7: Plot of optimum shade and radiator parameters, p', $\hat{h}_{sh}$, and a_{ra}, versus radiator surface temperature for a radiator on the lunar equator.

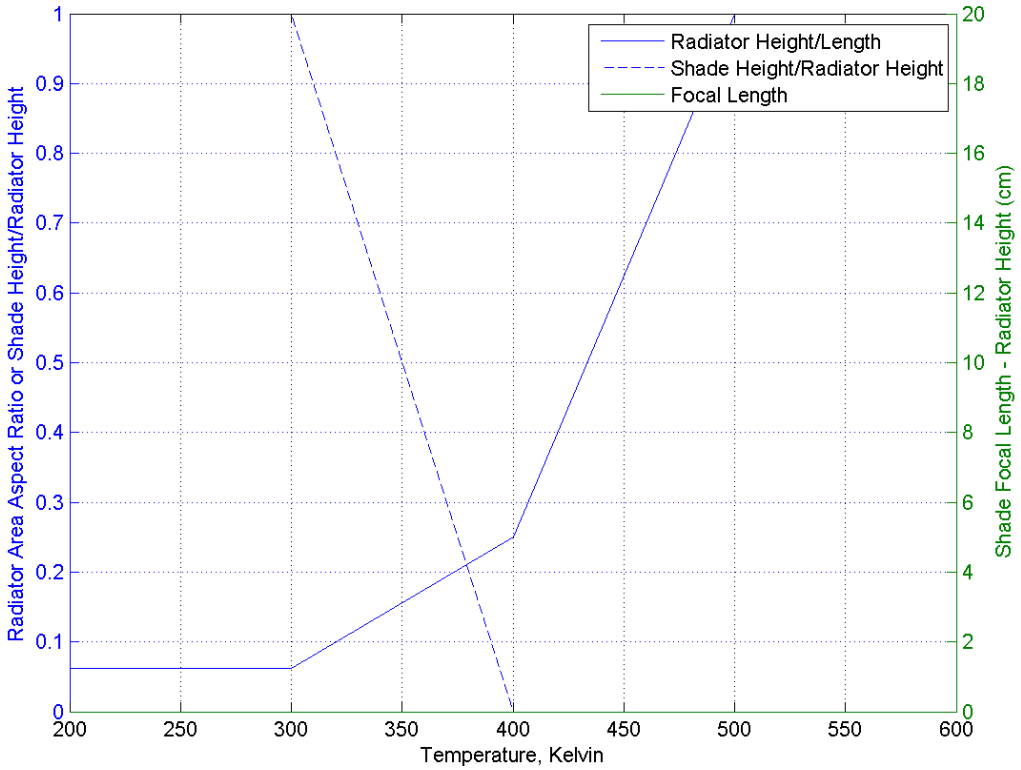

Fig. 4.8: Plot of optimum shade and radiator parameters, p', $\hat{h}_{sh}$, and a_{ra}, versus radiator surface temperature for a radiator at 45°N.

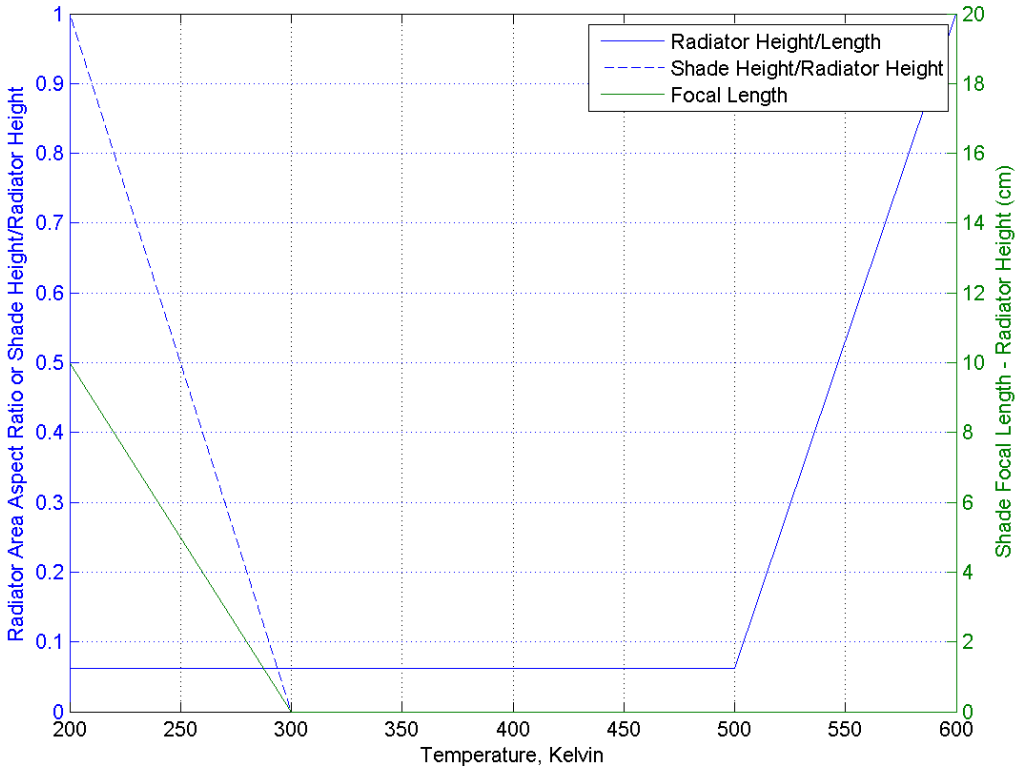

Fig. 4.9: Plot of optimum shade and radiator parameters, p', $\hat{h}_{sh}$, and a_{ra}, versus radiator surface temperature for a radiator at the lunar hot pole.

Table 4.1: Optimum parameters from control model testing.

		T_{ra}, Kelvin				
Latitude	Parameter	200	300	400	500	600
Equator	$\hat{h}_{sh}$	1	1	0	0	0
	p'	10	10	10	10	10
	a_{ra}	0.0625	0.0625	0.0625	0.25	1
45°N	$\hat{h}_{sh}$	1	1	0	0	0
	p'	0	0	0	0	0
	a_{ra}	0.0625	0.0625	0.25	1	1
Hot Pole	$\hat{h}_{sh}$	1	0	0	0	0
	p'	10	0	0	0	0
	a_{ra}	0.0625	0.0625	0.0625	1	1

From the results it is shown that the shade is the most useful for a sub-polar system that has a radiator with a temperature lower than or close to the maximum lunar surface temperature. For reference, the highest surface temperature at noon on the equator is 384 Kelvin; the highest surface temperature at noon at 45°N is about 320 Kelvin.

4.1.6 Shade Mass Sensitivity

Shade area mass for the previous was 10 kg/m^2. However, many shade masses could have been considered for analysis; one source[14,15] neglected shade structure and used a shade area mass of 0.56 kg/m^2, and another[13] used 20 kg/m^2. Fig. 4.10 shows the minimum radiator temperature threshold where a shaded radiator performs better in terms of heat radiated per unit radiator and shade mass than a vertical or horizontal radiator of the same temperature. It is fairly obvious that when the shade has a lower area mass than the radiator (less than 3 kg/m^2 or so), the shade is useful for any temperature of radiator tested.

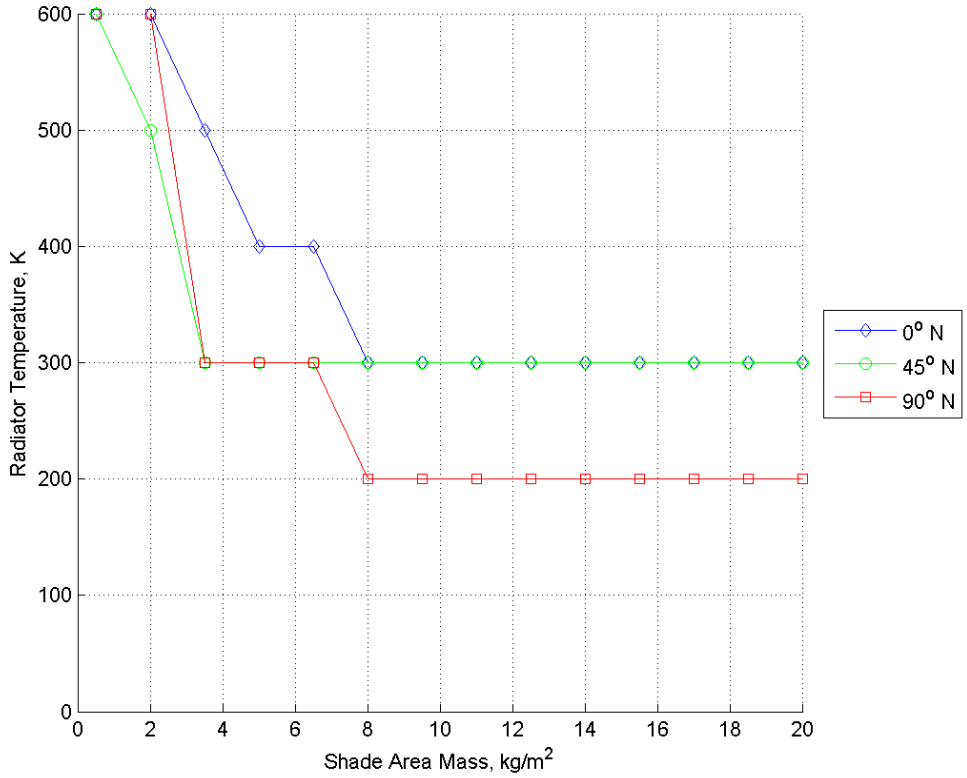

Fig. 4.10: Minimum radiator temperature threshold versus shade area mass.

4.2 Heat Pipe Radiators and Systems

This section begins with the results from Thermal Desktop tests of heat pipe radiators with optimal shade geometry factored in. Figs. 4.11, 4.12, and 4.13 are plots of specific heat rejection versus the radiator temperature for horizontal, bare vertical, and vertical with optimized shade configurations for the three lunar latitudes tested (equator, 45°N, and hot pole). No shaded configurations were tested for temperatures above 400 K; above this temperature, it seems the shade actually hampers heat transfer, and the additional mass a shield requires is a detriment, and will not be considered.

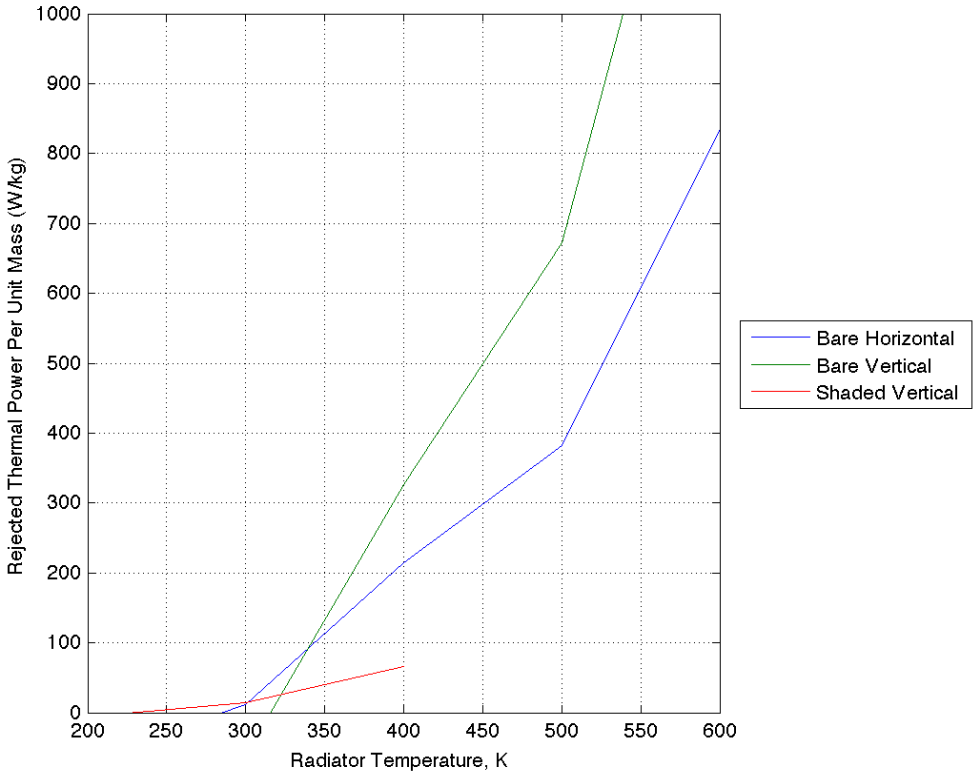

Fig. 4.11: Rejected heat per unit mass versus radiator surface temperature at equator; horizontal and vertical radiators aligned with lunar latitude line.

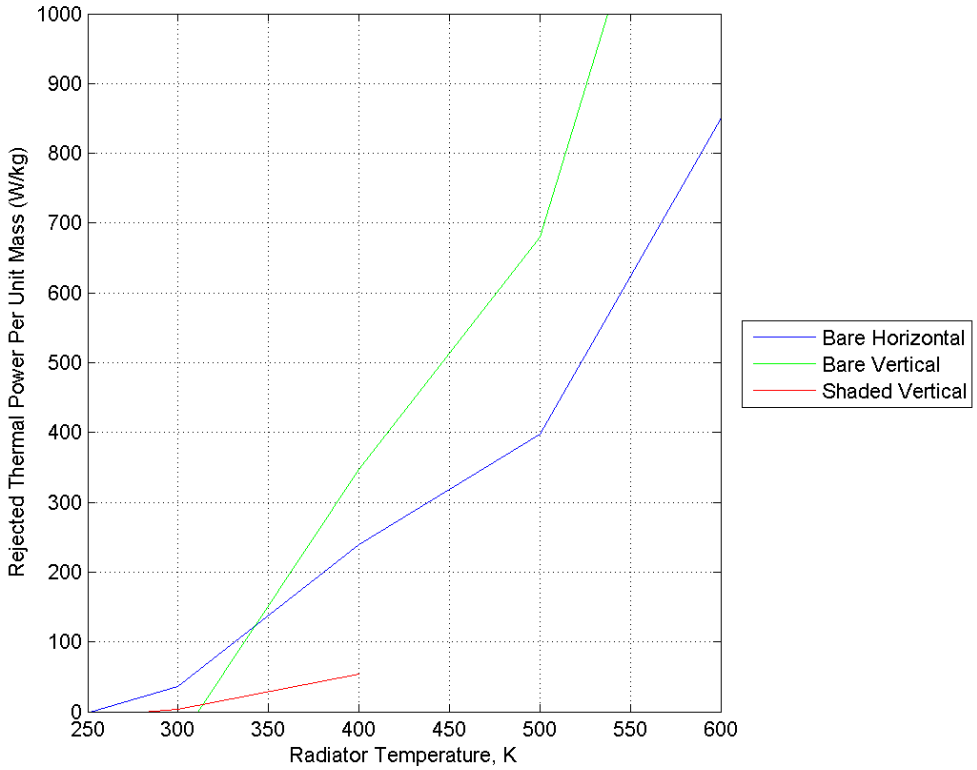

Fig. 4.12: Rejected heat per unit mass versus radiator surface temperature at 45°N; horizontal and vertical radiators aligned with lunar latitude line.

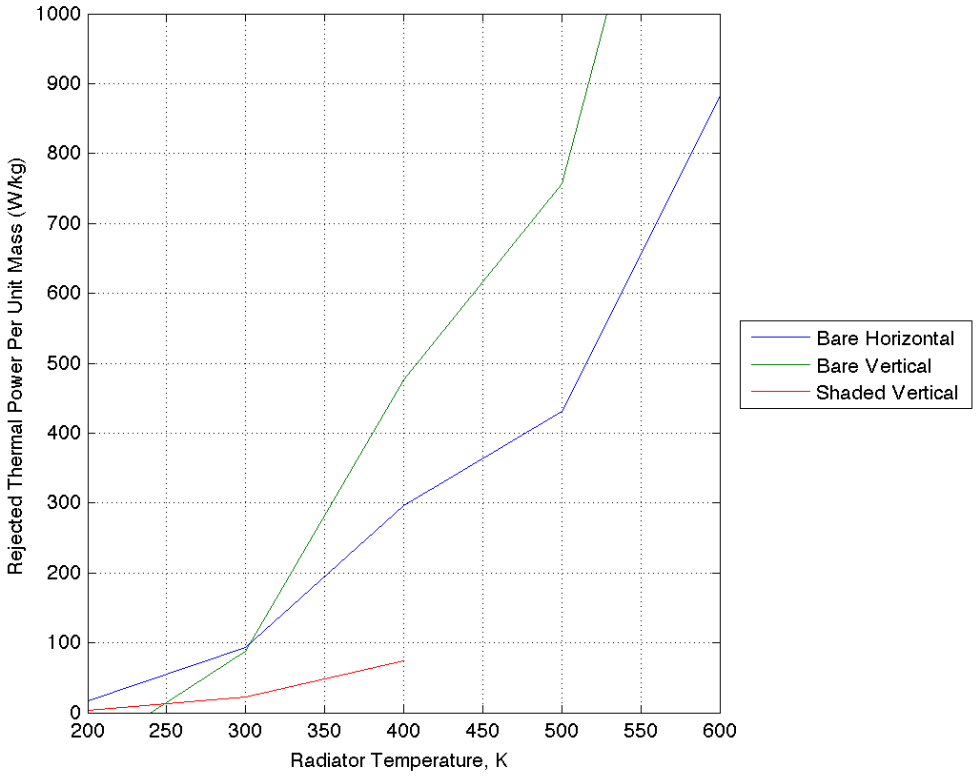

Fig. 4.13: Rejected heat per unit mass versus radiator surface temperature at the hot pole; horizontal and vertical radiators.

The curves in these plots mimic the curves in the previous graphs of rejected heat per unit mass versus radiator temperature; shadow shielding shines for the lower temperature radiators at the lunar equator. Shadow shielding does not seem to be useful for higher latitudes.

Figs. 4.14, 4.15, and 4.16 are the results from heat-pipe radiator coupled with reactor mass calculations. A 25% Carnot efficiency was used to determine reactor outlet temperature from the radiator temperature, drawing from the previously found results in the Introduction.

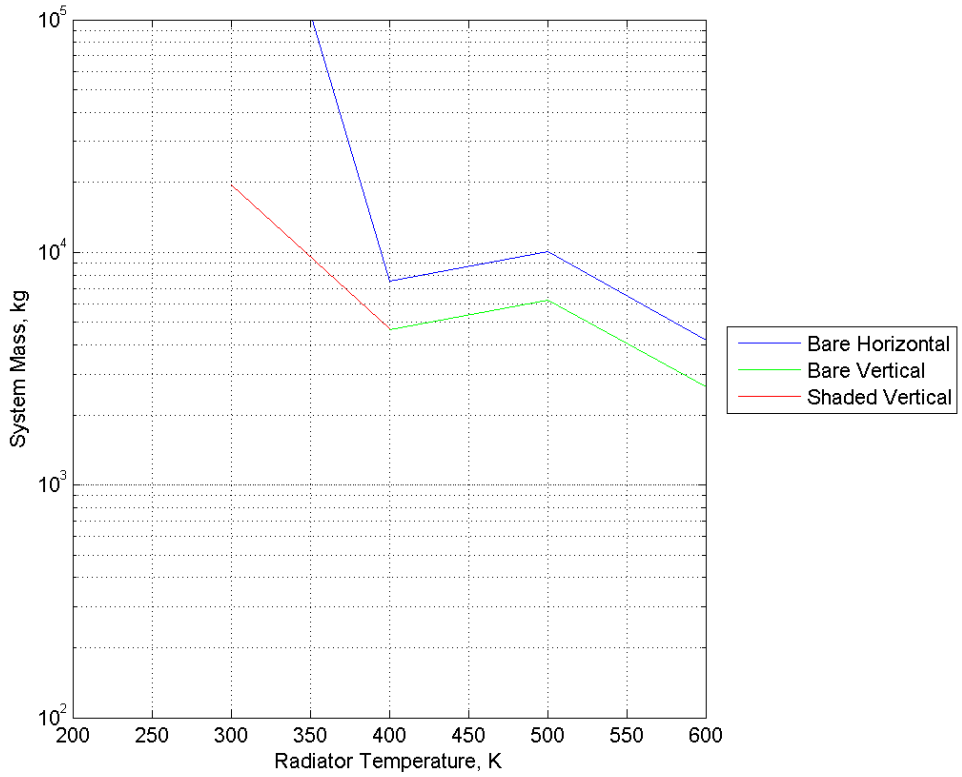

Fig. 4.14: System mass versus radiator surface temperature at equator; shaded and vertical radiators aligned with lunar latitude line.

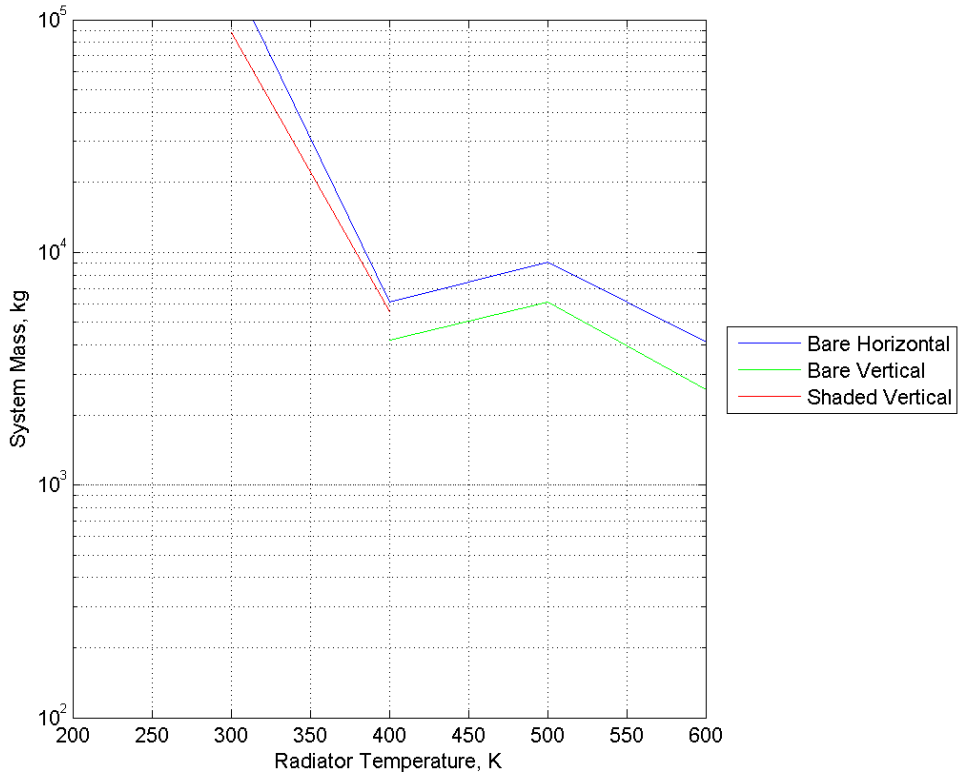

Fig. 4.15: System mass versus radiator surface temperature at 45°N; horizontal and vertical radiators aligned with lunar latitude line.

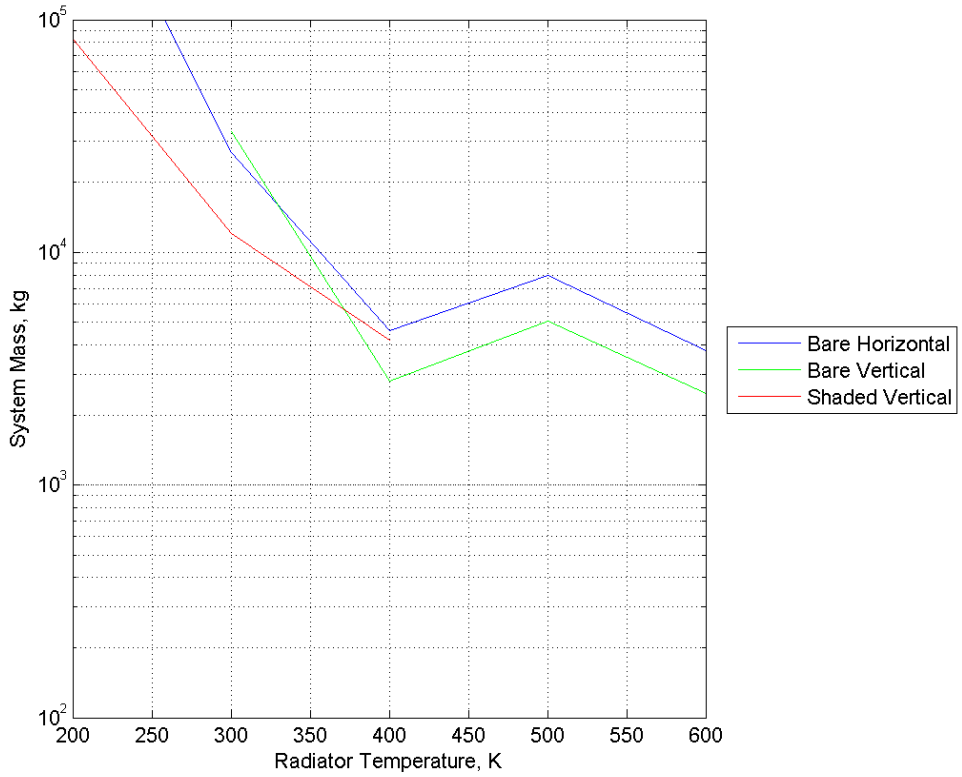

Fig. 4.16: System mass versus radiator surface temperature at hot pole.

The shade allowed a low temperature radiator provide a fairly viable option. At no point in any of the graphs does the horizontal radiator provide the lowest mass radiator and reactor combination. For the systems at 45°N and the equator, a shaded radiator is the lowest mass option below a radiator temperature of 400 K; the threshold is about 375 K for the hot pole system. The shaded radiator is still

5. SUMMARY AND CONCLUSIONS

Shadow shielding is a novel and practical concept for waste heat rejection from lunar surface spacecraft systems. A shadow shield is a light shield that shades the radiator from parasitic thermal radiation from the sun or lunar surface. Radiator size and mass can reduce if the radiator is not required to account for parasitic heat loads in addition to system energy rejection requirements.

The lunar thermal environment can be very harsh towards radiative heat rejection. Parasitic heat loads force the radiator to expand in size and mass to compensate. On the Moon, there are three types: surface infrared, solar insolation, and albedo. Surface infrared thermal radiation is emitted by the lunar surface during all times of the lunar day but is most extreme where surface temperatures are highest (i.e. the lunar equator at noon). Solar insolation directly comes from the sun, which circles overhead at lower latitudes (causing a day and night cycle) but circles around the horizon at the lunar hot pole. Albedo is solar thermal radiation reflected by the lunar surface; it is the least intense of the three types. Shadow shielding is meant to block a vertical radiator's view of the lunar surface, minimizing surface infrared and albedo loads; it also occasionally blocks out the radiator's view of the sun at the hot pole.

This thesis tests shadow shielding geometry and its effect on the radiator and nuclear reactor mass in a reactor-powered Carnot heat engine. The Carnot heat engine cycle was used for all thermodynamic system calculations. It is an ideal cycle that ignores irreversibilities and provides an upper limit on thermodynamic efficiency; cooling by means of a radiator, however, adds another constraint. It was proved that due to the nature of cooling by radiative heat transfer, the maximum shaft work a Carnot system can produce and the minimal required radiator area occurs when the Carnot efficiency is 25%. This precedent was used throughout the system analysis.

First, a case for shadow shielding is made using an isothermal, control radiator model in Thermal Desktop. Six radiator temperatures and three latitudes are considered in the

tests. Test variables in this section include radiator shapes and shade geometry. The simulations found that shadow shielding is most useful for a low-temperature radiator at the lunar equator. Optimized parabolic shade geometry includes a focus right above or at the top of the radiator and full to three-quarter height shading. Additionally, the most useful radiator shape for shadow shielding is that which has a low height and long width.

Optimized shade and radiator geometry results were then factored into a second model where the radiator is comprised of heat pipes similar to radiators from actual lunar nuclear system designs. The study found that shadow shielding allowed the system to use a low-temperature radiator where other configurations were not viable, and that shadow shielding drastically improves heat transfer by lowering the sink temperature (by up to 100 Kelvin), but consequentially adds mass to the radiator.

The final systems analysis found that although the shadow shielded radiator performs better than bare configurations in terms of radiated heat per system mass, however a shadow-shielded system is heavier than its bare counterparts; however, this is mostly a materials consideration.

Further testing could consider many other factors. As far as lunar tests are concerned, this body of work did not test the effect of the rotation angle, confirm shade optical properties, test alternate shade materials, or consider the thermal impact of dust on shaded radiator performance. This thesis also did not consider other bodies in the solar system such as planets Mars and Mercury as well as asteroids.

REFERENCES

1. Poston, D., Kapernick, R., and Guffee, R., "Design and Analysis of the SAFE-400 Space Fission Reactor," *AIP Conference Proceedings*, Vol. 608, No. 1, 2002, pp. 578–588.

2. Houts, M. and Mason, L., "Fission Surface Power System Technology for NASA Exploration Missions," Department of Energy, 2005.

3. Elliott, J., Reh, K., and MacPherson, D., "Lunar Fission Surface Power System Design and Implementation Concept," *AIP Conference Proceedings*, Vol. 813, No. 1, 2006, pp. 942–952.

4. Dieckamp, H., *Nuclear Space Power Systems*, Atomics International, Canoga Park, CA, 1967.

5. Chang, H., "Optimization of a Heat Pipe Radiator Design," *AIAA Thermophysics Conference*, Vol. 1, No. AIAA-84-1718-686, June 1984.

6. Truong, H. and Mancuso, R., "Performance Predictions of Radiating Annular Fins of Various Profile Shapes," *American Society of Mechanical Engineers and American Institute of Chemical Engineers, Joint National Heat Transfer Conference*, July 1980.

7. Cengel, Y. and Boles, M., *Thermodynamics: An Engineering Approach*, McGraw-Hill, Boston, 6th ed., 2007.

8. Modest, M., *Radiative Heat Transfer*, Academic Press, 2nd ed., 2003.

9. Gilmore, D., *Spacecraft Thermal Control Handbook: Fundamental Technologies*, Aerospace Press, Los Angeles, 2nd ed., 2002.

10. Christie, R., Plachta, S., and Hasan, M., "Transient Thermal Model and Analysis of the Lunar Surface and Regolith for Cryogenic Fluid Storage," Technical Memorandum 20080039640, National Aeronautics and Space Administration, Glenn Research Center, Cleveland, Ohio 4413, August 2008.

11. Dallas, T., Diaguila, A., and Saltsman, J., "Design Studies on the Effects of Orientation, Lunation, and Location on the Performance of Lunar Radiators," Tech. Rep. NASA-TMX-1846, National Aeronautics and Space Administration, March 1971.

12. Costello, F. and Swanson, T., "Lunar radiators with specular reflectors," *Heat Transfer in Space Systems; Proceedings of the Symposium, AIAA/ASME Thermophysics and Heat Transfer Conference*, edited by S. Chan, R. S. E.E. Anderson, C. Chan, and D. Pepper, Jan. 1990, pp. 145–150.

13. Barron, C., Castro, N., and Phillips, B., "Preliminary Design of a Radiator Shading Device for a Lunar Outpost," Contractor Report NASA-CR-192016, National Aeronautics and Space Administration, January 1991.

14. Keller, J., "A Parametric Study of Parabolic Radiator Shades for Lunar Base Thermal Control Systems," *25th International Conference on Environmental Systems*, SAE International, Warrendale, PA, July 1995.

15. Ewert, M., Graf, J., and Keller, J., "Development of a Lunar Radiator Parabolic Shading System," *25th International Conference on Environmental Systems*, SAE International, Warrendale, PA, July 1995.

16. Clark, C. and Ewert, M., "Analysis and Conceptual Design of a Lunar Radiator Parabolic Shade," *Proceedings of the 26th Intersociety Energy Conversion Engineering Conference*, Vol. 4, American Nuclear Society, LaGrange Park, IL, August 1991, pp. 273–278.

17. Todreas, N. and Kazimi, M., *Nuclear Systems 1: Thermal Hydraulic Fundamentals*, Taylor & Francis, 1st ed., 1990.

18. Bragg-Sitton, S., *Analysis of Space Reactor System Components: Investigation Through Simulation and Non-Nuclear Testing*, Ph.D. dissertation, University of Michigan, Ann Arbor, MI, 2004.

19. Panczak, T., Ring, S., Welch, M., Johnson, D., and Bell, D., *Thermal Desktop Users Manual*, Cullimore and Ring Technologies, Inc., Littleton, Colorado, 5th ed., October 2008.

20. Angelo, J. and Buden, D., *Space Nuclear Power*, Orbit, a Foundation Series, Orbit Book Company, 1985.

APPENDIX A
DERIVATIONS

$$\dot{Q} = \frac{\dot{W}}{\eta_C},$$

then the heat rejected by the radiator, $\dot{Q}_R$, is the difference between the heat input and shaft work such that

$$\dot{Q}_R = \dot{Q} - \dot{W} = \dot{W}\left(\frac{1}{\eta_C} - 1\right).$$

If

$$\begin{array}{lcl} T_H & = & \text{System Heating Temperature} \\ T_R & = & \text{System Heat Rejection Temperature} \\ T_S & = & \text{Sink Temperature} \end{array}$$

then

$$\eta_C = 1 - \frac{T_R}{T_H}$$

and using a simplified radiative heat transfer equation,

$$\dot{Q}_R = A_{ra}\varepsilon_{ra}\sigma\left(T_R^4 - T_S^4\right),$$

where

$$\begin{array}{lcl} A_{ra} & = & \text{Radiator Area} \\ \varepsilon_{ra} & = & \text{Radiator Surface Emissivity} \\ \sigma & = & \text{Stefan-Bolzmann Constant} \end{array}$$

If one were to define a parameter θ_S as the ratio of the sink temperature to the system heat rejection temperature as

$$\theta_S = \frac{T_S}{T_R},\ \theta_S \in [0 \ldots 1],$$

then

$$\dot{Q}_R = A_{ra}\varepsilon_{ra}\sigma T_R^4\left(1 - \theta_S^4\right)$$

and furthermore

$$\dot{Q}_R = A_{ra}\varepsilon_{ra}\sigma T_H^4 \left(1-\eta_C\right)^4 \left(1-\theta_S^4\right).$$

Therefore one can find Eq. (A.1):

$$\frac{\dot{W}}{A_{ra}} = \varepsilon_{ra}\sigma T_H^4 \frac{\left(1-\eta_C\right)^4 \left(1-\theta_S^4\right)}{\frac{1}{\eta_C}-1}. \tag{A.1}$$

The maximum work (or minimal radiator area) occurs where

$$\frac{\partial}{\partial\theta_S}\left(\frac{\dot{W}}{A_{ra}}\right) = \frac{\partial}{\partial\eta_C}\left(\frac{\dot{W}}{A_{ra}}\right) = 0,$$

$$\frac{\partial}{\partial\theta_S}\left(\frac{\dot{W}}{A_{ra}}\right) = \varepsilon_{ra}\sigma T_H^4 \frac{\left(1-\eta_C\right)^4}{\frac{1}{\eta_C}-1} \frac{\partial}{\partial\theta_S}\left(1-\theta_S^4\right)$$

$$\frac{\partial}{\partial\theta_S}\left(1-\theta_S^4\right) = -4\theta_S^3$$

$$\rightarrow \frac{\partial}{\partial\theta_S}\left(\frac{\dot{W}}{A_{ra}}\right) = \varepsilon_{ra}\sigma T_H^4 \frac{\left(1-\eta_C\right)^4}{\frac{1}{\eta_C}-1} \cdot -4\theta_S^3$$

$$-4\theta_S^3 = 0 \Rightarrow \theta_S = 0$$

$$\frac{\partial}{\partial\eta_C}\left(\frac{\dot{W}}{A_{ra}}\right) = \varepsilon_{ra}\sigma T_H^4 \left(1-\theta_S^4\right) \frac{\partial}{\partial\eta_C}\left(\frac{\left(1-\eta_C\right)^4}{\frac{1}{\eta_C}-1}\right)$$

$$\frac{\left(1-\eta_C\right)^4}{\frac{1}{\eta_C}-1} = \left(1-\eta_C\right)^4 \cdot \frac{\eta_C}{1-\eta_C} = \eta_C\left(1-\eta_C\right)^3$$

$$\frac{\partial}{\partial\eta_C}\left(\eta_C\left(1-\eta_C\right)^3\right) = \left(1-\eta_C\right)^3 - 3\eta_C\left(1-\eta_C\right)^2$$

$$\rightarrow \frac{\partial}{\partial\eta_C}\left(\frac{\dot{W}}{A_{ra}}\right) = \varepsilon_{ra}\sigma T_H^4 \left(1-\theta_S^4\right) \cdot \left(\left(1-\eta_C\right)^3 - 3\eta_C\left(1-\eta_C\right)^2\right)$$

$$(1-\eta_C)^3 - 3\eta_C(1-\eta_C)^2 = 0$$

$$\rightarrow 1-\eta_C = 3\eta_C \Rightarrow \eta_C = \frac{1}{4}$$

APPENDIX B

DATA

Table B.1: Lunar environment properties

Property		Value	Units
Temperatures	Equator Noon	384	Kelvin
	Equator Night	120	
	Hot Pole	220	
	Cold Pole	70	
Regolith	Absorptivity, α_{ls}	0.93	Unit-Less
	Emissivity, ε_{ls}	0.93	
	Reflectance, ρ_{ls}	0.07	
Inclination of the Lunar Equator Relative to the Sun		1.53	Degrees
Solar Thermal Flux		1370	W/m^2

APPENDIX C

ADDITIONAL PLOTS

Radiator Surface Temperature and Configuration

Equator

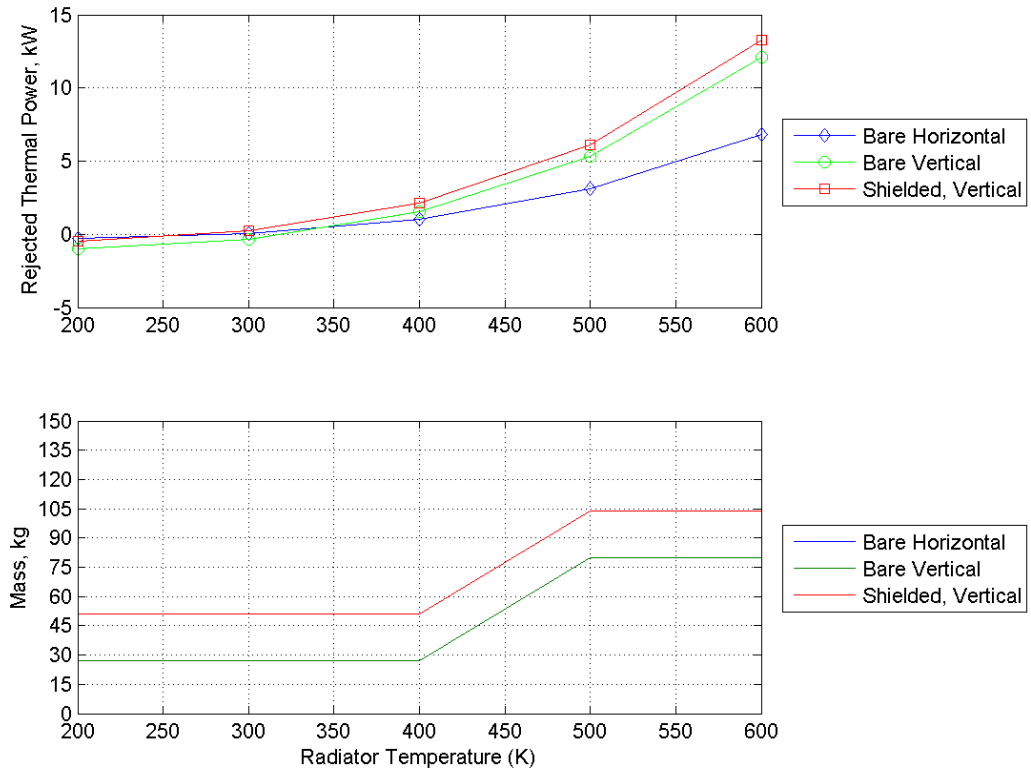

Fig. C.1: Radiated heat and radiator mass versus radiator surface temperature at equator; vertical and shaded radiators aligned with lunar latitude line ($\beta_{fs-\vartheta}$ =90°); full shade with focus 10 cm above radiator top.

45°N

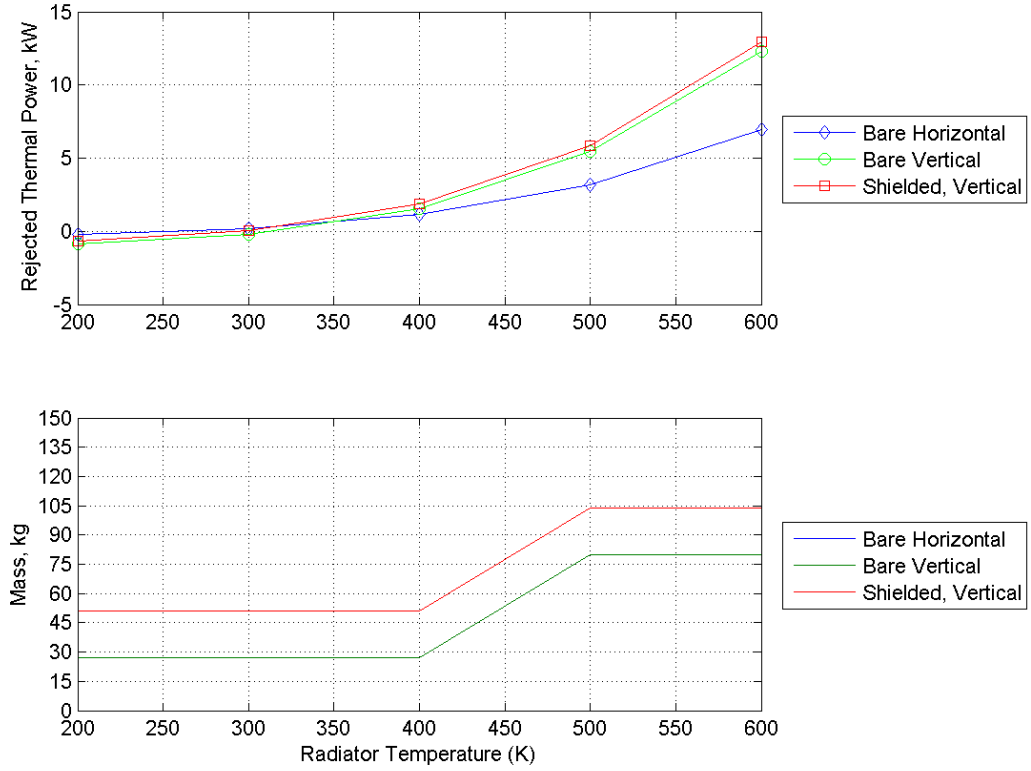

Fig. C.2: Radiated heat and radiator mass versus radiator surface temperature at 45°N; vertical and shaded radiators aligned with lunar latitude line ($\beta_{fs-\vartheta}$ =90°); full shade with focus 10 cm above radiator top.

Hot Pole

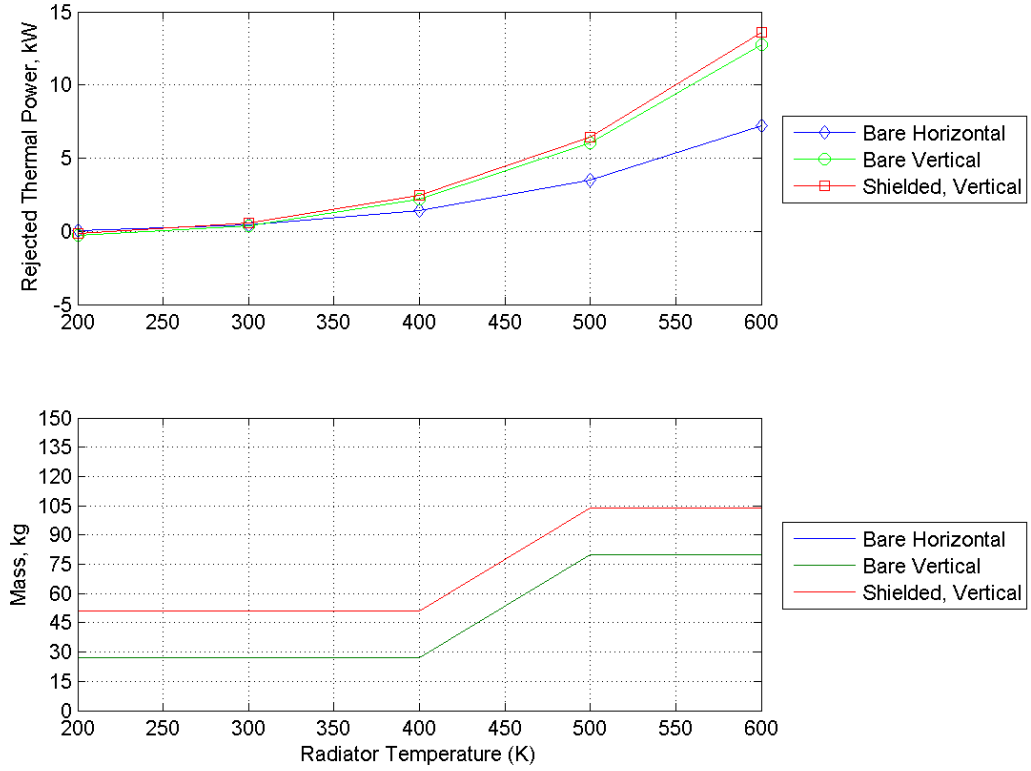

Fig. C.3: Radiated heat and radiator mass versus radiator surface temperature at hot pole; full shade with focus 10 cm above radiator top.

Radiator Area Configuration

Equator

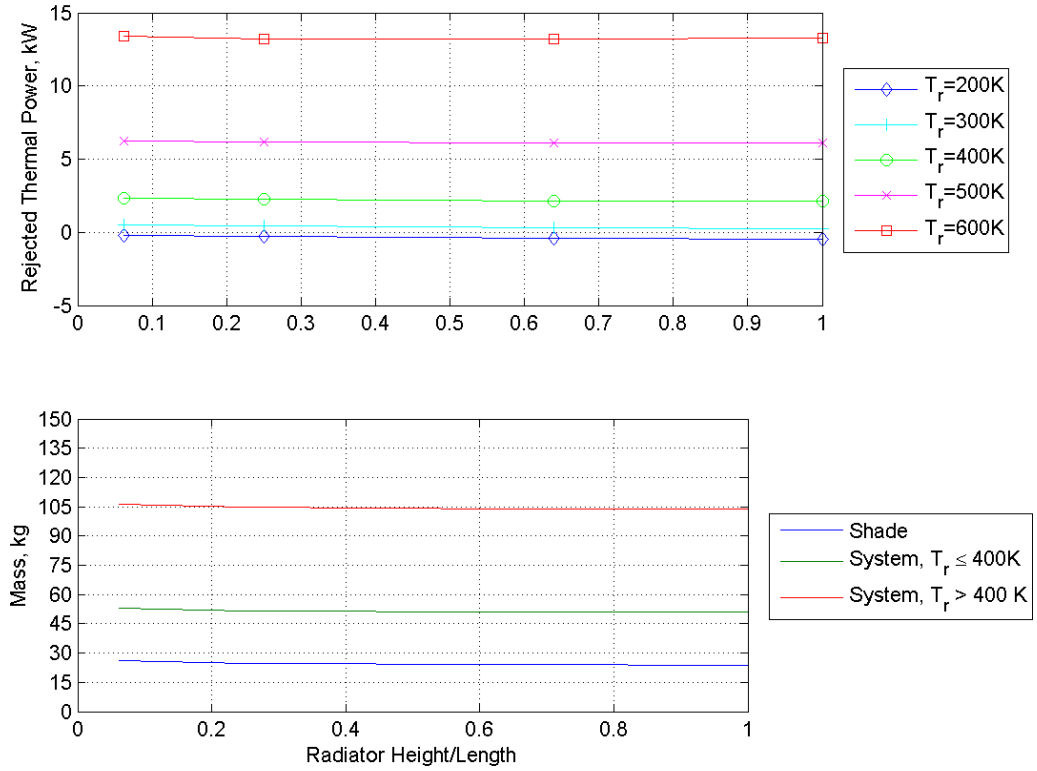

Fig. C.4: Radiated heat and radiator mass versus ratio of radiator height to length at equator and aligned with lunar latitude line ($\beta_{fs-\vartheta}$ =90°); full shade with focus 10 cm above radiator top.

45°N

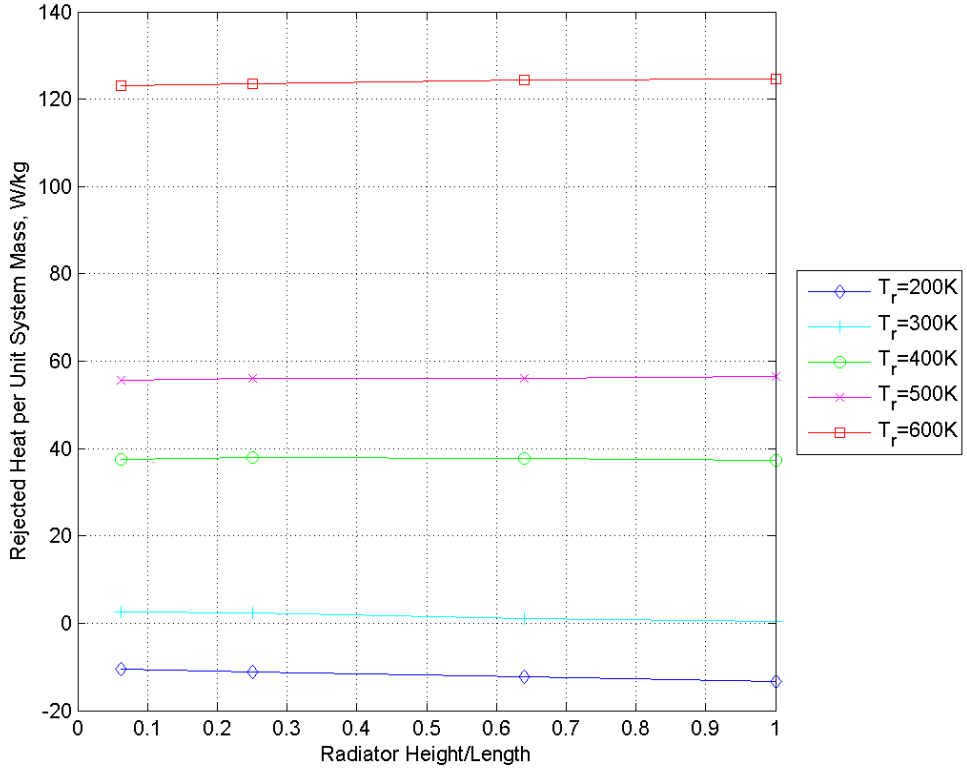

Fig. C.5: Radiated heat per unit mass versus ratio of radiator height to length at 45°N and aligned with lunar latitude line ($\beta_{fs-\vartheta}$ =90°); full shade with focus 10 cm above radiator top.

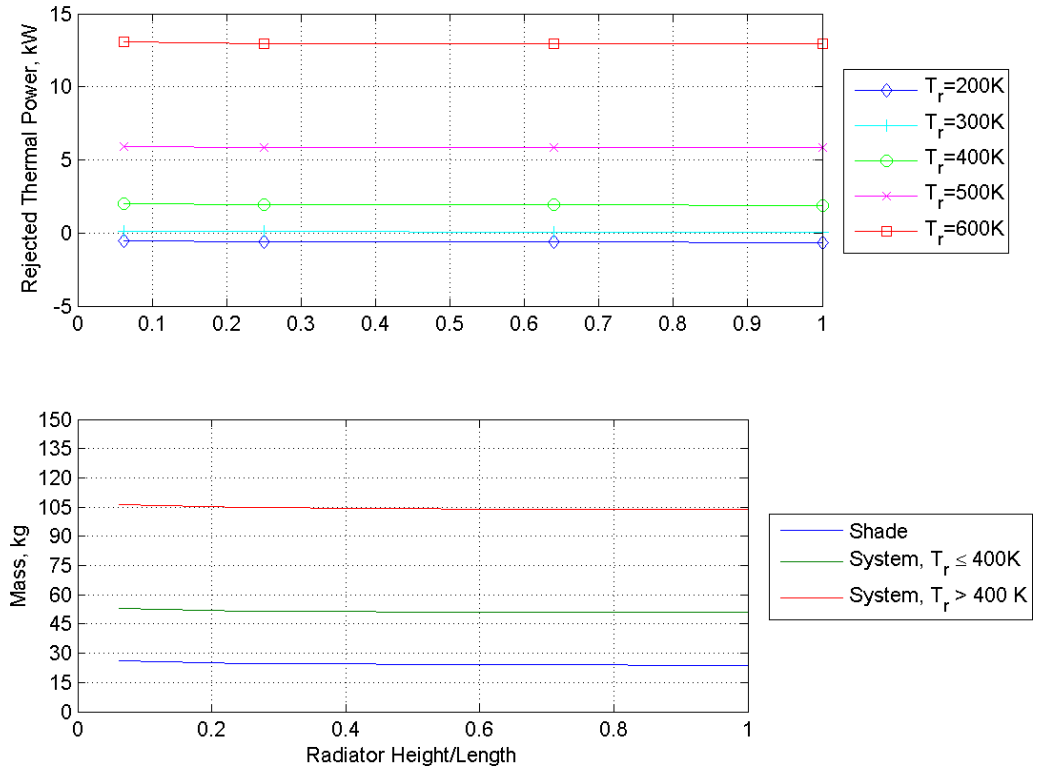

Fig. C.6: Radiated heat and radiator mass versus ratio of radiator height to length at 45°N and aligned with lunar latitude line ($\beta_{fs-\vartheta}$ =90°); full shade with focus 10 cm above radiator top.

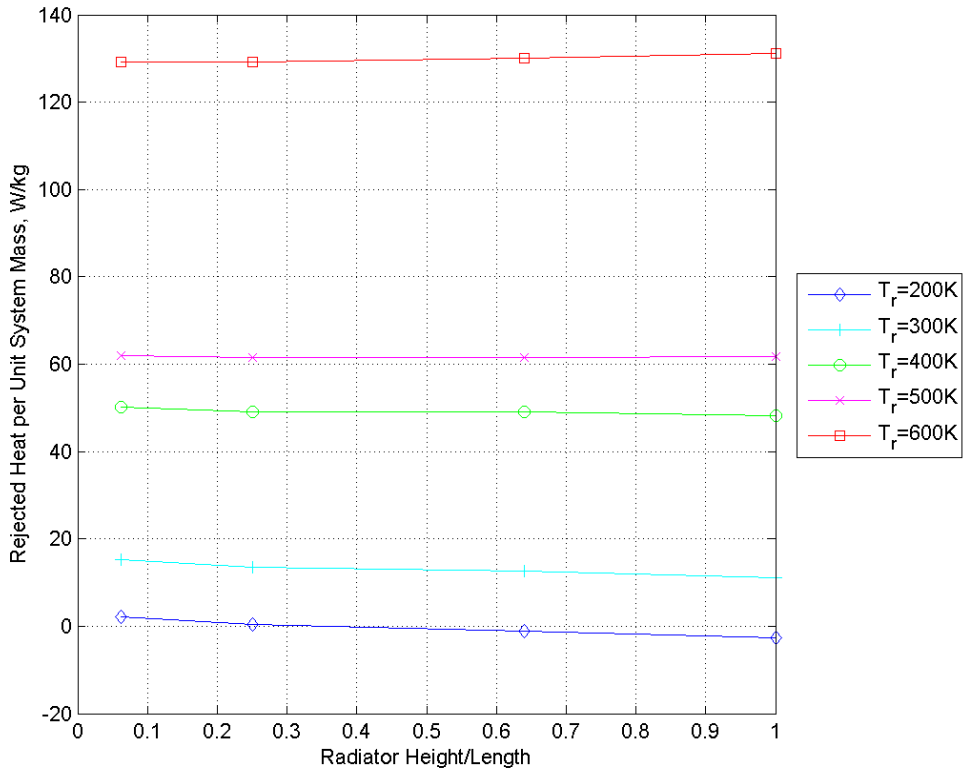

Fig. C.7: Radiated heat per unit mass versus ratio of radiator height to length at hot pole; full shade with focus 10 cm above radiator top.

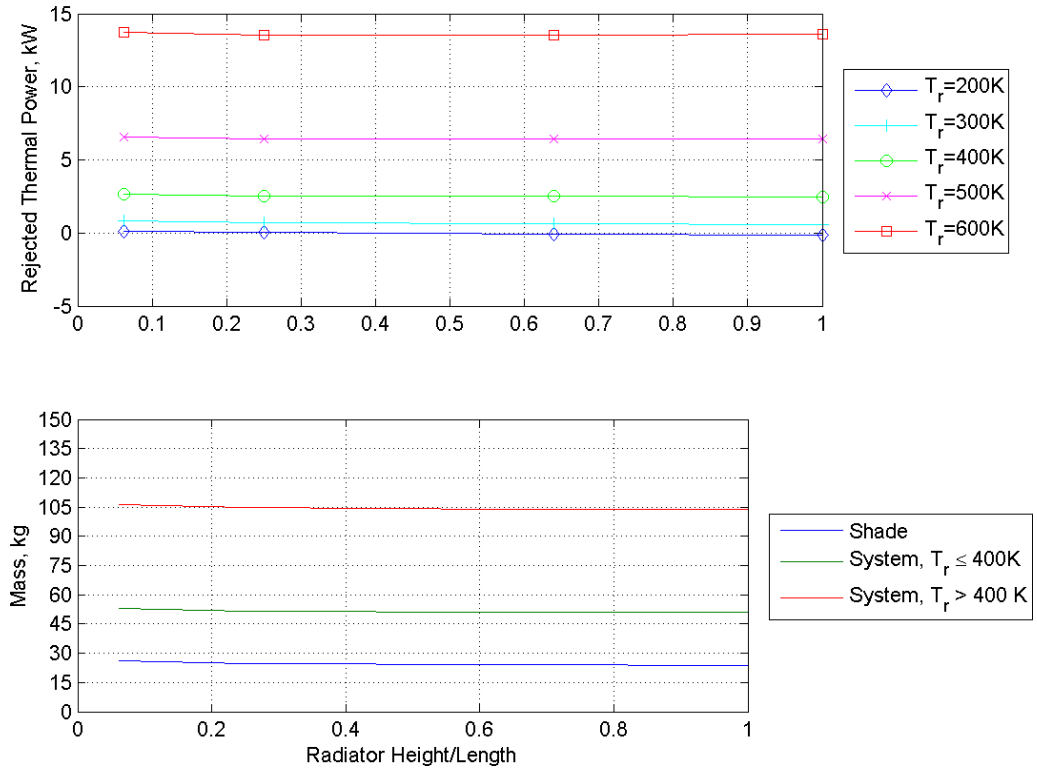

Fig. C.8: Radiated heat and radiator mass versus ratio of radiator height to length, equatorial radiator aligned with lunar latitude line ($\beta_{fs-\vartheta}$ =90°); full shade with focus 10 cm above radiator top.

Shade Height

Equator

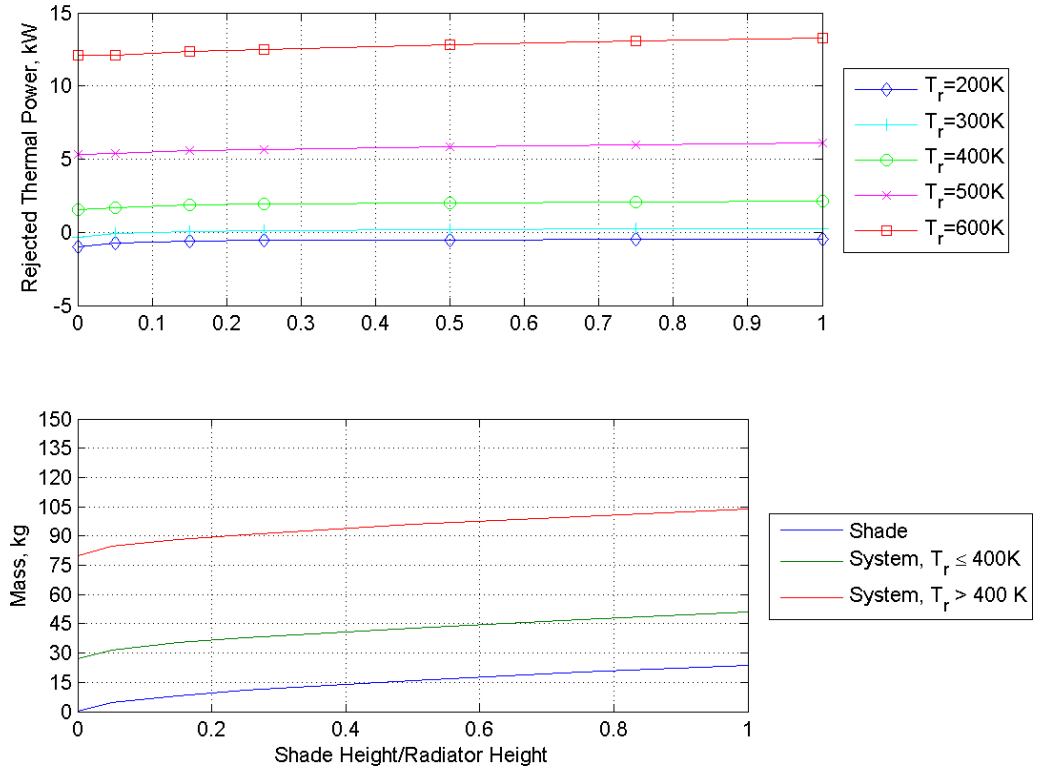

Fig. C.9: Radiated heat and radiator mass versus shade height; square, equatorial radiator aligned with lunar latitude line ($\beta_{fs-\vartheta} = 90°$); shade focus 10 cm above radiator top

45°N

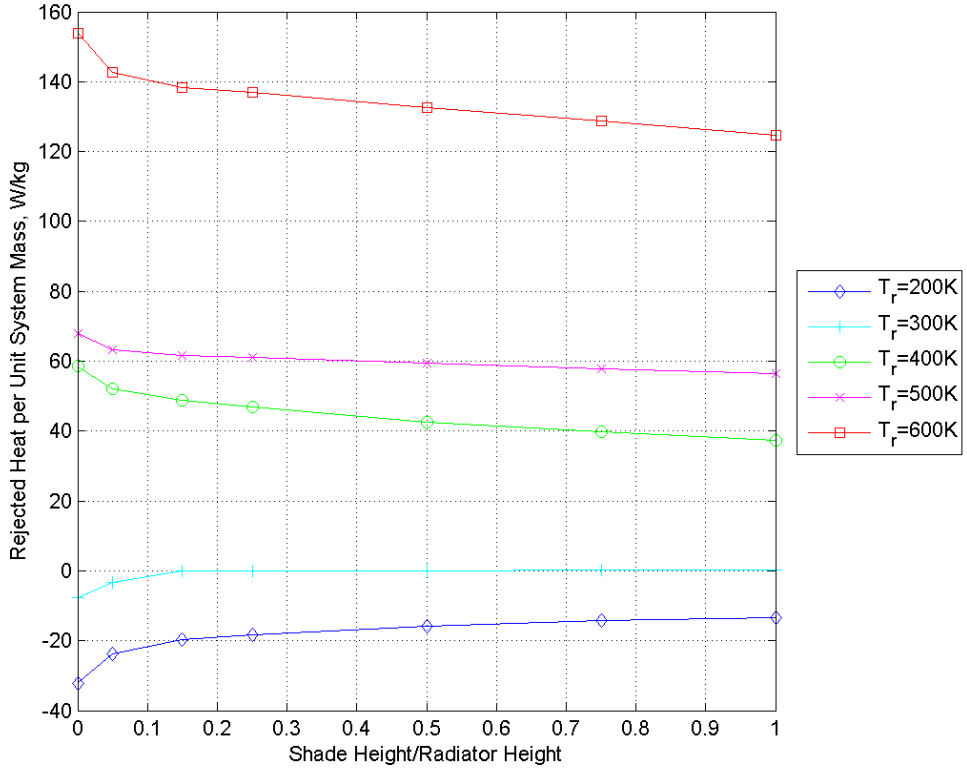

Fig. C.10: Radiated heat per unit mass versus shade height; square radiator at 45°N and aligned with lunar latitude line ($\beta_{fs-\vartheta}$ =90°); shade focus 10 cm above radiator top

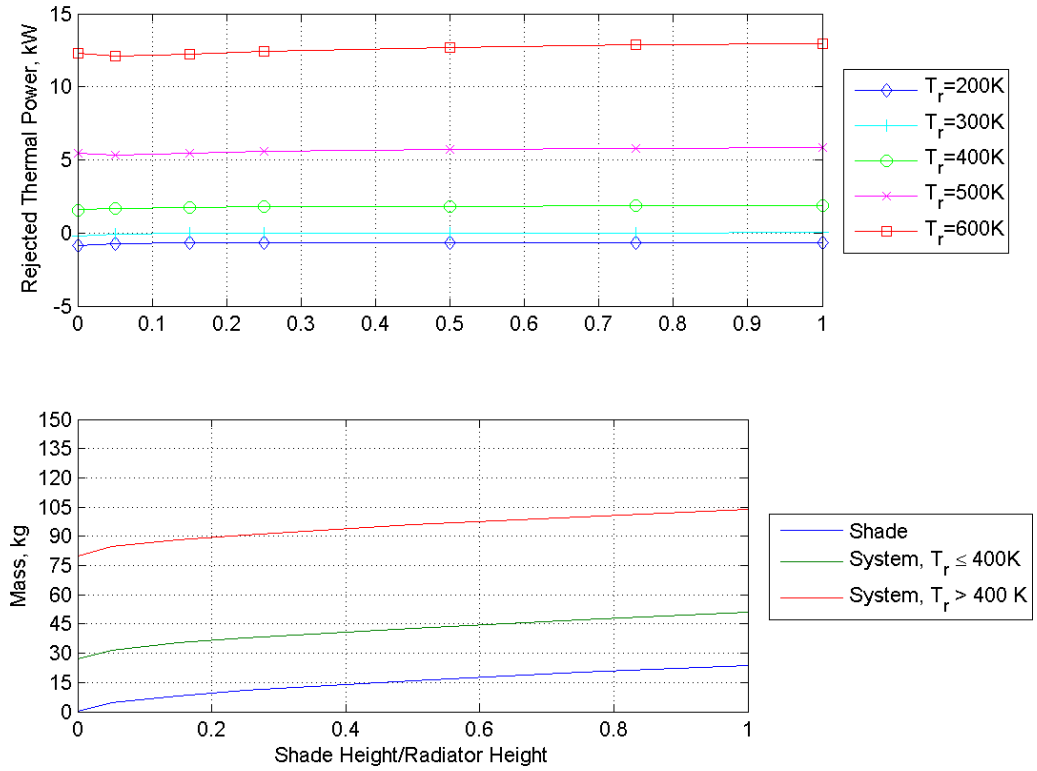

Fig. C.11: Radiated heat and radiator mass versus shade height; square radiator at 45°N and aligned with lunar latitude line ($\beta_{fs-\vartheta}$ =90°); shade focus 10 cm above radiator top

Hot Pole

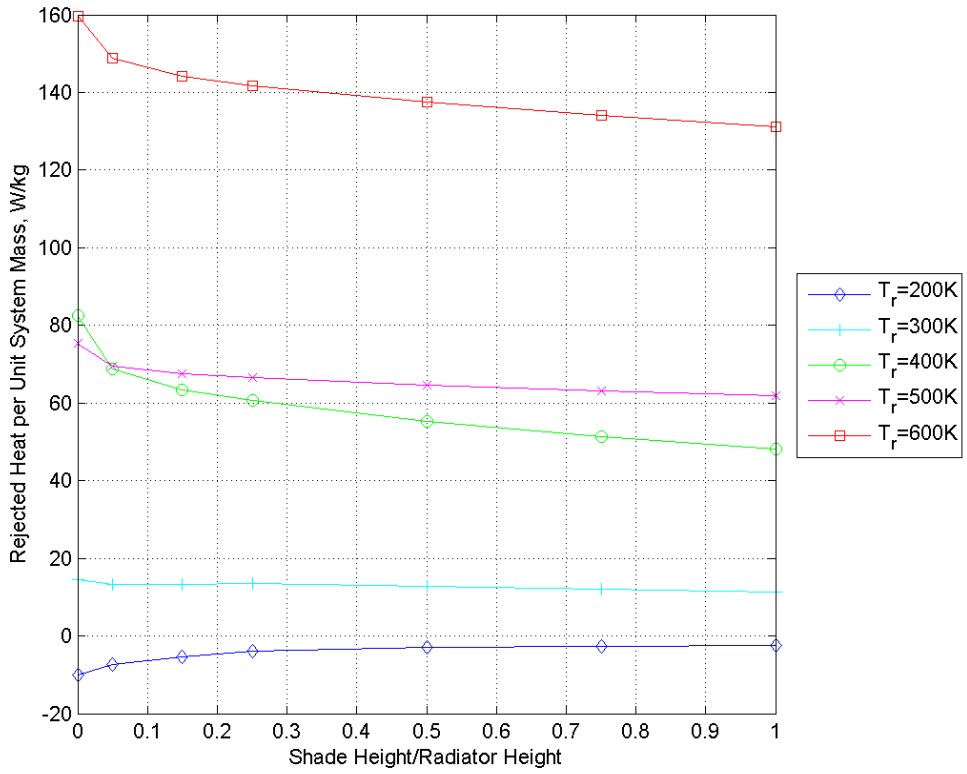

Fig. C.12: Radiated heat per unit mass versus shade height; square radiator at hot pole; shade focus 10 cm above radiator top

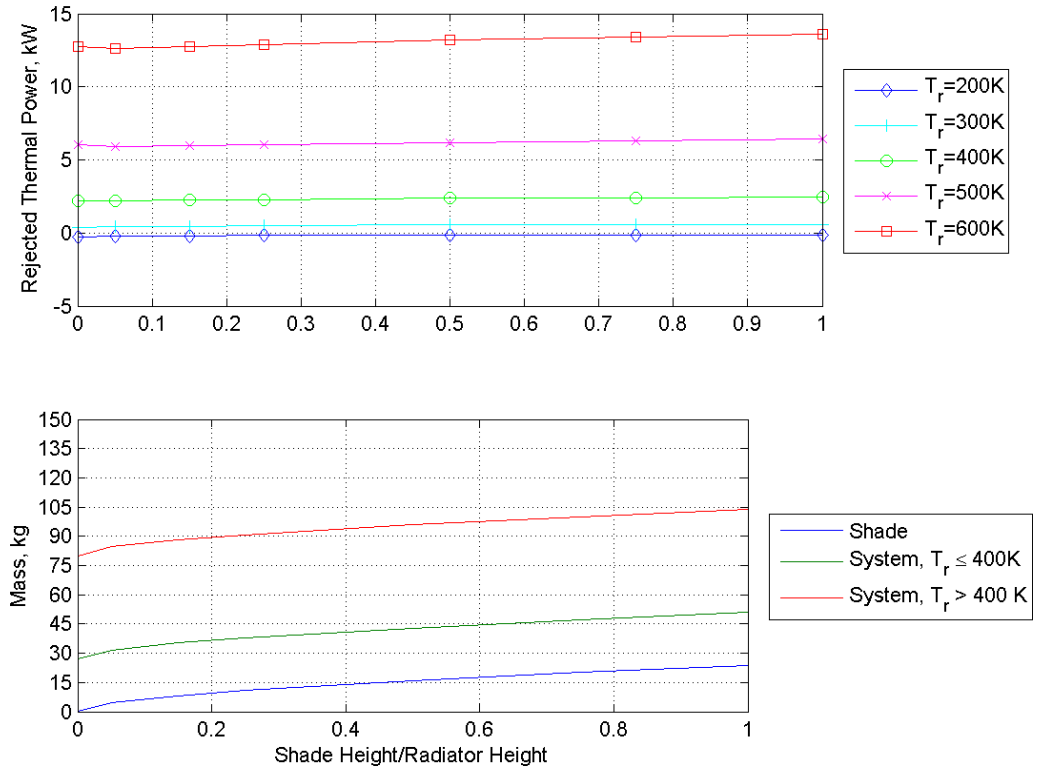

Fig. C.13: Radiated heat and radiator mass versus shade height; square radiator at hot pole; shade focus 10 cm above radiator top

Shade Focal Length

Equator

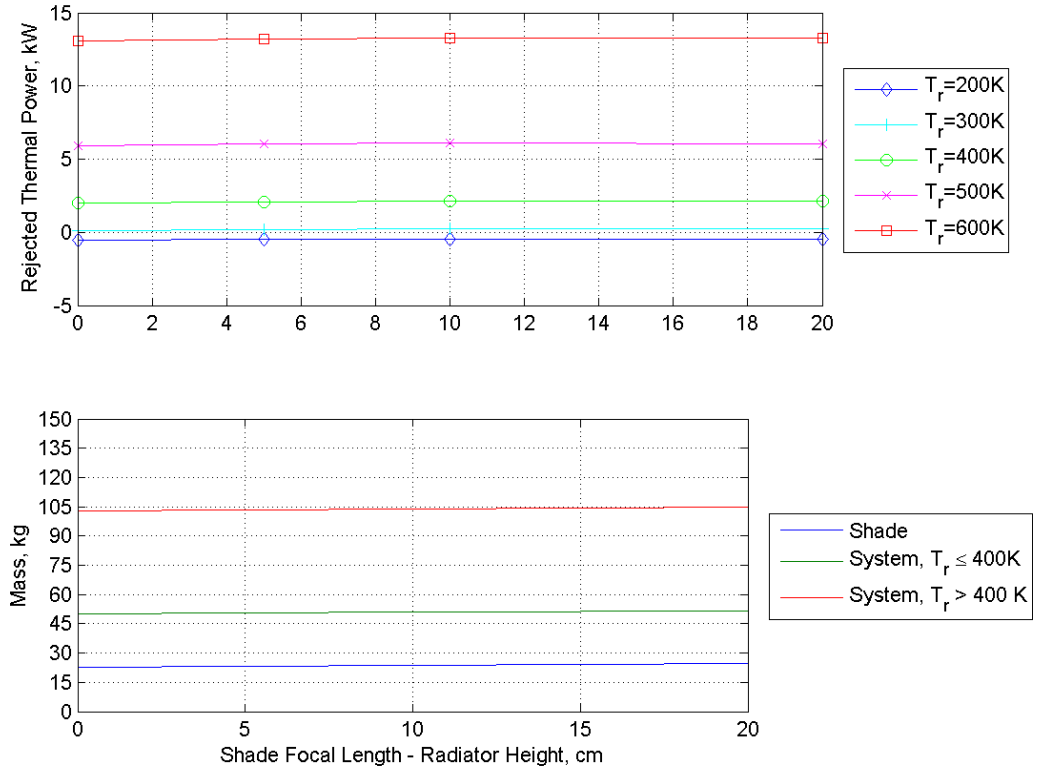

Fig. C.14: Radiated heat and radiator mass versus difference between shade focal length and radiator height; square, equatorial radiator aligned with lunar latitude line ($\beta_{fs-\vartheta}$ =90°); full shade.

45°N

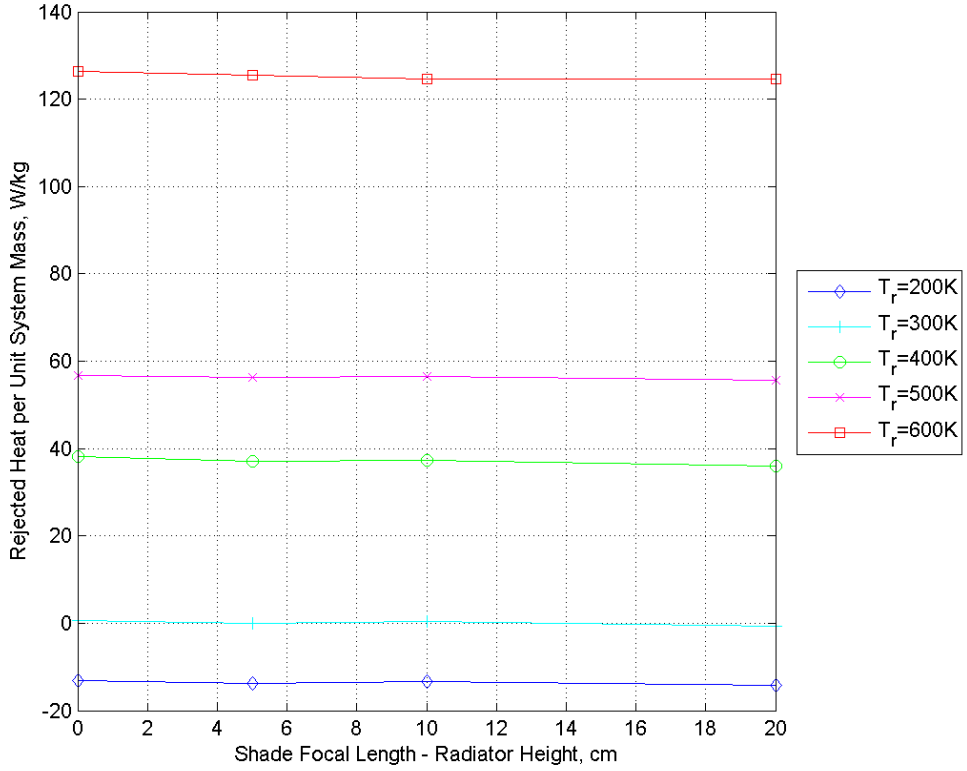

Fig. C.15: Radiated heat per unit mass versus shade height; square radiator at 45°N aligned with lunar latitude line ($\beta_{fs-\vartheta} = 90°$); shade focus 10 cm above radiator top

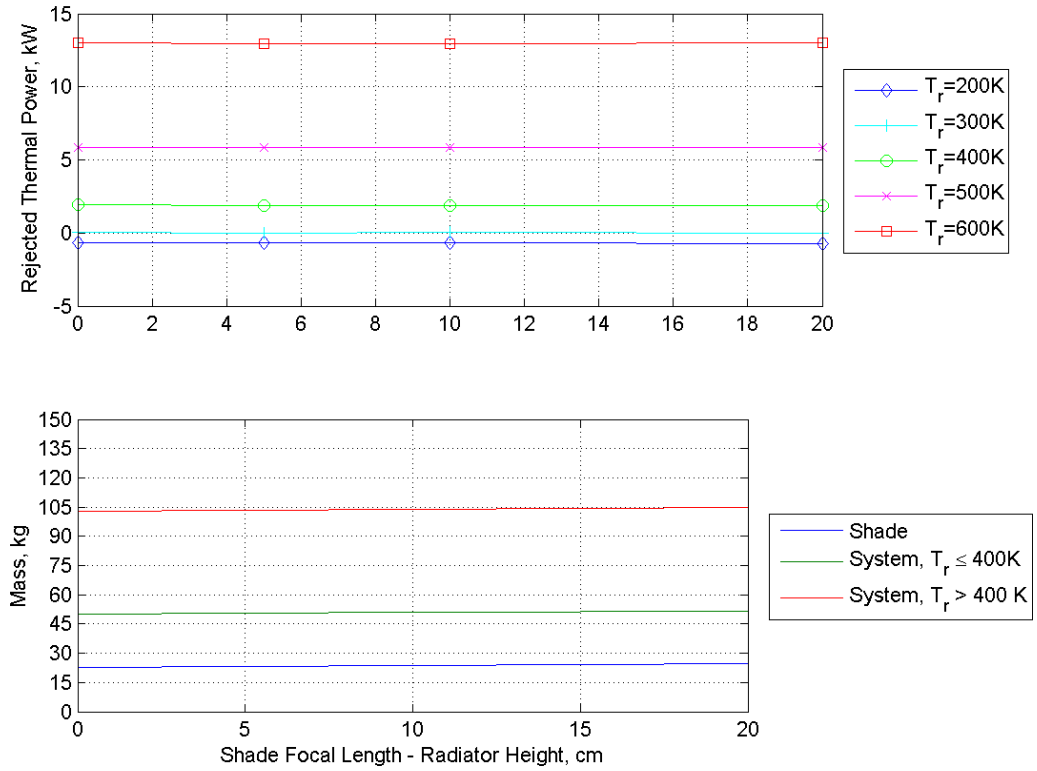

Fig. C.16: Radiated heat and radiator mass versus shade height; square radiator at 45°N aligned with lunar latitude line ($\beta_{fs-\vartheta}$ =90°); shade focus 10 cm above radiator top

Hot Pole

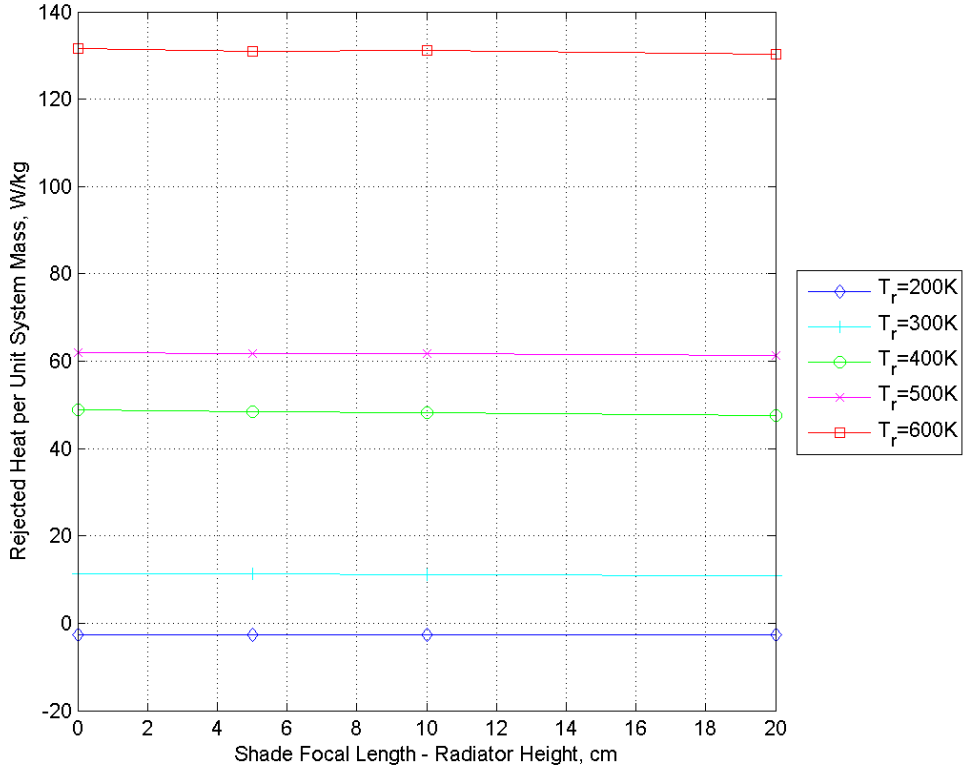

Fig. C.17: Radiated heat per unit mass versus shade height; square radiator at hot pole; shade focus 10 cm above radiator top

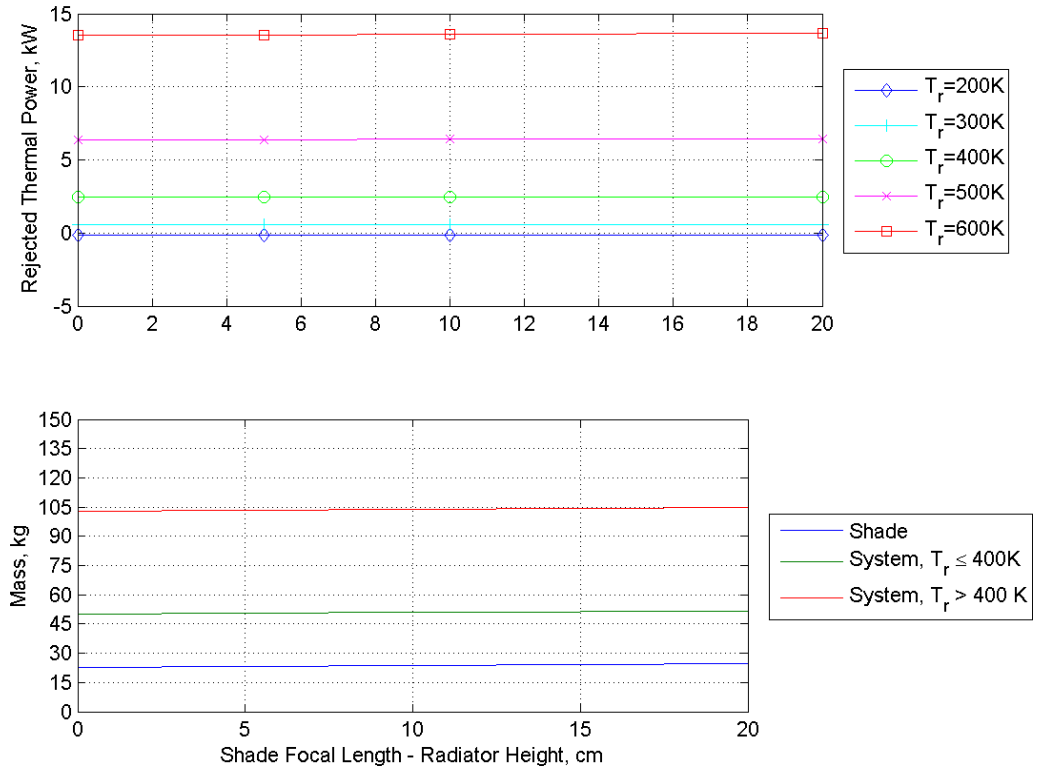

Fig. C.18: Radiated heat and radiator mass versus shade height; square radiator at hot pole; shade focus 10 cm above radiator top

APPENDIX D
CODE

Thermal Desktop produces its calculated results in the form of text files. Several Matlab codes were generated to read the text files, strip out pertinent numbers from the file name and contents, and plot the results. The file names are used to categorize the results from within the text files, e.g. latitude, radiator temperature, shade size, shade focal point. The general program procession is thus:

- Compile results from Thermal Desktop results files in a programing structure. For each individual Thermal Desktop file:
  - Read file name for latitude, rotation angle (if applicable), radiator size, surface temperature, configuration, shade height, distance between shade focus and radiator top. The last three parameters are omitted if the radiator configuration is bare vertical or horizontal.
  - Pick time of lunar day and heat transfer data from file.
  - Calculate radiator and shade masses.
  - Calculate waste heat rejected per unit system mass. The waste heat used in this calculation should be the smallest out of the heat transfer data to be conservative.
- For each plot:
  - Designate constants and variables.
  - Find data in the structure that fit the constants and variables.
  - Rearrange the data into a matrix and plot.
  - Determine optimal variable tested; usually variable that corresponds with maximum waste heat per unit mass.
- Plot optima.

VITA

Cheyn Layton Worn received his Bachelor of Science in nuclear engineering from Texas A&M University in May 2009. He entered the Nuclear Engineering graduate program at Texas A&M University in January 2010. His research interests include two-phase flow, heat transfer, and space nuclear systems.

Mr. Worn's mail can be forwarded through the Department of Nuclear Engineering, 129 Zachry, Texas A&M University, College Station, Texas 77843. His e-mail address is clworn@gmail.com.